Titre: Title:	Implantable Micro-Device for Epilepsy Seizure Detection and Subsequent Treatment
Auteur: Author:	Muhammad Tariqus Salam
Date:	2012
Type:	Mémoire ou thèse / Dissertation or Thesis
Référence: Citation:	Salam, M. T. (2012). Implantable Micro-Device for Epilepsy Seizure Detection and Subsequent Treatment [Thèse de doctorat, École Polytechnique de Montréal]. PolyPublie. https://publications.polymtl.ca/844/

Document en libre accès dans PolyPublie
Open Access document in PolyPublie

URL de PolyPublie: PolyPublie URL:	https://publications.polymtl.ca/844/
Directeurs de recherche: Advisors:	Mohamad Sawan, & Dang Khoa Nguyen
Programme: Program:	Génie Électrique

UNIVERSITÉ DE MONTRÉAL

IMPLANTABLE MICRO-DEVICE FOR EPILEPSY SEIZURE DETECTION
AND SUBSEQUENT TREATMENT

MUHAMMAD TARIQUS SALAM

DÉPARTEMENT DE GÉNIE ÉLECTRIQUE

ÉCOLE POLYTECHNIQUE DE MONTRÉAL

THÈSE PRÉSENTÉE EN VUE DE L'OBTENTION

DU DIPLÔME DE PHILOSOPHIAE DOCTOR (PH.D.)

(GÉNIE ÉLECTRIQUE)

Avril 2012

UNIVERSITÉ DE MONTRÉAL

ÉCOLE POLYTECHNIQUE DE MONTRÉAL

Cette thèse intitulée:

IMPLANTABLE MICRO-DEVICE FOR EPILEPSY SEIZURE DETECTION AND SUBSEQUENT TREATMENT

présentée par : Muhammad Tariqus Salam

en vue de l'obtention du diplôme de : Philosophiae Doctor

a été dûment acceptée par le jury d'examen constitué de :

M. AUDET Yves, Ph.D, président

M. SAWAN Mohamad, Ph.D., membre et directeur de recherche

M. NGUYEN Dang Khoa, Ph.D., membre et codirecteur de recherche

M. LESAGE Frédéric, Ph.D., membre

M. GHOVANLOO Maysam, Ph.D., membre

DÉDICACE

To my father

REMERCIEMENTS

RÉSUMÉ

L'émergence des micro-dispositifs implantables est une voie prometteuse pour le traitement de troubles neurologiques. Ces systèmes biomédicaux ont été exploités comme traitements non-conventionnels sur des patients chez qui les remèdes habituels sont inefficaces. Les récents progrès qui ont été faits sur les interfaces neuronales directes ont permis aux chercheurs d'analyser l'activité EEG intracérébrale (icEEG) en temps réel pour des fins de traitements.

Cette thèse présente un dispositif implantable à base de microsystèmes pouvant capter efficacement des signaux neuronaux, détecter des crises d'épilepsie et y apporter un traitement afin de l'arrêter. Les contributions principales présentées ici ont été rapportées dans cinq articles scientifiques, publiés ou acceptés pour publication dans les revues IEEE, et plusieurs autres tels que «Low Power Electronics» et «Emerging Technologies in Computing». Le microsystème proposé inclus un circuit intégré (CI) à faible consommation énergétique permettant la détection de crises d'épilepsie en temps réel. Cet CI comporte une pré-amplification initiale et un détecteur de crises d'épilepsie. Le pré-amplificateur est constitué d'une nouvelle topologie de stabilisateur d'hacheur réduisant le bruit et la puissance dissipée. Les CI fabriqués ont été testés sur des enregistrements d'icEEG provenant de sept patients épileptiques réfractaires au traitement antiépileptique. Le délai moyen de la détection d'une crise est de 13,5 secondes, soit avant le début des manifestations cliniques évidentes. La consommation totale d'énergie mesurée de cette puce est de 51 μW.

Un neurostimulateur à boucle fermée (NSBF), quant à lui, détecte automatiquement les crises en se basant sur les signaux icEEG captés par des électrodes intracrâniennes et permet une rétroaction par une stimulation électrique au même endroit afin d'interrompre ces crises. La puce de détection de crises et le stimulateur électrique à base sur FPGA ont été assemblés à des électrodes afin de compléter la prothèse proposée. Ce NSBF a été validé en utilisant des enregistrements d'icEEG de dix patients souffrant d'épilepsie réfractaire. Les résultats révèlent une performance excellente pour la détection précoce de crises et pour l'auto-déclenchement subséquent d'une stimulation électrique. La consommation énergétique totale du NSBF est de 16 mW. Une autre alternative à la stimulation électrique est l'injection locale de médicaments, un traitement prometteur de l'épilepsie. Un système local de livraison de médicament basé sur un nouveau détecteur asynchrone des crises est présenté. Ce dernier système dépendant des calculs

de données réduit jusqu'à 49% la consommation énergétique en comparaison avec le neurostimulateur synchrone précédemment présenté. Le détecteur a été validé à partir d'enregistrements icEEG de sept patients ayant déjà subi des examens intracrâniens pour une chirurgie d'épilepsie. Le déclenchement du système de livraison de médicaments a été testé et une dose prédéfinie de médicament est libérée environ 16 secondes après le début des crises électrographiques.

Dans le but d'améliorer les performances du dispositif implantable, de nouvelles électrodes sous-durales seront présentées. Elles offrent une meilleure qualité d'enregistrement des icEEG et permettent de délimiter la zone épileptogène durant l'évaluation pré-chirurgicale. De plus, le nouveau réseau d'électrodes a une nouvelle forme et permet de minimiser certaines complications (i.e. infection, œdème et hémorragie au niveau du cerveau) habituellement rencontrées avec l'utilisation des électrodes sous-durales actuelles. Ces nouvelles électrodes ont été testées in vitro dans une solution saline et in vivo pendant une période de trois semaines. Le rapport signal sur bruit a été amélioré de 6 dB en comparaison avec des électrodes commerciales actuellement disponibles.

ABSTRACT

Emerging implantable microdevices hold great promise for the treatment of patients with neurological conditions. These biomedical systems have been exploited as unconventional treatment for the conventionally untreatable patients. Recent progress in brain-machine-interface activities has led the researchers to analyze the intracerebral EEG (icEEG) recording in real-time and deliver subsequent treatments.

We present in this thesis a long-term safe and reliable low-power microsystem-based implantable device to perform efficient neural signal recording, seizure detection and subsequent treatment for epilepsy. The main contributions presented in this thesis are reported in five journal manuscripts, published or accepted for publication in IEEE Journals, and many others such as Low Power Electronics, and Emerging Technologies in Computing. The proposed microsystem includes a low-power integrated circuit (IC) intended for real-time epileptic seizure detection. This IC integrates a front-end preamplifier and epileptic seizure detector. The preamplifier is based on a new chopper stabilizer topology that reduces noise and power dissipation. The fabricated IC was tested using icEEG recordings from seven patients with drug-resistant epilepsy. The average seizure detection delay was 13.5 sec, well before the onset of clinical manifestations. The measured total power consumption of this chip is 51 µW.

A closed-loop neurostimulator (CLNS) is next introduced, which is dedicated to automatically detect seizure based on icEEG recordings from intracranial electrode contacts and provide an electrical stimulation feedback to the same contacts in order to disrupt these seizures. The seizure detector chip and a dedicated FPGA-based electrical stimulator were assembled together with common recording electrodes to complete the proposed prosthesis. This CLNS was validated offline using recording from ten patients with refractory epilepsy, and showed excellent performance for early detection of seizures and subsequent self-triggering electrical stimulation. Total power consumption of the CLNS is 16 mW. Alternatively, focal drug injection is the promising treatment for epilepsy. A responsive focal drug delivery system based on a new asynchronous seizure detector is also presented. The later system with data-dependent computation reduces up to 49% power consumption compared to the previous synchronous neurostimulator. The detector was validated using icEEG recordings of 7 patients who have previously undergone intracranial investigations for epilepsy surgery. The triggering of the drug

viii

delivery system was tested and a predefined seizure suppression dose was delivered ~16 sec after electrographical seizure onsets.

In order to improve performances of the whole implantable device, a novel subdural electrode is presented for better icEEG recording quality and delineation of the epileptogenic zone during the presurgical evaluation. Moreover, the new subdural grid electrode has a new shape and several attributes to address some of the problems (e.g. brain infection, swelling and hemorrhage) encountered with currently used subdural electrodes. These electrodes are tested *in vitro* saline solution and *in vivo* experiments for 3 weeks, and signal-to-noise ratio is improved up to 6 dB compared to using commercial electrodes.

TABLE DES MATIÈRES

LISTE DES TABLEAUX

LISTE DES FIGURES

LISTE DES SIGLES ET ABRÉVIATIONS

Au	Gold
ADC	Analog-to-Digital Conversion
AFED	Asynchronous Front-End Detector
AM	Amplitude Detectors
ASIC	Application-Specific Integrated Circuit
ATN	Anterior Thalamic Nucleus
Au	Gold
BER	Bit Error Rate
BES	Brief Electrical Seizures
CAM	Current Amplifier
CCPA	Canadian Council for the Protection of Animals
CHUM	Centre Hospitalier de l'Université de Montréal
CIBPAR	Comité Institutionel des Bonnes Pratiques Animales en Recherche
CLNS	Closed-Loop Neurostimulator
CMOS	Complementary Metal–Oxide–Semiconductor
CNC	Computer Numerical Controlled
CSF	Cerebrospinal Fluid
DAC	Digital-to-Analog Converter
DBS	Deep Brain Stimulation
DC	DC current
DD	Digital Demodulators
DDS	Drug Delivery System

DFF	D Flip Flop
DPE	Depth electrode
DSP	Digital Signal Processor
DTD	Detection Delay
EBSD	Event Based Seizure Detector
EEG	Electroencephalography
EEG-fMRI	EEG-Functional MRI
eRNS	External Responsive Neurostimulator
ES	Electrical Stimulator
ESD	Event-based Seizure Detector
EZ	Epileptogenic Zone
FD	False Detection
FD	Frequency Detectors
FDA	Food and Drug Administration
FEP	Feature Extraction Process
FPGA	Field-Programmable Gate Array
FQRNT	Fonds Québécois de la Recherche sur la Nature et les Technologies
FSK	Frequency-shift keying
GTC	Generalized Tonic-Clonic
HFB	High Frequency Band
HFD	High-Frequency Detector
HSE	Hybrid Subdural Electrode
icEEG	Intracerebral EEG
LDA	Linear Discriminant Analysis

LFB	ow Frequency Band
MEG	Magnetoencephalographic
MICS	Medical Implant Communication Service
MRE	Microelectrode
MRI	Magnetic Resonance Imaging
MUX	Multiplexer
NLESD	Nonlinear Energy Seizure Detector
OLS	Open Loop Neurostimulation
OTA	Operational Transconductance Amplifier
PC	Power Consumption
PCB	Printed Circuit Board
PDMS	Polydimethylsiloxane
PET	Positron Emission Tomography
PLCS	Post-Layout Circuit Simulation
PS	Power Supply
PSD	Power Spectral Densities
Pt	Platinum
ReSMiQ	Microsystems Strategic Alliance of Québec
RNS	Responsive Neurostimulator
SD	Seizure Detector
SDE	Subdural Electrode
SE	Silver epoxy
SEM	Scanning Electron Microscope
SESD	Spectral Energy Seizure Detector

SNR	Signal-to-Noise Ratio
SOD	Seizure Onset Detector
SPECT	Ictal Single-Photon Emission Computed Tomography
SW	Switch
SXT	Sensitivity
TFS	Time Frame Selector
VLD	Voltage Level Detector
VNS	Vagus Nerve Simulation
VWD	Voltage Window Detector
WANN	Wavelet Artificial Neural Network

LISTE DES APPENDIXES

INTRODUCTION

Epilepsy is a neurological disorder affecting 1.3% of Canadians and up to 1% of the world population. Each year, an average of 15,500 Canadians learns that they have epilepsy. Epilepsy is a common chronic neurological disorder characterized by a predisposition to unprovoked recurrent seizures. A seizure is the manifestation of an abnormal, hypersynchronous discharge of a population of cortical neurons. Several causes may disturb the normal pattern of brain activity and trigger an epileptic seizure, such as head injury, brain infection, developmental malformations, brain tumors, cerebrovascular disease, vascular malformations, genetic disorders, and hippocampal sclerosis. Antiepileptic drugs are the mainstay of treatment, but many patients have systemic and central nervous system side effects and a third of them are refractory. Because most drug-resistant epileptics suffer from focal epilepsy, these patients may benefit from epilepsy surgery. Many studies have shown that resection of the epileptogenic zone may lead to seizure freedom (ENGEL, 2009). Success of the surgery is dependent on the accurate localization and complete resection of the epileptogenic zone. Unfortunately, not all refractory patients with focal epilepsy benefit from resective surgery; some have an epileptogenic zone overlying eloquent areas (language, primary motor or visual areas) that cannot be resected without permanent sequelae, while others have multifocal epilepsy (SPENCER, 2009). Therefore, the poor neurological outcome of these cases combined with the lack of efficacy and adverse effects of antiepileptic drugs provide sufficient justification to have an alternative treatment to supplement conventional treatments. The details motivation behind the neurostimulator therapies and the improved presurgical procedure for the treatment of epilepsy are discussed below.

Motivation

Over the last quarter century, the vast progression in neurotechnology has allowed the Food and Drug Administration (FDA) to approve stimulators for the treatment of neurological disorders, such as multichannel cochlear implant for hearing loss, deep brain simulation for Parkinson diseases, and vagus nerve simulation (VNS) for epilepsy. Commercially available VNS provides scheduled stimulation (open-loop) to the left vagus nerve to reduce seizure frequency by a yet unclear mechanism. However, seizure freedom is rare, and only 30 – 40% of patients show a significant decrease in seizure frequency (SCHACHTER, 2009). More recently, there has been growing interest in the development of responsive therapeutic devices to abort seizures at their

onset. The responsive device (detection and treatment) identifies seizures at their onset and triggers focal treatment to the epileptogenic zone to abort the seizure, whether by electrical stimulation, cooling, or drug release. To do so, an efficient seizure detection algorithm is required for accurate seizure onset detection without false alarms, and which can be implemented in a custom integrated circuit.

Several mathematical models have been developed to detect electrographic seizures onset. Intracerebral EEG-based models have shown much better performance than scalp EEG-based models, as lesser artifacts are encountered with the former. Several others studies have shown better seizure detection performances than random predictor. These models were developed using desktop computers for off-time data processing. These types of algorithms cannot be employed in a low-power implantable microchip. However, a power-efficient epileptic seizure detection algorithm can be integrated in novel therapeutic devices for epilepsy that the system could run on a button cell battery for more than 8 years. Currently, only a few clinically applicable seizure detectors exist (e.g. Responsive Neurostimulation System, NeuroPace Inc., and Seizure Advisory System, NeuroVista Corporation). Apart from the seizure detection performance, the other concerns are safety, low-power techniques, miniaturized devices and determination of optimal stimulation parameters. The several proof-of-concept experiments were introduced for the treatment of epilepsy, among them the surgical treatment, focal electrical stimulation, and direct drug delivery.

Surgical treatment of epilepsy

Patients with refractory epilepsy may benefit from epilepsy surgery if the epileptogenic zone (EZ) can be identified and resected without harm. Due to the limited spatial or temporal resolution of currently available non-invasive localization techniques, accurate delineation of the EZ may sometimes be arduous, particularly with nonlesional refractory epilepsy (SPENCER, 2009). As such, invasive EEG recordings may be necessary prior to resective surgery. An intracerebral EEG (icEEG) study consists of implanting intracerebral subdural strip, grid or depth electrodes to sample suspected areas of epileptogenicity. Intracranial electrodes will overcome the sensitivity limitations of extracranial (scalp) electrodes because they are closer to generators of epileptiform activity. Whereas a large cortical surface is required to generate a recordable signal by extracranial electrodes, intracranial electrodes can pick up potential changes occurring over only a few

millimeters of cortex. When seizures occur, the icEEG signal is analyzed to identify the EZ for subsequent resection. But there are some risks associated with icEEG recordings using available commercial intracranial electrodes, such as brain infection, cerebral edema and failure to adequately localize the EZ from inadequate brain sampling

Focal electrical stimulation

In a pilot trial, Osorio et al. (2005) demonstrated the feasibility and short-term safety of automated high-frequency electrical stimulation in blocking seizures using an external prototype composed of an electrocorticographic acquisition system, a desktop computer, and a stimulator (Grass S12). Another external responsive neurostimulator (eRNS) has been shown to terminate electrographic seizures as well (KOSSOFF, 2004). Apart from seizure detection performance, the other concerns are the safety of chronic electrical stimulation and the determination of optimal stimulation parameters. It is generally agreed that limiting the maximum charge density to 30 μC/cm^2 per phase can avoid tissue damage (AGNEW, 1990); however, no cell damage in human cortex has been found for 50 to 60 μC/cm^2 per phase stimulation (GORDON, 1990; RISINGER, 1995).

Direct drug delivery

The currently available orally administered antiepileptic drugs are associated with variable systemic side effects (adverse effects in liver, bone marrow, and central nervous system). Focal drug delivery directly onto the epileptogenic zone could enhance the efficacy of drugs while limiting side effects to a minimum. Experiments in the past showed that focal diazepam infusion using a programmable pump in response to automated seizure detection could suppress the seizure (STEIN, 2000; DAVID, 2004). Other drugs such as DP-valproic acid (FISHER, 2002), gabapentin (OOMMENA, 2007), and adenosine (ANSCHEL, 2004) have been used but with less success. Much work lies ahead prior to clinical application in optimal drug selection, the delivery system, automated seizure detection, the refilling procedure, etc. To date, technological barriers limit the exploration of direct drug delivery for the long-term treatment of focal epilepsy.

Thesis Works

The new technologies give us the opportunity to solve drawbacks of the available treatments and extend the traditional neurostimulation therapies and resective surgical treatment procedures

for better treatments of epilepsy. In this thesis, our objectives are to propose new technologies for implantable device therapies and presurgical evaluation for epilepsy. We introduce long-term, safe and reliable low-power microsystems-based implantable devices to perform efficient neural signal recording, seizure detection and subsequent treatment. We have accomplished three specific objectives in the implantable device therapies: (i) Designed and implemented a low-power neural preamplifier and real-time seizure onset detection algorithm in a microchip using advanced integration technology; (ii) Designed a low-power closed-loop electrical stimulators and constructed a responsive neuromodulator by assembling the detector chip and stimulator together; and (iii) Modeled and implementated of an implantable responsive focal drug delivery system as an alternative promising treatment. For the epilepsy presurgical evaluation, we have introduced novel intracranial electrodes and a wireless icEEG recording system in order to improve EZ localization and reduce morbidity.

Contributions

The main contributions of this thesis have been reported in several peer-reviewed scientific journals and international conferences. These contributions are:

1. Design, simulation, implementation, and validation of novel power-efficient epileptic seizure detection algorithms for refractory epilepsy patients (SALAM, 2009(a), (b); SALAM, 2010 (a), (b); SAFI-HARB, 2011(b)).

2. Design, fabrication and testing of new preamplifiers and novel low-power implantable epileptic seizure-onset detectors. The systems were implemented using 0.18µm CMOS technology and discrete components in miniaturized printed circuit boards (PCBs). The implemented devices were validated using icEEG recordings of several refractory epilepsy patients (SALAM, 2011(a), (c); SAFI-HARB, 2011(b)).

3. Modeling, implementation and validation of new implantable closed-loop epilepsy prosthesis. The system was assembled with an embedded microchip (0.18µm CMOS technology) and field-programmable gate array (FPGA) in miniature PCBs, and tested using icEEG recordings of ten refractory epilepsy patients (SALAM, 2010(c), SALAM, 2012(a); SALAM, 2012(c)).

4. Design, implementation and testing of an implantable asynchronous responsive drug delivery system for Treatment of Epilepsy. The system was assembled with commercial discrete

components in miniature PCBs and validated using icEEG recording of refractory epilepsy patients (SALAM, 2011(a); SALAM, 2012(b)).

5. Design and fabrication of new subdural porous and notched mini grid electrodes for wireless icEEG recordings. The electrodes were validated *in vivo* icEEG recording experiments and demonstrated comparative studies with the commercial electrodes (SALAM, 2011(b); SALAM, 2012(c)).

Thesis organization

This thesis is divided into 8 chapters. The first chapter of this thesis describes a comprehensive literature review on the alternative treatment for epilepsy. Chapters 2 through 6 address the design, implementation and validation of the new implantable device. The last chapters summarize the entire thesis, and draw attention to the contribution of this research and the recommended future works. The following is the brief chapter-wise summary of this thesis.

Chapter 1 reviews the fundamental concepts of implantable device therapies and presurgical evaluation for the treatment of epilepsy. This chapter begins with basic theories, design issues and design criteria of the implantable device. We discuss about subdural electrodes, preamplifiers front-end, seizure detectors and stimulators in the prospect of state-of-the-art, and highlight factors limiting performance in implantable device therapies for epilepsy.

Chapter 2 investigates electrographic seizure onset detection criteria and noises affect for limiting performance in the responsive neuromodulation therapies. A modified chopper stabilized preamplification method and a new power efficient seizure onset detection algorithm are proposed for the responsive neuromodulation therapy. The ultra low-power detector is implemented and validated using icEEG recordings from seven refractory epileptic patients.

Chapter 3 describes electrical stimulation therapy, a new low-power circuit design, implementation and testing of a new closed-loop electrical stimulator. The proposed FPGA embedded neurostimulator is triggered by the seizure onset detector chip for disrupting an upcoming seizure. Experimental results demonstrated safety and reliability for the automated triggering of the bipolar electrical stimulator.

Chapter 4 demonstrates modeling, implementation and validation of a new closed-loop electrical stimulator (second prototype). The new electrical stimulator has lower power

consumption, wider range of parameter variation, better precision, and larger memory. Experimental results show spatial voltage distribution in brain due to the current stimulation and suggest optimum electrical stimulation parameters for the suspected epileptic focus.

Based on the design and implementation trend in the previous chapters, which aims at closed-loop electrical stimulator; chapter 5 presents an asynchronous closed-loop drug delivery system. A new power saving strategy is employed to design this direct drug delivery device. This chapter also describes a new preamplifier, an asynchronous seizure onset detector, a drug delivery system, and a hybrid subdural electrode. The experimental results demonstrate efficiency of the device and wide range of drug dosing capacity at seizure onset.

Chapter 6 describes novel subdural electrodes to improve icEEG recording quality as well as localization of the epileptogenic zone with less morbidity. The new subdural mini grid electrode has new a shape and several attributes to overcome some of the currently encountered problems with intracranial recordings. This chapter also demonstrates the design of the novel electrodes, method of fabrication, architecture of a wireless EEG recording system, and *in vitro* and *in vivo* experimental results.

Finally, a discussion chapter is presented in Chapter 7 followed by a conclusion and recommendation for future works in chapter 8.

CHAPTER 1   MICROELECTRONIC SYSTEM FOR TREATMENT OF EPILEPSY

In the last decade, implantable microelectronic systems have been exploited as unconventional treatment for the conventionally untreatable patients. Several microelectronic devices have been commercialized for treatment of heart disease, Parkinson's disease, Epilepsy, and deaf. Recent progress in brain-machine-interface (BMI) has led to the idea of using the medical devices to analyze the intracerebral EEG (icEEG) recorded data in real-time in order to provide subsequent treatments. The combination of the online icEEG analysis and responsive treatment approaches ensure consistent link in between neuronal pathways for normal brain activities and break the pathway for the abnormalities. Thus, microelectronic therapeutic devices offer new attractive treatment option for the neurological disorders. However, many challenges are involved in designing the implantable microelectronic devices. The design issues and factors limiting performances of microelectronic therapeutic devices are discussed in the chapter. This review work published in "Journal of Healthcare Engineering" is reproduced in following pages.

1.1   LOW-POWER IMPLANTABLE DEVICE FOR ONSET DETECTION AND SUBSEQUENT TREATMENT OF EPILEPTIC SEIZURES: A REVIEW

Muhammad Tariqus Salam[1], Mohamad Sawan[1], and Dang Khoa Nguyen[2]

[1]Polystim Neurotechnologies Laboratory, École Polytechnique de Montréal, Québec

[2]Neurology service, Notre-Dame Hospital (Centre Hospitalier de l'Université de Montréal)

Abstract - Over the past few years, there has been growing interest in neuro-responsive intracerebral local treatments of seizures, such as focal drug delivery, focal cooling, or electrical stimulation. This mode of treatment requires an effective intracerebral electroencephalographic acquisition system, seizure detector, brain stimulator, and wireless system that consume ultra-low power. This review focuses on alternative brain stimulation treatments for medically intractable epilepsy patients. We mainly discuss clinical studies of long-term responsive stimulation and suggest safer optimized therapeutic options for epilepsy. Finally, we conclude our study with the proposed low-power, implantable fully integrated device that automatically detects low-voltage

fast activity ictal onsets and triggers focal treatment to disrupt seizure progression. The detection performance was verified using intracerebral electroencephalographic recordings from two patients with epilepsy. Further experimental validation of this prototype is underway.

1.2 MICROELECTRONIC SYSTEM DESIGN CRITERIA FOR CHRONIC BRAIN IMPLANTS

Microelectronic systems are generally implanted on the skull under the skin and interface directly with the recording/stimulation sites for the treatment of epilepsy. Thus, the system size needs to be small, lightweight and invisible after surgical implantation. The microelectronic implants are safety-critical in nature; high reliability is an essential system attribute. Moreover, the implants must operate under stringent low-power constraints for minimal heat dissipation in surrounding tissues and to avoid frequent surgical battery replacement. Energy harvesting is essential to recharge the implanted battery from an external power source. The rechargeable implantable battery needs short-circuit protection mechanism and constant current discharge state for longer time. The implant must ideally function for 8 – 10 years without having to replace the battery. The electronic components of an implant must be sealed with biocompatible casing which is implanted in a viable places for energy harvesting, data communication, and battery replacement without a major surgery. Apart from the long lasting implantation facts, the other concerns are proper device functionalities, accurate icEEG monitoring, personalized treatment parameters, and external tuning. The key challenges of a BMI are the icEEG monitoring for true electrographic seizure activity in real-time and the trigger of focal treatment at seizure onset. Thus, noise reduction or isolation from the icEEG recordings is essential for device performance. Moreover, the abnormal icEEG detection criteria and focal treatment parameters may vary from patient to patient, and these criteria and parameters for a patient may change over the time. Therefore, a remote tunability is required in the device for adjusting detection criteria and increase/decrease intensity of the treatment.

1.3 ICEEG RECORDING METHOD

The icEEG records the activity of thousands of neurons in the region across the ~5 mm diameter of an intracranial electrode contact. A frequency analyzer can decompose the icEEG

recording and extract brain state information (e.g. normal and abnormal). Recent studies using higher sampling rates (1000 – 2000Hz) have showed high-frequency oscillations in preictal activities (JACOBS, 2010). Until we obtain a better understanding of the significance of these high-frequency oscillations with regards to epileptogenesis, most clinical epileptologists still rely on the analysis of a limited frequency range in the low-frequency bandwidth (10 – 40Hz) of icEEG recording (OSORIO, 2009(b)). In order to acquire the brain state information of a patient, a data acquisition system with low gain-bandwidth product and low noise are required. Commercial instrumentation has poor noise performance for the low-spectral neural signal amplification. Therefore, microelectronic circuit design problems increase due to the various noises located in the low frequency band that degrade the input icEEG recordings. As a result, the icEEG recording may translate erroneous brain state information.

Partial seizure generally begins in the EZ, spreading to adjacent regions. However, electrographic seizure onsets may vary in terms of onset morphology, discharge frequency, focality, and spread pattern. The most common seizure onset pattern in a partial epilepsy patient is characterized by a low-voltage high-frequency discharge. Figure 1-1(a) shows icEEG recording from the EZ (V_{in}) using a 200 Hz sampling frequency with the sudden appearance of this typical low-voltage fast activity at seizure onset. Figure 1-1(b) illustrates the spectrogram analysis of V_{in}. Magnitude of short-time Fourier transformation |SF| reveals low frequency activity (< 3 Hz) before seizure onset and high frequency activity (> 10 Hz) at seizure onset and during the seizure. The frequency at seizure onset may vary from patient to patient but generally stands between 10 – 40 Hz in epileptic human icEEG recordings (OSORIO, 2009(b); SALAM, 2011(a)).
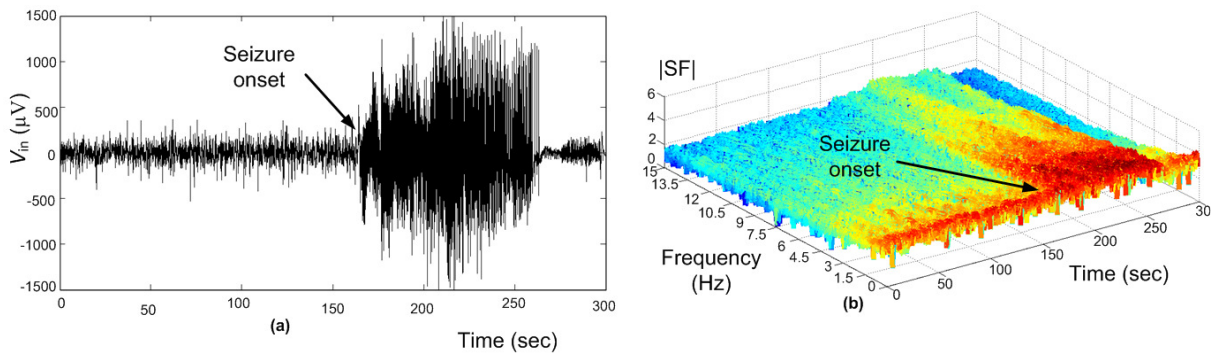
Figure 1-1: Seizure signal analysis: (a) is icEEG recording V_{in} from the epileptogenic zone during a seizure and (b) is |SF| of V_{in}.

1.4 NOISE FIGURES

Unlike scalp EEG recordings, icEEG recordings are relatively devoid of motion and muscle artifacts. However, several other noises may degrade the icEEG recording and subsequent automated evaluation in microelectronic implant may lead to erroneous brain state translation. Figure 1-2 illustrates the noises influence in the input icEEG recording V_{in}. In this situation, the subdural electrodes placed directly on the brain tissue and the electrode-tissues interface create a capacitive double layer that generates dc offset (V_{OS}) in the millivolts range. But, the front-end amplifier has a low dynamic input range due to the microvolt input neuronal signal and V_{OS} saturates the amplifier. Therefore, V_{OS} needs to be suppressed adequately so that V_{in} can dominate over V_{OS} in front-end amplification. Moreover, flicker noise V_{nF} contributes a major amount of noise in the low frequency band due to fundamental physics properties of instrumentation. Thermal noise V_{nT} dominates in higher frequency (above the flicker corner frequency) due to internal resistance of instrumentation and wire resistance. Finally, 60 Hz noise V_{n60} is a large
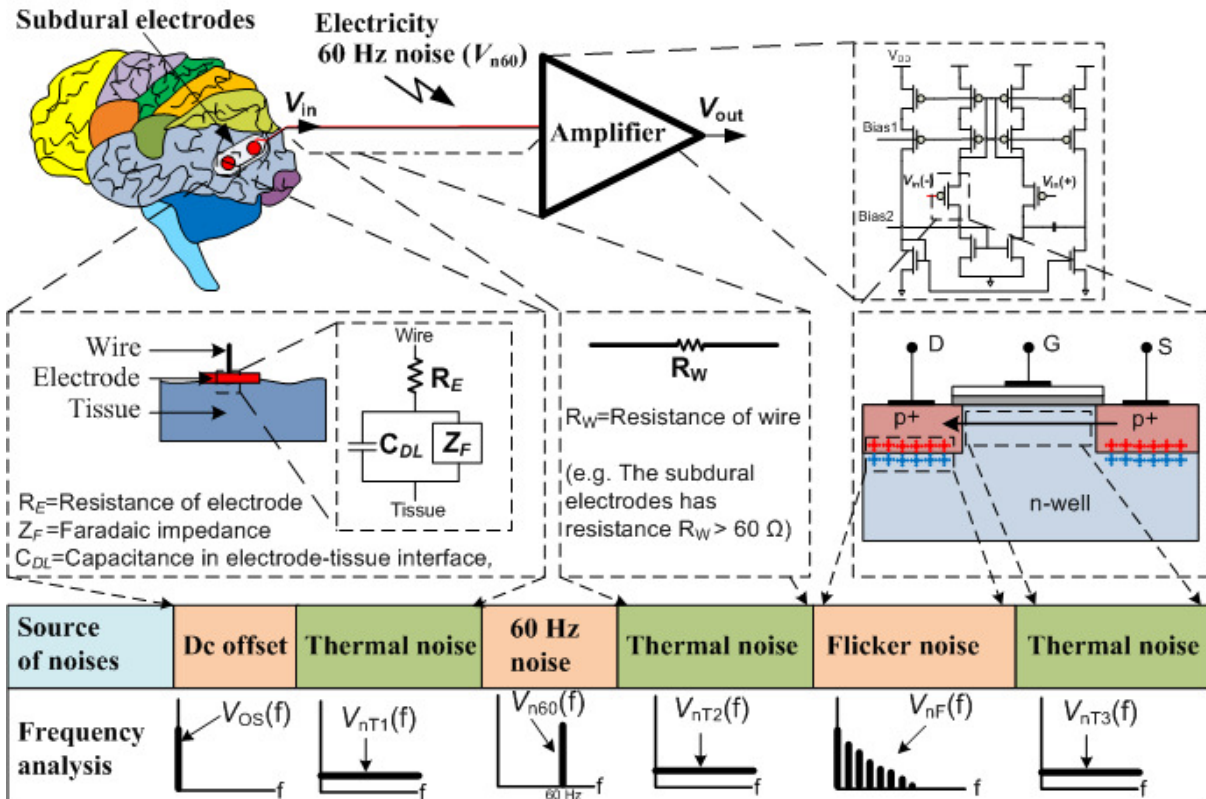
Figure 1-2: Various noise sources affect icEEG recording V_{in}.

source of noise generated from the AC power supply; this noise may completely degrade the V_{in}.

1.5   INTRACRANIAL ELECTRODE CONTACT

Noises generated from electrodes, electrode-tissues interface, and from instruments may modulate the neural signal and degrade the signal-to-noise ratio (SNR). The custom integrated amplifiers could reduce instrument noise effect for the low-spectral neural signal amplification, but optimum SNR values can be obtained by modifying intracranial electrode contacts (SALAM, 2011(b)). Microelectrode (MRE) arrays are widely used in neurological research to improve spatial resolution in icEEG recording (CHEN, 2011). But MRE arrays have high resistivity in electrode-tissues interface which may impede icEEG neural recording (CHEN, 2011). Macroelectrodes (e.g. subdural (SDE) and depth electrodes (DPE)) have been used for the last sixty years in epilepsy presurgical evaluation. Dimensions of a SDE and a DPE are well suited to delineate the EZ. Due to their larger electrode-tissues interface, these electrodes have different electrical characteristics (compared to microelectrodes) including lower electrode impedance. Platinum (Pt) and stainless steel materials are commercially used in SDE and DPE, with Pt having better biocompatibility properties. Gold (Au) has been used in subdural electrodes (REN, 2010) but no significant improvement on icEEG recording has been reported. The details drawbacks of the available intracranial electrode contacts are described in chapter 6.

1.6   NEURAL SIGNAL AMPLIFIER

Over the past few decades, many neural signal amplifiers have been developed to overcome several challenges (e.g. low-power, low-noise, and minimal chip area). Many integrated amplifiers have been proposed, but very few designs meet the requirements for epilepsy device therapies or presurgical evaluation. The intracranial electrodes potential mismatch creates input dc offset (SALAM, 2011(a)). There are two schemes for the dc offset suppression. The first scheme is capacitive feedback of an operational transconductance amplifier (OTA) (HARRISON, 2003). MOS-bipolar pseudo-resistor elements in parallel with the capacitive feedback were used to provide a very low high-pass cutoff frequency as well as a fast settling time (ZARIFI, 2008). The capacitive feedback scheme removes the dc offset, but it may increase input referred noise (GOSSELIN, 2007(c)).

The second scheme is based on closed loop control of dc level (GOSSELIN, 2007(c); GOSSELIN, 2010(a)). This scheme is made of active components that are placed in the feedback path of an instrumentation amplifier. It can reduce low-spectrum noise and provide high input impedance. Further high-pass and low-pass filters are needed to suppress significant amount of noise. CMOS technology is widely used for bioamplifier due to the low-power dissipation, but this technology has relatively poor noise performance and the amplifier requires low input-referred noise (GOSSELIN, 2007(c); GOSSELIN, 2010(a), (b); GOSSELIN, 2009). Chopper preamplifiers have been constructed using CMOS technology and reported performance have been satisfactory (GOSSELIN, 2007(c); MASAYA, 2010; JAWED, 2009). The chopper preamplifier is based on modulation, amplification, demodulation, and filtering. The restrictions on the power consumption and size of an implantable device limit increasing the biasing current of the amplifier. Therefore, design trade-offs between the biasing current and noise are required to optimize the performance of a device. For the seizure detection application, the neural signal amplifier needs low frequency bandwidth (10 – 40 Hz). However, many amplifiers are made for neural spike detection and the amplifiers bandwidth starts from 100 Hz (GOSSELIN, 2007(c)); GOSSELIN, 2009). But the main challenge in seizure detection application is to record neural signal from the lower frequency band where noises are prominent.

1.7   LOW-POWER SEIZURE DETECTOR

In recent years, there has been growing interest in developing seizure detection algorithm. Several mathematical models have been proposed for this task, such as support vectors (MEIER, 2008), artificial neural networks (GHOSH-DASTIDAR, 2008), wavelet transformation (ZANDI, 2009), wavelet decomposition (SAAB, 2005), nonlinear time series analysis (LEHNERTZ, 1995), and mean nonlinear decision function (TITO, 2009). IcEEG-based models (MEIER, 2008; GHOSH-DASTIDAR, 2008; LEHNERTZ, 1995; TITO, 2009) perform much better than scalp EEG-based models (ZANDI, 2009; SAAB, 2005) owing to motion/muscle artifacts on scalp EEG recordings. Table 1.1 briefly summarizes different detection algorithms. These mathematical models have been implemented in high-speed computer for short-term EEG/icEEG monitoring applications. These models cannot be employed in an implantable device due to heavy mathematical computation involved and high-power dissipation. So far, few seizure detection algorithms have been proposed for low-power implantable microelectronic devices.

The detection algorithm presented in (RAGHUNATHAN, 2009) is based on classifying icEEG data into events, which are defined by two threshold voltages in icEEG recording. An ictal event is translated by high-frequency discharges. Recent studies have showed that high-frequency discharges can be very brief (few seconds), remain very focal (without spread), do not evolve in time or frequency, and are clinically silent (electrical seizures) (SALAM, 2010(a); SALAM 2009(b)). This device may result in false positive detection due to the high-frequency discharge

Table 1.1: Summary of seizure detection algorithms

Reference	Method	Description	Application
MCSHARRY, 2002	Multi-modal probability evaluation	Time evolution of the probability density function.	SESD
SHOEB, 2004	Wavelet and neural network	Wavelet decomposition constructs feature vector and the support-vector machine classification algorithm that determine seizure onset.	SESD
SUFFCZYNSKI, 2006	Bistable mathematical model	Predict time of seizure occurrences using a Poisson process and a random walk process.	IEBSD
MOXON, 2001	Correlation	Similarity between a reference and dynamically recorded signal.	IEBSD
IASEMIDIS, 2003(a)	Nonlinear, Lyapunov exponent	Convergence and divergence of short-term maximum Lyapunov exponents (STLmax) among critical electrode sites.	IEBSD
IASEMIDIS, 2003(b)	Phase changes	Measure average angular frequency and optimize the techniques.	IEBSD
MORMANN, 2000	Coherence	Statistical measurement of phase synchronization of signals.	IEBSD
TETZLAFF, 2006	Features extraction	Automated technique for the detection of a preseizure state.	IEBSD
ARNHOLD, 1999	Signals synchronization	Detect weak interdependences of signal.	IEBSD
NAGARAJ, 2006	Synchronization	Cross-correlationship used to find dissimilarity of signals between interictal periods and epileptic seizures.	IEBSD
SUKHI, 2005	Bayes' theorem	Spectral feature extraction, Bayes' theorem and spatiotemporal analysis.	IEBSD

SESD: Scalp EEG recording and software in desktop computer.
IEBSD: Intracranial electrodes, band pass filter and software in desktop computer.

detection. The support vector seizure detection algorithm (VERMA, 2010) has good flexibility but based on only spectral content of icEEG recording. Moreover it requires a large number of support vectors to define the complex decision boundary between a patient's seizure and non-seizure activity. This explains its high-power consumption and cost. Similarly, another detector (PATEL, 2009) based on linear discriminant analysis classifiers requires higher complexity of the digital signal processor to improve sensitivity and specificity. In order to avoid redundancy, further discussions on the low-power seizure detectors are described in chapters 2, 3, 4, and 5.

1.8   IMPLANTABLE DEVICES FOR THE TREATMENT OF EPILEPSY

Few implantable devices for the treatment of epilepsy have been commercialized. The only FDA-approved implantable device for the treatment of epilepsy is the vagal nerve stimulator (VNS). The VNS is an open-loop (non-responsive) system comprising an implantable stimuli generator, two leads incorporating two bipolar electrodes, and an external pulse programming system for the stimuli generator (Table 1.2). The stimuli generator of the VNS is inserted through an incision in the left axilla and implanted under the skin in the left chest below the clavicle under general anesthesia. The lead is tunneled to the neck, and the two helical bipolar stimulating electrodes are placed around the left vagus nerve. After the operation, the VNS can be turned on by a computer and programming wand. The most common settings for the stimulator are a frequency of 20 – 30 Hz, a pulse width of 250 – 500 µsec, time on of 30 sec, and time off of 3 – 5 min. The advantages of VNS include (a) no need to exactly delineate the epileptogenic zone, (b) no craniotomy, (c) a lower rate of surgical complications, and (d) mild and infrequent side effects due to stimulation (hoarseness, cough). The main disadvantage is that, while 30 – 40% of cases show a reduction in seizure frequency of more than 50%, only about 3% of them attain seizure freedom (RYCHLICKI, 2006; SETHI, 2008).

Deep Brain Stimulation (DBS) featuring, for example, 1-10 V, 90 µsec pulse width, 100 – 165 Hz frequency for the treatment of Parkinson's disease has been shown to be safe and effective as evidenced by FDA approval (BLAD, 2007). A 1 min on and 5 min off stimulation paradigm was used during an investigational DBS trial for epilepsy. DBS has also been investigated for the treatment of drug-refractory epilepsy by providing scheduled stimulation (open-loop) via depth electrodes to various sites such as the hippocampus, thalamus, cerebellum, caudate nucleus,

Table 1.2: Comparison of two commercially available neurostimulators for the treatment of epilepsy.

VNS	RNS
FDA approved	Clinical trial
Vagal Nerve Stimulation Cyberonic Inc. Houston, USA	Neuropace RNS-300 Mountain Biew, California, USA
Features: • Battery powered • Stimulate vagus nerve • External remote • Applicable for refractory generalized and focal epilepsy.	**Features**: • Battery powered • Controlled by microcontroller • Store neural signal • Detect signature of seizure onset • Applicable for motor simple partial seizure and complex partial seizure

	Min dose	Max dose		Min dose	Max dose
Stimulation Parameters	0.25 mA 30 Sec ON 3 hr OFF 130 µsec PW	3.5 mA 30 sec ON 5 min OFF 500 µsec PW	Stimulation Parameters	1 mA 40 µsec PW	12 mA 1000 µsec PW
Frequency	0.25 Hz	30 Hz	Frequency	1 Hz	333 Hz

Source: SCHACHTER, 2009; RYCHLICKI, 2006; SETHI, 2008	Source: SKARPAAS, 2009; MORRELL, 2006

centromedian thalamus, anterior thalamic nucleus, and neocortical seizure foci (LEGA, 2009; ZHONG, 2011; CHABARDES, 2002; HANDFORTH, 2006; HODAIE, 2002). Recently, a large and multicenter trial (SANTE: Stimulation of the Anterior Nucleus of the Thalamus for Epilepsy)

was conducted and subsequently with encouraging results, making anterior thalamic nucleus the most well-established target for DBS in the treatment of epilepsy to date (ZHONG, 2011). The mechanism through which DBS affects seizure frequency is yet unknown, the results so far have been modest in the same line as the VNS (FISHER, 2011).

Most of the reported experiments have shown abortion of seizure activity by electrical stimulation, but there is indication that low-frequency stimulation (lower than 10 Hz delivered to either posterior hypothalamus or thalamus) may induce a seizure (OSORIO, 2001). It may very well be that proper stimulation parameters need to be individualized during the presurgical intracerebral EEG study for maximum efficacy prior to the implantation of a closed-loop responsive stimulation device. Many stimulation parameters have shown promising performance. For example, Osorio et al. (2005) used a biphasic, charge-balanced square pulse (100 µsec/phase width, 100 – 500 Hz frequency) for 1 sec. If the stimulation failed to terminate the seizure, the next seizure detection begins within 1 minute. A maximum of five stimulations are allowed to terminate a seizure. More recently, the cranially implanted Responsive Neurostimulator (RNS, closed-loop) system has been proposed for the treatment of refractory epilepsy (MORRELL, 2011). It consists of a programmable, battery-powered microprocessor-controlled device (the RNS neurostimulator) implanted in the cranium, which delivers a short train of electrical pulses to the epileptogenic zone through intracranial electrodes (depth and cortical strip leads) when a seizure onset is detected. An external programmer, laptop computer, wand, and telemetry interface enable communication with the implanted RNS neurostimulator, allowing the physician to modify the parameters of detection and stimulation of RNS through wireless communication. This investigational responsive device is still under clinical trial (MORRELL, 2011; SCHACHTER, 2009; THEODORE, 2004; MORRELL, 2002). Table 1.2 compares the RNS features with those of the VNS.

1.9 CONCLUSION

Drug-resistant epileptic patients may be candidates for non-pharmacological therapies, such as epilepsy surgery and implantable medical device therapies. Unfortunately, currently available commercial intracranial electrodes used to delineate the EZ for surgery or implantable devices for non-operable patients have some limitations. A number of strategies hold promise for improving their effectiveness. Closed-loop implantable responsive systems for the focal treatment of

refractory partial epilepsy are promising therapeutic avenues that show potential for effective treatment with minimal side effects. Novel approaches in direct electrical stimulation, drug delivery, and new subdural electrode design could offer a chance for long-term seizure remission or even cure.

CHAPTER 2   CMOS BASED EPILEPTIC SEIZURE DETECTOR

This chapter concerns implementation of a low-power epileptic seizure detector for the treatment of epilepsy. The design and experimental results of the fabricated seizure detector chip are demonstrated using icEEG recordings from seven refractory epilepsy patients. This seizure detector has low-power consumption, accurate seizure detection, tuneable neural signal amplifier, sophisticated noise reduction techniques, excellent seizure detection sensitivity, higher specificity, and short seizure detection delay. This work published in "IEEE Transactions on Biomedical Circuits and Systems" is reproduced in following pages.

2.1   A NOVEL LOW-POWER IMPLANTABLE EPILEPTIC SEIZURE-ONSET DETECTOR

Muhammad Tariqus Salam[1], Mohamad Sawan[1], and Dang Khoa Nguyen[2]

[1]Polystim Neurotechnologies Laboratory, Polytechnique Montréal, Québec, Canada

[2]Notre-Dame Hospital, Centre Hospitalier de l'Université de Montréal (CHUM), Québec, Canada

Abstract – A novel implantable low-power integrated circuit is proposed for real-time epileptic seizure detection. The presented chip is part of an epilepsy prosthesis device that triggers focal treatment to disrupt seizure progression. The proposed chip integrates a front-end preamplifier, voltage level detectors, digital demodulators and a high-frequency detector. The preamplifier uses a new chopper stabilizer topology that reduces instrumentation low frequency and ripple noises by modulating the signal in the analog domain and demodulating it in the digital domain. Moreover, each voltage level detector consists of an ultra low-power comparator with adjustable threshold voltage. The digitally integrated high-frequency detector is tunable to recognize the high-frequency activities for the unique detection of seizure patterns specific to

each patient. The digitally-controlled circuits perform accurate seizure detection. A mathematical model of the proposed seizure detection algorithm was validated in Matlab and circuits were implemented in a 2 mm^2 chip using CMOS 0.18-µm process. The proposed detector was tested using intracerebral electroencephalography (icEEG) recordings from seven patients with drug-resistant epilepsy. The seizure signals were assessed by the proposed detector and the average seizure detection delay was 13.5 sec, well before the onset of clinical manifestations. The measured total power consumption of the detector is 51 µW.

2.2 INTRODUCTION

Epilepsy is a common medical condition characterized by a predisposition to unprovoked recurrent seizures. A seizure is the manifestation of an abnormal, hypersynchronous discharge of a population of cortical neurons (SPENCER, 2009). Approximately 30% of patients, the majority of which suffer from partial (focal) seizures with or without secondary generalization, are refractory to anticonvulsants. Not all refractory patients are good epilepsy surgery candidates due to an extensive area of epileptogenic zone (EZ), multifocal, inability to localize the EZ, and an EZ overlying eloquent areas (language, primary motor or visual areas) that cannot be resected without permanent sequelae (SPENCER, 2009). As a result, the uncontrolled seizures bring a devastating impact on their quality of life.

Proof-of-concept experiments conducted in animals and humans with epilepsy have demonstrated that focal electrical, thermal, or pharmacological manipulations of the EZ can suppress seizure activity (SCHACHTER, 2009; SALAM, 2010(a); FISHER, 2010; OSORIO, 2005).Over the last few years, there has been growing interest in the development of implantable devices as an adjunctive treatment for patients with refractory partial epilepsy. So far, the vagus nerve stimulator (VNS) is the only Food and Drug Administration (FDA) approved medical device for the treatment of epilepsy. This scheduled (open-loop) stimulation device provides a reduction in seizure frequency; however, the overall effectiveness is modest (SCHACHTER, 2009; SALAM, 2010(a)). A cranially implanted responsive neurostimulator that triggers stimulation only upon detection of a seizure holds the promise of better seizure control, lower systemic, peripheral and central nervous system side effects, as well as lower battery consumption (SCHACHTER, 2009; SALAM, 2010(a); OSORIO, 2005; OSORIO; 2009(a); OSORIO, 2009(b)). Preliminary results on a new responsive device for the treatment of epilepsy (RNS

system, Neuropace Inc.) have been promising (SCHACHTER, 2009). Several issues remain to be addressed, such as the necessity of a reliable seizure detection system that is sensitive enough to detect seizures early on but also specific enough to prevent unwarranted triggering of focal intervention.

The initial steps required for the development of any responsive focal therapy device for epilepsy are the recording of intracerebral electroencephalography (icEEG) followed by the automated detection of seizures. IcEEG recordings are generally performed using subdural strip and/or depth electrode contacts. The recorded icEEG represents synchronous firing of many neurons throughout a region across the diameter of an electrode contact. It is generally characterized by a low-amplitude signal (microvolts) and low-frequency bandwidth. Due to the microvolt-level range, the neural signal must be amplified very carefully before further analysis (e.g. detection, digitization). CMOS technology has relatively poor noise performance and the low-amplitude amplification requires a CMOS amplifier with low input-referred noise (SALAM; 2009(a); SALAM; 2009(a); SALAM; 2010(b); GOSSELIN; 2010(a); GOSSELIN; 2010(b); GOSSELIN; 20o9; GOSSELIN; 2007; GOSSELIN; 2004). However, the restrictions on the power consumption and size of an implantable device limit increasing the biasing current. Therefore, design trade-offs between the biasing current and noise are required to optimize the performance of a device.

The challenges of seizure detection are variability in epileptic seizure onset pattern, signal amplitude and spectral content. Over the past few decades, many seizure detection and prediction algorithms have been proposed (BERDAKH; 2009; ZANDI, 2009; NAGARAJ, 2006; SUKHI, 2005; YADAV, 2009). However, these algorithms are carried out offline using high-performance computers. These types of algorithms cannot be employed in a low-power implantable microchip. More recently, a few implantable integrated seizure detectors have been proposed (SALAM; 2009(a); SALAM; 2009(a); SALAM; 2010(b); RAGHUNATHAN, 2009; VERMA, 2010; PATEL, 2009; BHAVARAJU, 2006; AZIZ, 2006; AZIZ 2007). Earlier design of our seizure detectors (SALAM; 2009(a); SALAM; 2009(a); SALAM; 2010(b)) are based on several detection criteria in different amplitude levels, details will be explained in section II and IV. The detection algorithm presented in (RAGHUNATHAN, 2009) is based on classifying icEEG data into events, and the events are related to a threshold voltage in the icEEG during high frequency discharges at seizure state. Because the detector (RAGHUNATHAN, 2009) relies only on two threshold

voltages (positive and negative), there is a high risk for false positive detections. The support vector seizure detection machine (VERMA, 2010) needs a high number of support vectors in order to define the complex decision boundary between a patient's seizure and non-seizure activity, explaining its high power consumption and cost. Similarly, the detector based on linear discriminant analysis classifier requires higher complexity in digital signal processor (DSP) and application-specific integrated circuit (ASIC) implementation to improve sensitivity and specificity (PATEL, 2009).

In this paper, we present a low-power implantable CMOS integrated seizure onset detector (SOD) for patients with medically intractable epilepsy. The detector is part of an epilepsy prosthesis that triggers focal treatment to disrupt seizure progression. This SOD includes implanted electrodes, a data acquisition system, as well as analog and digital signal processors in order to acquire and process real-time icEEG. The proposed SOD chip uses the specific seizure onset features of a patient in order to detect their progressive increase of low-voltage fast-activity ictal pattern. The system is designed to have tunable parameters, which would allow for trade-off between sensitivity (SXT), false detection (FD) and detection delay (DTD). The tunability of the SOD provides higher accuracy on seizure detection. The adjustable gain of an amplifier can emphasize the amplitude level of interest, and variable threshold voltages of the voltage level detectors (VLD) delimit the detected signal locations and extract the information of frequency as well as progressive increase in amplitude. The SOD chip was tested offline on seven patients with refractory epilepsy. The measured results have shown that the SOD maximizes the SXT and minimizes the FD, which would trade-off for longer the DTD, but prior to first clinical manifestations of the patients. The detection is expected to be reliable in an implantable device without risking false detections of physiological rhythms (e.g. sleep spindles).

The epileptic seizure detection algorithm is described in Section II and the global system in Section III. The proposed circuits and their implementations are the subject of Section IV. Experimental results are presented in Section V, and Conclusions are summarized in the last Section of this paper.

2.3 EPILEPTIC SEIZURE DETECTION ALGORITHM

Partial seizures originate primarily within discretely localized or more widely distributed networks limited to one cerebral hemisphere. They may subsequently generalize as the epileptic discharge spreads contralaterally. Seizure onsets may vary from patient to patient in terms of onset morphology, discharge frequency, focality, and spread pattern. Electrographically, several patterns can be seen at seizure onset such as low-voltage and high-voltage fast activities or rhythmic spiking (SPENCER, 2009). Figure 2-1(a) shows the sudden appearance of the typical low-voltage fast activity recorded from two intracerebral contacts positioned over the EZ, increasing in frequency (Figure 2-1(b)), and amplitude (Figure 2-1(c)). The icEEG is analyzed over the seizure onset (Figure 2-1(a)-(c)) and the SOD detects the high frequency discharge in icEEG, which may suggest an upcoming electroclinical seizure. However, as seen in many icEEG recordings, some of these high frequency discharges (e.g. Figure 2-1(d)) can be very brief (few seconds), remain very focal (without spread), do not evolve in time or frequency, and are clinically silent (electrical seizures). For most patients, it is probably not necessary to target them as 'seizures' warranting
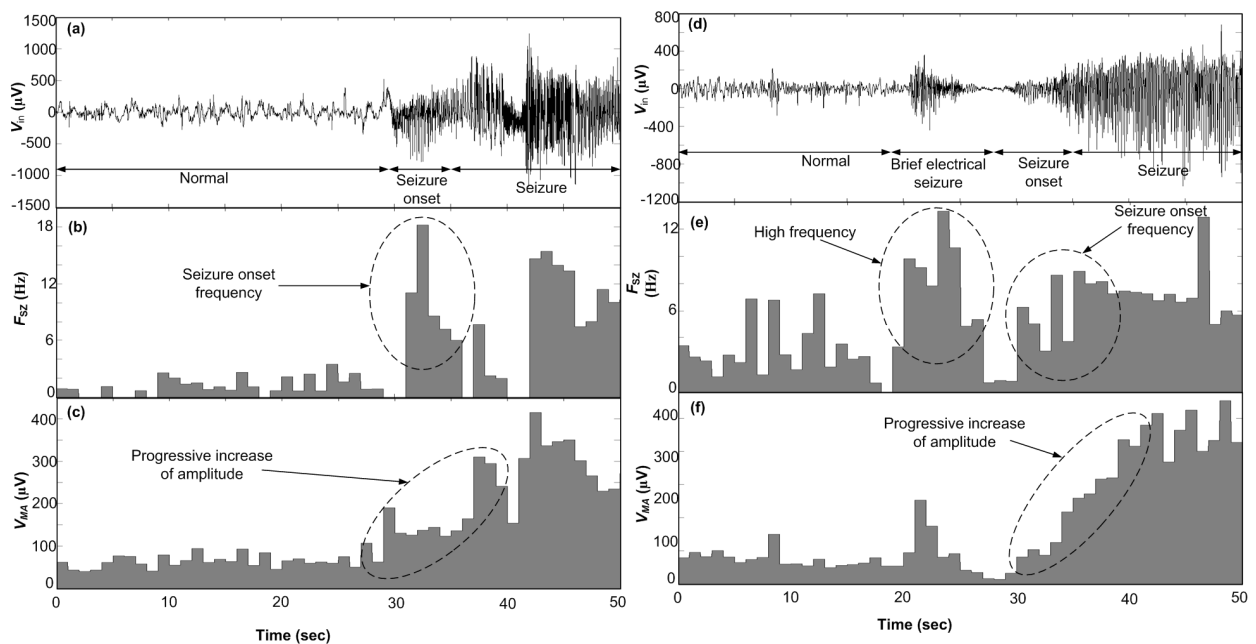
Figure 2-1: IcEEG recordings of two patients with refractory focal epilepsy and signal analyses: (a) Start of seizure activity characterized by low-amplitude fast activity, (b) Frequency analysis (F_{SZ}) of (a), (c) Mean absolute amplitude (V_{MA}) analysis of (a), (d) Seizure activity of second patient with an initial brief electrical seizures (BES) followed by an electroclinical seizure, (e) F_{SZ} of (d), and (f) V_{MA} of (d).

focal treatment, they can simply be ignored. For this reason, the seizure onset detection criteria are preferably set as a high frequency activity (Figure 2-1(b) and (e)) showing progressive increase in amplitude (Figure 2-1(c) and (f)). This should avoid false detections of interictal spikes and polyspikes, movement artifacts, physiological rhythms (e.g. sleep spindles), and brief asymptomatic high frequency voltage activities or very brief electrical seizures which would erroneously trigger unwarranted focal treatment.

The proposed seizure detector is specialized to detect very specific type of seizure characterized by their progressive increase of low voltage fast activity. In this algorithm, the input signal (V_{in} in Figure 2-2 (a)) is modulated into high frequency ($F_s = 1/T_s$) so that the instrumentation's low frequency noise does not affect the signal. Moreover, this modulation (Eq. (2.1)) converts negative signal amplitudes to positive amplitudes (Figure 2-2 (b)). Thus, positive hyper-excited threshold voltages ($V_{i,HET1,2}$) of a voltage level detectors (VLD) are sufficient to detect the high frequency of V_{in}. The discrete modulated signal (V_{mod}) confined to a time frame (T_f) passes through N number of VLDs to detect the specific features (Eq. (2.2)) characterized by progressive increase in amplitude and high-frequency variation. Figure 2-2(c) shows the output of a VLD V_{comi} when it detects fast activities following Eq. (2.2).

$$V_{\mathrm{mod}}(n) = \sum_{n=1}^{\frac{T_f}{T_S}} V_{in}(nT_s)(-1)^n \tag{2.1}$$

where n =1, 2, 3, ..., T_f/T_S
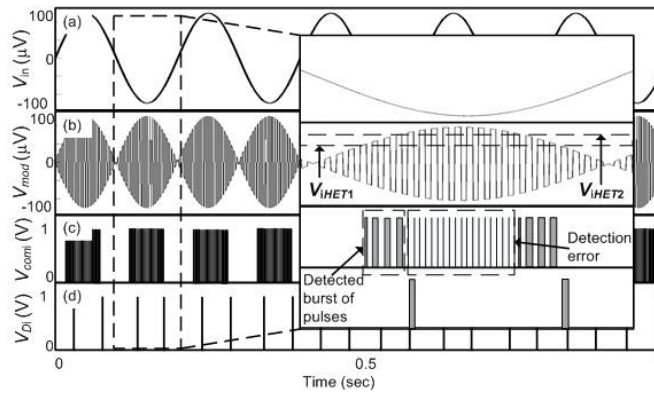
Figure 2-2: Seizure detection algorithm: (a) Input signal V_{in}, (b) Modulated signal of V_{in}, (c) Output of VLDs V_{comi}, and (d) Digital demodulation V_{Di}.

$$V_{comi}(n) = \begin{cases} \text{'1'}, & for \quad V_{i,HET1} > V(n) > V_{i,HET2} \\ \text{'0'}, & for \qquad otherwise \end{cases} \qquad (2.2)$$

where i = 1, 2, 3, ..., N. $V_{i,HET1,2}$ and T_f are tuned to the specific seizure onset frequency (F_Z) of a patient so that no false alarms happen during seizure detection. Due to the modulation, VLDs detect a burst of pulses and unwanted high-frequency samples (Figure 2-2(c)). The following Eq. (2.3) shows the elimination of false positive detections for the unwanted high- frequency samples.

$$V_{SEi}(n) = \begin{cases} \text{'1'}, & for \quad PW \geq T_S \\ \text{'0'}, & for \quad otherwise \end{cases} \qquad (2.3)$$

where PW is the pulse width of $V_{comi}(n)$. The detected burst pulses are converted to a single pulse by Eq. (2.4).

$$V_{Di}(n) = \begin{cases} \text{'1'}, & for \quad V(n-1) = 1 \quad and \quad V(n) = 0 \\ \text{'0'}, & for \qquad otherwise \end{cases} \qquad (2.4)$$

The signal frequency (F_{SZi}) is defined by the total number of identified pulses V_{Di} confined to T_f as follow.

$$F_{SZi} = \frac{\sum_{n=1}^{T_f/T_s} V_{Di}(n)}{T_f} \qquad (2.5)$$

Thus, seizure onset will be declared based on following conditions (Eq. (2.6)).

$$V_{SO}(n) = \begin{cases} \text{'1'}, & Seizure, \quad F_{SZi} > F_Z \\ \text{'0'}, & No \quad Seizure, \quad otherwise \end{cases} \qquad (2.6)$$

The SXT of the algorithm is enhanced, and several decision boundaries are introduced to reduce the number of FDs for the patient's specific seizure onset pattern. Signal analysis of this algorithm demonstrates that the early modulation and proper rectification of icEEG can identify the seizure onset efficiently.

2.4   PROPOSED SYSTEM

The proposed implantable SOD provides continuous long-term monitoring of icEEG from the EZ. Figure 2-3(a) illustrates the implant configuration of the SOD and the functional block diagram of Figure 2-3(b) presents its architecture. The device will be implanted within the skull and interfaced directly with the recording site using standard subdural/depth electrodes
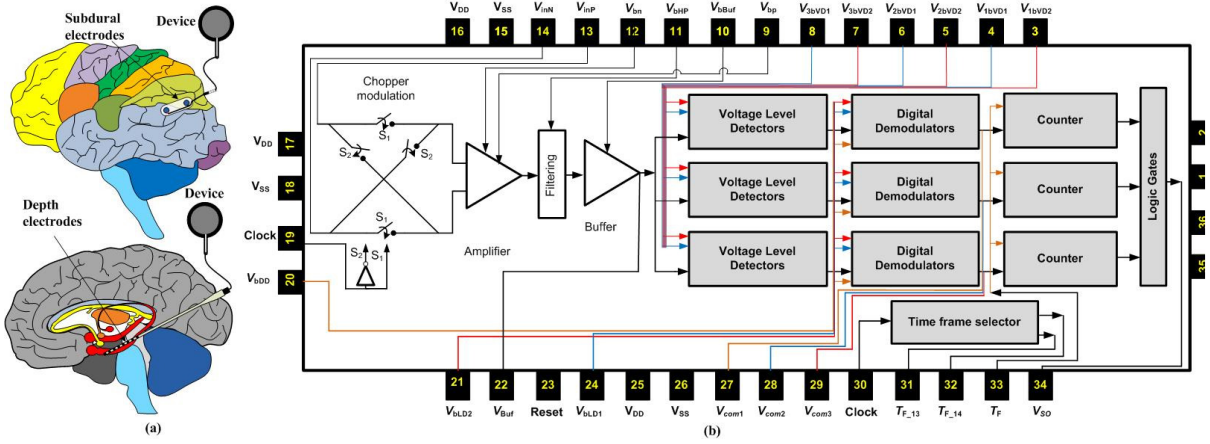
Figure 2-3: The proposed integrated SOD: (a) Implant configuration which shows the devices and two sets of electrodes; the sensing subdural electrodes and depth electrodes, and (b) Block diagram of the proposed SOD chip.

(diameter/size: 5mm and interelectrode spacing: 10 mm). This SOD consists of a preamplifier, voltage level detectors (VLD), digital demodulators (DD) and a high-frequency detector (HFD). In this SOD, several variable parameters (V_{REF}, $V_{i,HET1,2}$ and T_F) are introduced to facilitate higher accuracy in real-time seizure onset detection. V_{REF} controls the amplification of neural signals, $V_{i,HET1,2}$ are used to adjust the threshold voltages of VLDs, and T_F in HFD sets the tunability of the frequency detection. Figure 2-3(b) shows that most of the signal processing in the SOD is accomplished in the digital domain because of the relatively poor noise performance of CMOS technology. The preamplifier initially modulates the neural signal in F_s and amplifies the input amplitude level of interest. Subsequently, the VLDs convert the amplified signal V_{Buf} to a digital signal V_{comi}. Once the signal is digitalized, there is little further possibility to add noises in this signal. Then the V_{comi} is demodulated to the original digital signal V_{Di}. Finally, the HFD determines the seizure onset frequency from processed signals and declares a seizure detection (V_{SO}) without false alarm.

2.5   CIRCUIT IMPLEMENTATION

As illustrated in Figure 2-3, the SOD consists of four main functional blocks. Details are given below.
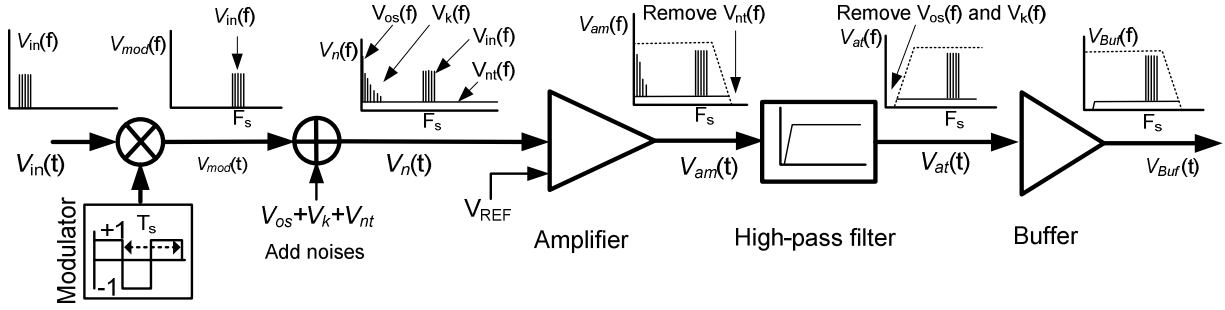
Figure 2-5: The dedicated chopper stabilizer circuit and corresponding frequency analysis of signals in different nodes.

2.5.1 Preamplification

A dedicated chopper preamplification method was introduced in our previous work (SALAM, 2009(a)). Figure 2- 4 shows the block diagram of the preamplifier and the frequency analysis of signals in different nodes. This figure demonstrates that the preamplifier input signal is modulated by a signal with frequency F_s, and the flicker noise V_k and dc-offset voltage noise V_{os} of the amplifier are attenuated by the high-pass filter, while the finite bandwidth of the amplifier and buffer band limits the thermal noise V_{nt}. The proposed preamplifier is advantageous over the conventional chopper preamplifier for the detection of epileptic seizures.

The comparison of the preamplifiers is shown in Table 2.1. Figure 2-5(a) illustrates the preamplifier construction, which comprises an operational transconductance amplifier (OTA) (Figure 2- 5(b)), high-pass filter, and a buffer. These circuits give a band-pass frequency response, which is produced by the preamplifier (Figure 2-5(a)) and the band-pass filter that has a maximum
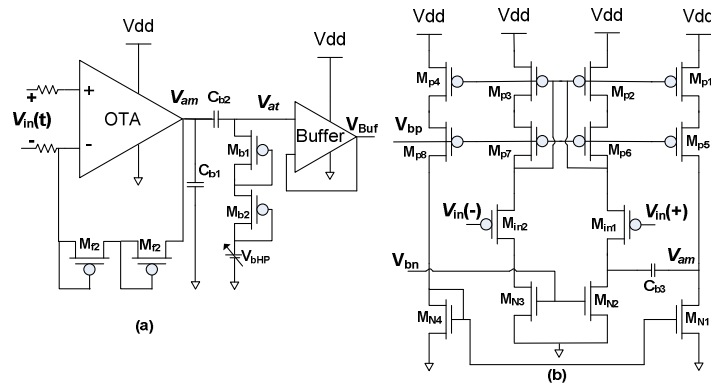
Figure 2-4: Preamplification front-end: (a) Band-pass filter comprising an OTA, a high-pass filter and a buffer, (b) Circuit of the OTA used in preamplifier.

of 80 dB midband gain and 17 kHz (2 kHz to 19 kHz) bandwidth with 6 µVrms input-referred noise. Moreover, the OTA has variable gain that can emphasize a specific amplitude range of the neural signal.

Table 2.1: Comparison of the conventional and the proposed chopper preamplifier.

The preamplifier [15]	The proposed preamplifier
A demodulator adds ripple noise.	No demodulator
A low-pass filter with sharp cutoff frequency consumes extra power.	No low-pass filter is used.
Thermal noise is attenuated by the low-pass filter.	Thermal noise is attenuated by the band limited amplifier.
Flicker noise is shifted to high frequency and attenuated by the low-pass filter.	Flicker noise is attenuated by high-pass filter (a capacitor and 2 PMOS transistors).
Design complexity is high.	Design complexity is low.
Moderate input referred noise.	Lower input referred noise
Medium power consumption (24µW).	Lower power consumption (6µW)

2.5.2 Voltage Level Detector

A VLD consists of comparators, logic gates, DFF and a buffer (Figure 2-6(a) an (b)). A low-power comparator has been reported in (Tangel, 2004) that includes two cascaded CMOS inverters, with the threshold voltage set by the aspect ratios of the transistors. The main disadvantage of this comparator is the fixed threshold voltage in an integrated device. However, a modified version of the comparator (Figure 2-6(c)) provides variable threshold voltages $V_{i,HET1,2}$.

$$V_{i,HET1,2} = \frac{V_{DD} - V_{SGp1} - |V_{tp}| + V_{tn}\sqrt{K_n/K_p}}{1 + \sqrt{K_n/K_p}} \tag{2.7}$$

where V_{tp} and V_{tn} are the threshold voltage of the NMOS and PMOS devices, respectively; V_{SGp1} is the source to gate voltage of Mcp1 transistor; and $K_n = (W/L)_n \mu_n C_{ox}$ and $K_p = (W/L)_p \mu_p C_{ox}$. Eq. (7) shows that V_{SGp1} is the only variable parameter that can adjust the value of V_{HETi} in an integrated circuit. The variation of V_{SGP1} is proportional to the bias voltage $V_{i,bVD1,2}$. The other advantages of the modified comparator are (i) negligible static power consumption, (ii) no hysteresis effect, and (iii) relatively small transistor area.
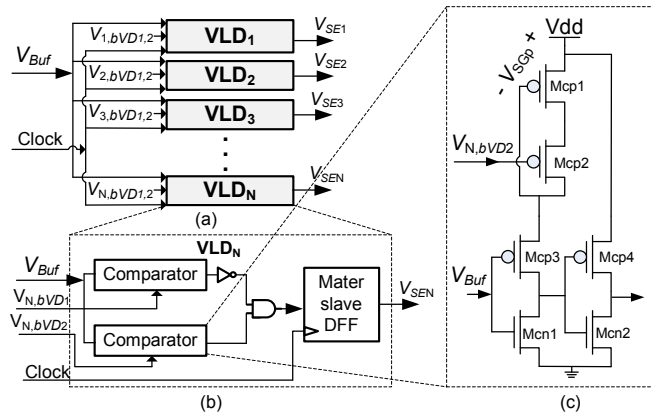
Figure 2-6: Construction of VLDs: (a) Block diagram of VLDs, (b) Schematic of a VLD, and (c) Circuit of a comparator.

In order to construct a VLD, two modified comparators are used. Figure 2-6(a) shows several VLDs; the bias voltages $V_{i,bVD1}$ and $V_{i,bVD2}$ set the variable lower ($V_{i,HET1}$) and upper ($V_{i,HET2}$) threshold voltages, respectively. The DFF circuit removes unnecessary high-frequency samples.

2.5.3 Digital Demodulator

A digital demodulator (DD) includes a RC circuit and a VLD (Figure 2-7(a)) that converts a burst of pulses to a single pulse. During a seizure, the VLD (Figure 2-6) detects the abnormalities in signals and generates several bursts of pulses (V_{SEi}) due to modulation in the preamplification stage. In the DD, each of these input pulses V_{SEi} (Figure 2-7(b)) charges the capacitor (Ceb) quickly, but the discharging time (T_{eb}) of Ceb is longer than the duration (T_E) between two consequent pulses of clock (Figure 2-7(c)). Thus, the Ceb cannot be discharged completely
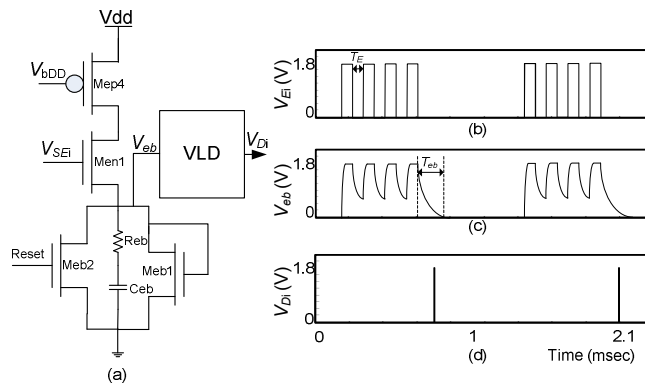
Figure 2-7: The digital demodulator (DD): (a) Circuit, (b) Burst of pulses detected by VLD, (c) Voltage V_{eb} across the RC circuit, and (d) Output V_{Di}.

during a burst of pulses. However, a VLD connected to a RC circuit detects the end of a burst, where the Ceb discharges completely through a diode connection of Meb1 transistor and generates a pulse V_{Di} (Figure 2-7(d)).

2.5.4 High-Frequency Detector

The high-frequency detector (HFD) (Figure 2-7(b)) has two main building blocks: a time frame selector (TFS) and three frequency detectors (FDs). The TFS is based on a 14-bit counter that generates two different time frames T_{f13} (= $2^{13}/F_s$) and T_{f14} (= $2^{14}/F_s$) in 13th and 14th bit, respectively. The FD counts the number of pulses received from the DD (V_{Di}) and resets all FDs at the end of every T_f. Finally, the logic gates analyze the outputs of FD and declare an upcoming seizure (V_{SO}).

2.6   EXPERIMENTAL RESULTS

The SOD was fabricated in a CMOS 0.18-µm process and occupies 2 mm x 1 mm of silicon area. A photograph of the fabricated chip is shown in Figure 2-8.
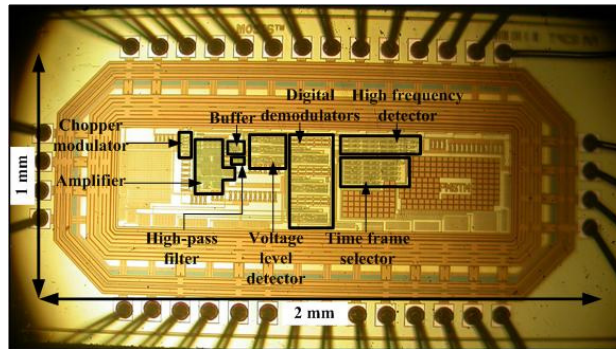
Figure 2-8: Microphotograph of the fabricated SOD chip.

2.6.1 Integrated Circuit Measured Performance

The test bench measurements were performed on five samples of the fabricated chip and presented consistency in results. The test bench supply voltage was set to 1.8 V and the measurements shown in Table 2-2 are based on averages over the set of test chips. The observed measured variation over the test chips was within ±5%.

Table 2.2: Measured features for the fabricated SOD

Block	Parameter		Value
Preamplifier	Midband gain		66 dB
	High-pass cutoff frequency		100 Hz
	Low-pass cutoff frequency		6500 Hz
	Bandwidth		6.1 kHz
VLD	Highest threshold voltage		496 mV
	Lowest threshold voltage		6 mV
	Threshold incremental step		30 mV
HFD	Detectable seizure frequency	Min	5 Hz
		Max	15 Hz
	Time frame T_f	Min	0.5 sec
		Max	163 sec
SOD	Supply voltage		1.8 V
	Supply current		28 µA
	Area (in 0.18µm- CMOS)		2 mm^2

The measured input-output characteristics (Figure 2-9(a)) of the front-end preamplifier show that the variable gain of the preamplifier can emphasize a specific amplitude range of the neural signal.
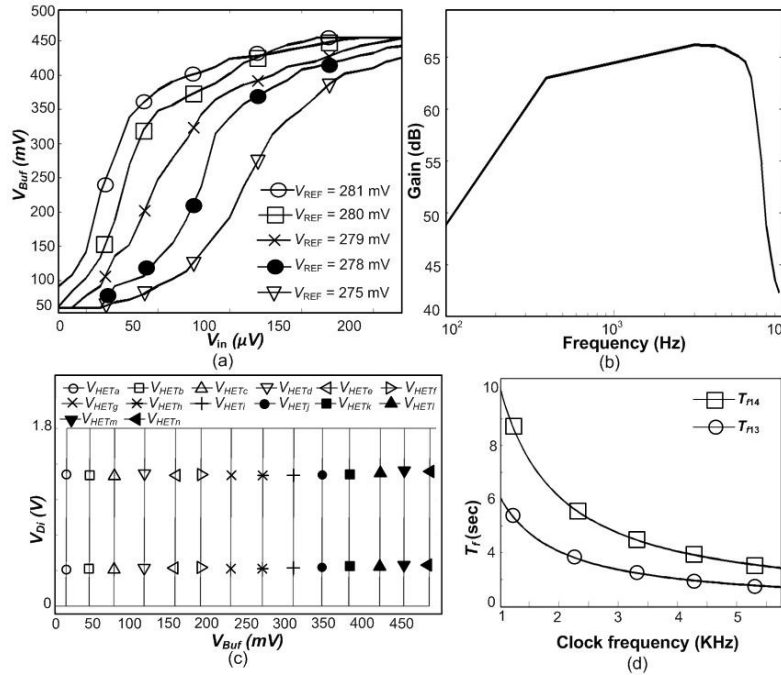
Figure 2-9: Measured results: (a) Variable gain of the preamplification front-end with changing of V_{REF}. (b) Gain response of the front-end preamplifier; (c) Comparator threshold levels; (d) Time frame (T_f) generation.

The preamplifier gain frequency response is shown in Figure 2-9(b). The maximum achieved measured gain of 66 dB was obtained over a 3 kHz to 5 kHz frequency, and the cutoff frequencies were measured at 100 Hz and 6.5 kHz. The output voltage V_{Buf} range is 50 mV to 450 mV while the VLD detects the desired amplitude of V_{Buf} with 30 mV incremental/decremental steps very precisely. Figure 2-9(c) shows the dc sweeping of the modified comparator with different threshold voltages $V_{i,HET1,2}$. Table 2.2 shows the lowest and highest threshold voltages $V_{HETa} = 6$ mV and $V_{HETn} = 495$ mV, respectively. Figure 2-9(d) shows the variable time frames T_{f13} and T_{f14} generated using different clock frequencies. The generated T_f varied from 1.3 to 8 sec.

2.6.2 Patient selection methodology

This study was conducted at Notre-Dame Hospital, Centre Hospitalier de l'Université de Montréal (CHUM). The proposed detector was validated using intracerebral recordings from seven patients with refractory epilepsy who underwent an intracranial study to better delineate the epileptogenic zone. Previously these patients had undergone a comprehensive presurgical evaluation, such as video-scalp EEG, a brain magnetic resonance study (MRI), an ictal single-photon emission computed tomography (SPECT), a positron emission tomography (PET), a magnetoencephalographic (MEG) study, and an EEG-functional MRI (EEG-fMRI). These complementary non-invasive studies failed to adequately localize the epileptogenic zone and invasive intracranial electrode studies were required to delineate with more precision the EZ. In these studies, intracranial electrodes were implanted of through a craniotomy or burr holes under general anaesthesia. Later, patients were transferred to the epilepsy monitoring unit for continuous video-EEG telemetry to record seizures. The patients, who had seizure onsets characterized by progressive increase of low-voltage fast-activity in icEEG recordings, were good candidates for the proposed detection validation.

2.6.3 Method of Case Studies

Seven patients (age: 15 to 49) with intractable nonlesional partial epilepsy who were candidates for epilepsy surgery underwent an intracranial study to better delineate the EZs (Table 2.3). A combination of depth and subdural (strip and/or grid) electrodes were implanted over suspected areas of epileptogenicity (e.g. hippocampus, insula, medial frontal gyrus, orbital frontal cortex etc.) through a craniotomy window or burr holes. Following the implantation of intracranial

electrodes, the patient underwent long-term video-EEG recording in the epilepsy monitoring unit (Notre-Dame Hospital, Montréal). The use of intracerebral recordings from epileptic patients undergoing an invasive study for the validation of our system was approved by the Notre-Dame Hospital ethics committee. Recorded seizures were carefully analyzed to identify the EZ. The EZ, seizure characteristics, and seizure detection results of the 7 patients in this study are listed in Table 2.3. Commercially available equipment was used to record the icEEG signal during a seizure from two contacts located in the EZ. The seizure signals of cases 1, 2, 3, 5 and 6 were recorded using depth electrodes and the signals of cases 4 and 7 were recorded using subdural strip electrodes. These signals were fed into the proposed seizure detection algorithm (Matlab software) and SOD chips. The proposed detector can handle up to two contacts subdural electrodes or depth electrodes. Seizure detections were tested on various seizures from seven patients (average of 5 seizures of each patient) due to the heterogeneity in signal amplitude and

Table 2.3: Case studies of seven patients with partial epilepsy and Matlab Analysis.

Case No.	Age/ sex	Origin	Seizures characterized by	Matlab simulation results					
				$V_{1,HETi}$ (μV)		$V_{2,HETi}$ (μV)		F_{SZ} (Hz)	T_{Det} (sec)
				i=1	i=2	i=1	i=2		
1	24/M	Right hippocampus	Warmth and dizziness, confusion ± GTC[a].	100	160	200	260	12	12
2	49/F	Left hippocampus	Déjà vu, visual flash, and confusion ± GTC[a].	50	100	100	160	8	7
3	41/M	Right amygdala/ hippocampus	Viscerosensory symptoms, and confusion	50	70	100	120	10	10
4	36/M	Left lateral temporal neocortex	Arrest of speech and inability to comprehend ± GTC[a]	100	160	200	260	10	24
5	32/M	Left hippocampus	Left somatosensory symptoms, dizziness, flushing, déjà vu, confusion ± GTC[a]	50	70	100	120	5	12
6	15/M	Right lingual gyrus	Visual flash, déjà vu, nausea, confusion, ± GTC[a].	50	100	100	150	4	25
7	44/M	Left premotor cortex	Right cephalic deviation, confusion, ± GTC[a].	50	70	100	120	10	7

[a]GTC : generalized tonic-clonic seizure

frequencies observed at ictal onset. Parameters of the detector were tuned for each patient based on time frequency and time amplitude analysis of a seizure signal and 3 or 4 brief electrical seizures. The detection performances in terms of DTD (T_{Det}) of both Matlab analysis and the fabricated chip results are presented in the next section.

2.6.4 Validation of the Seizure Detection Algorithm

The proposed seizure detection algorithm is evaluated by applying the recorded icEEG from seven patients. The performance of the algorithm is shown in Table 2.3. Case 1 is a 24 year-old male with drug-resistant partial epilepsy since age 18 years. During the intracranial study, several seizures were recorded, all originating from the right medial temporal lobe (hippocampus) and spreading to the lateral temporal neocortex and the insula (Figure 2-10(a)). The seizure signal is analyzed in time and frequency domains (inset of Figure 2-10(a)) in order to set the $V_{i,HET1}$, $V_{i,HET2}$ and F_{SZ}. The frequency domain demonstrates that the seizures were electrically characterized by an initial low-voltage tonic alpha activity (12 Hz) evolving into rhythmic spiking while amplitude in the time domain increased progressively. Table 2.3 shows that the seizure was detected T_{Det} =12 sec after ictal onset. In case 2, seizures similarly started from the left hippocampus with an initial low-voltage fast activity pattern, before spreading to the left occipital region. The signal analysis (Figure 2-10(b)) shows that the increase of signal frequency and progressive amplitude were found at T_{Det} =7 sec. Case 3 shows a higher signal frequency (20 Hz) at seizure onset (Figure 2-10(c)) that started to decrease with the progressive increase of its amplitude. The seizure of case 3 was detected at T_{Det} =10 sec.

Case 4 had seizures which electrically started as a diffuse slow wave followed by desynchronization and regional low-voltage high-frequency activity over several temporal neocortical contacts (Figure 2-11(a)). The algorithm ignored the brief electrical seizure (as specified by the clinician) and detected the electroclinical seizure after 24 sec. The seizure onset of case 5 was initially characterized by fast-activity without increasing of amplitude (Figure 2-11(b)). The signal frequency then suddenly drops for 2 sec followed by a higher frequency signal and progressive increase in amplitude which are detected (T_{Det} =12 sec). Figure 2-11(c) shows icEEG recordings from case 6 of two brief electrical seizures (ES) followed by an electroclinical seizure that started with low-voltage fast activity quickly increasing in amplitude and decreasing in frequency. Finally, the seizure onset of case 7 was characterized by rapid increase of frequency

(a) Case 1

(b) Case 2

(c) Case 3

[a]T : Medial temporal lobe, [b]G : Frontotemporal lobe, [c]F : Frontal lobe, [d]U : Insula, [e]H : Hippocampus, [f]O : Occipital, and [g]A : Amygdala
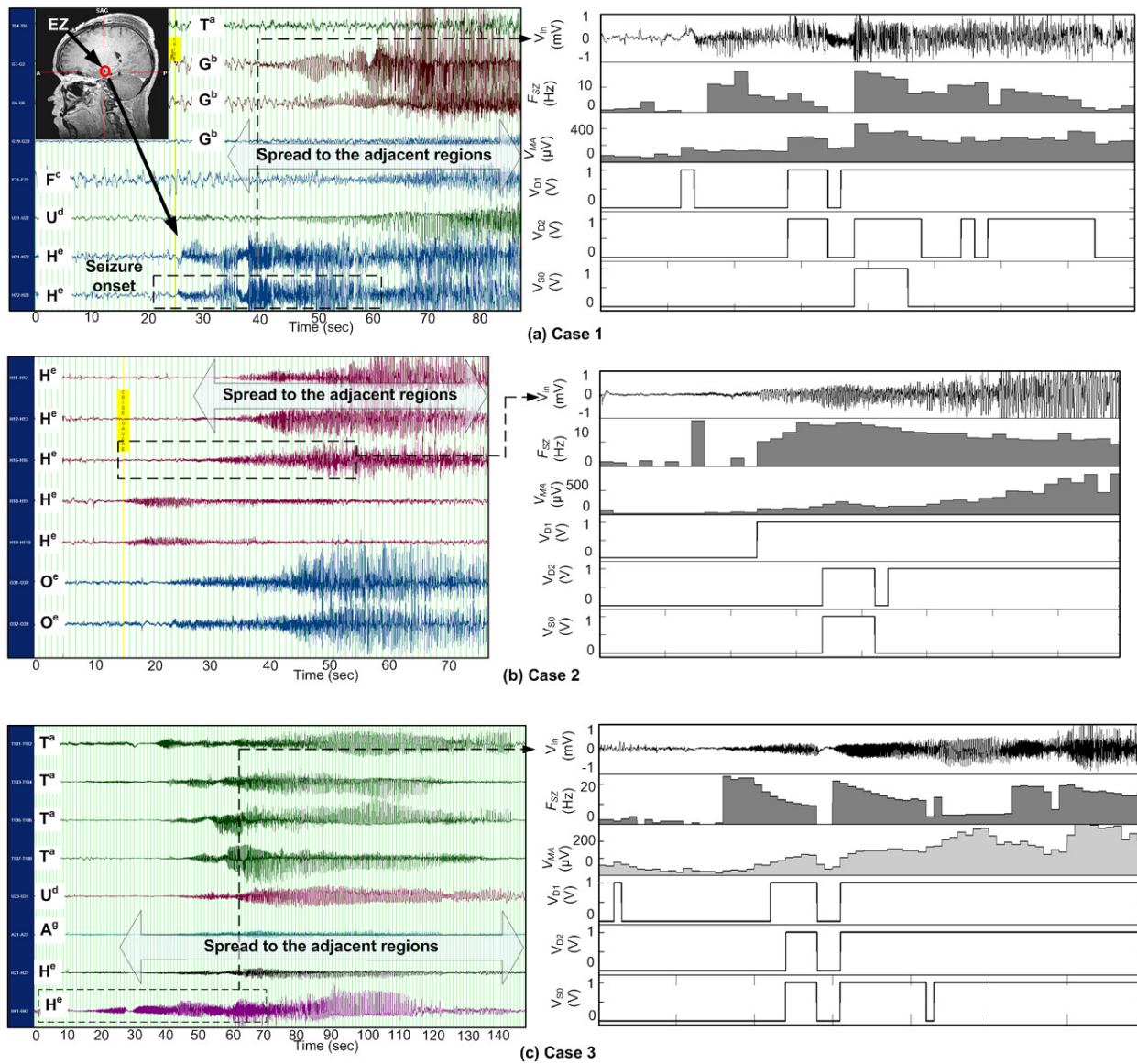
Figure 2-10: Seizure onset detections where icEEGs were recorded from different locations in patients, the zoom inset shows signal analysis and detection: V_{in} is icEEG of seizure recorded using two contacts from the EZ, F_{SZ} is frequency analysis of V_{in}, V_{MA} is mean absolute amplitude analysis of V_{in}, $V_{D1} - V_{D2}$ are high frequency detections, and V_{SO} is seizure onset detection: (a) Case 1, (b) Case 2, and (c) Case 3.
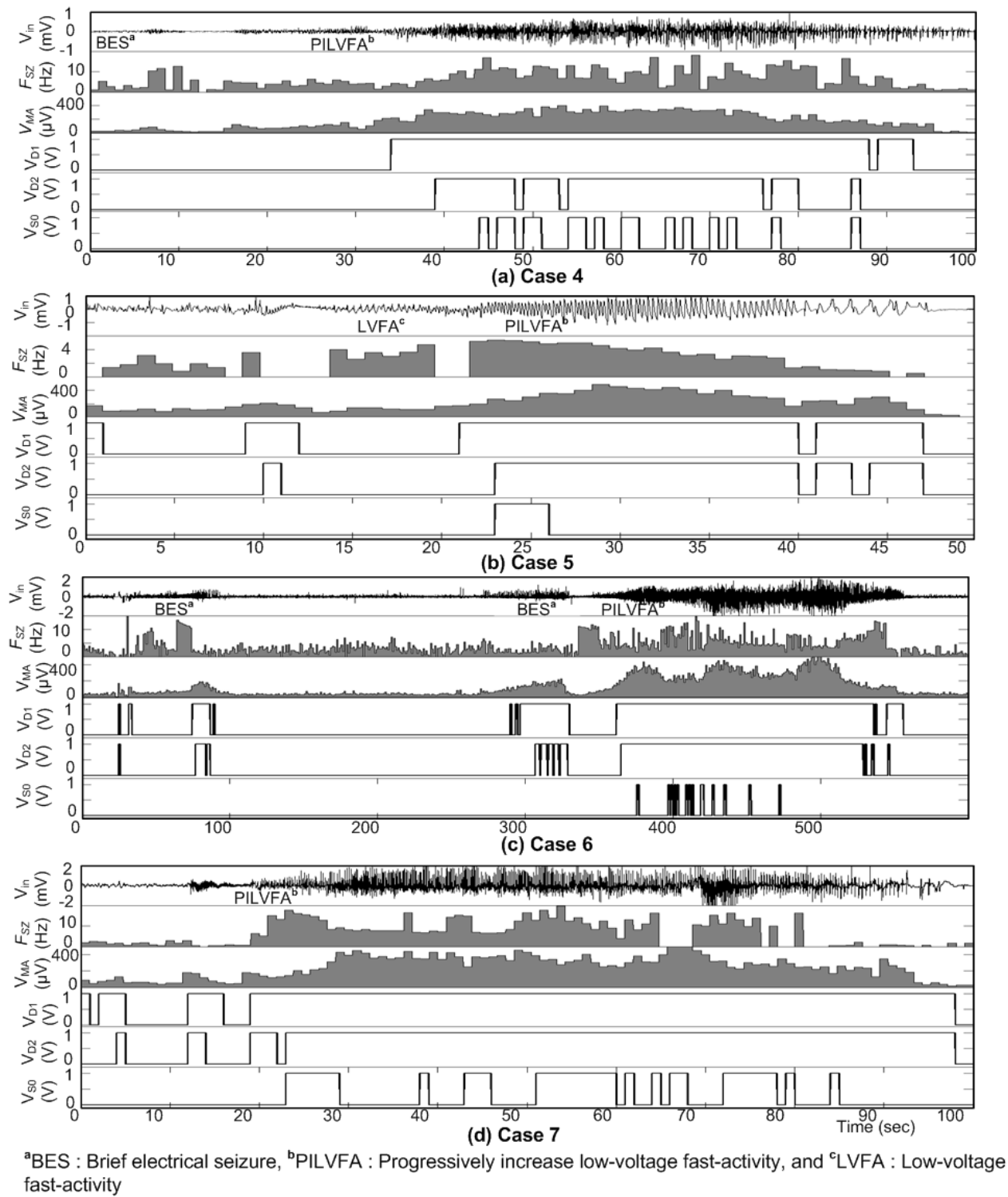
^aBES : Brief electrical seizure, ^bPILVFA : Progressively increase low-voltage fast-activity, and ^cLVFA : Low-voltage fast-activity

Figure 2-11: IcEEG analysis and seizure onset detection using Matlab. The icEEG (V_{in}) of a seizure recorded using two contacts from the EZ, frequency analysis F_{SZ}, mean absolute amplitude analysis V_{MA}, the high frequency detections $V_{D1} - V_{D2}$, and V_{SO} is seizure onset detection: (a) Case 4, (b) Case 5, (c) Case 6, and (d) Case 7.

[a]BES : Brief electrical seizure, [b]PILVFA : Progressively increase low-voltage fast-activity, and [c]LVFA : Low-voltage fast-activity

Figure 2-11: IcEEG analysis and seizure onset detection using Matlab. The icEEG (V_{in}) of a seizure recorded using two contacts from the EZ, frequency analysis F_{SZ}, mean absolute amplitude analysis V_{MA}, the high frequency detections $V_{D1} - V_{D2}$, and V_{SO} is seizure onset detection: (a) Case 4, (b) Case 5, (c) Case 6, and (d) Case 7.

and progressive amplitude increase of the signal (Figure 2-11(d)). Overall, the proposed algorithm maximizes the sensitivity and specificity of the detection, with a slightly longer detection delay as a trade off. In these experiments, the seizures of seven patients were detected on an average of 13.8 sec (min: 7 sec and max: 25 sec) prior to first clinical manifestations.

2.6.5 Validation of the SOD Chip

Following the validation of the seizure detection algorithm in Matlab, the integrated circuit of the SOD was tested using the same seizure recordings from the seven patients mentioned above. The icEEG recordings were modulated, amplified, and analyzed in frequency and time domain in order to set the threshold voltages of two VLDs (Table 2.4). The seizure detection on icEEG recordings (V_{in}) of 3 patients is shown in Figure 2-12. Outputs of the VLDs (V_{D1} and V_{D2}) were fed into a HFD to extract the frequency information (the zoom inset of Figure 2-12). The HFD had three 3-bit counters and a variable T_F generator that detected the seizure onset at an early stage of a seizure. The SOD ignored all the preictal activities (as set by the clinician) and detected the electroclinical seizures of the seven patients ~13.5 sec after onset, well before onset of clinical manifestations (~12 sec prior). Table IV shows the tunable parameters values and the average seizure detection delays of the SOD chips for all cases.

The proposed system is compared with recently published seizure detectors based on events (ESD) (RAGHUNATHAN, 2009), nonlinear Energy (NLESD) (PATEL, 2009), and spectral energy (SESD) (VERMA, 2010) in Table 2.4. The detectors presented in (RAGHUNATHAN,

Table 2.4: The tuneable parameters' values of the SOD chips and average detection delays.

Case No.	V_{REF} (mV)	$V_{1,HETi}$ (μV)		$V_{2,HETi}$(μV)		T_f (sec)	T_{Det} (sec)
		i=1	i=2	i=1	i=2		
1	272	300	320	340	360	2	6
2	275	90	110	120	140	2	12
3	278	100	130	200	230	2.7	15
4	272	300	320	340	360	2	15
5	278	100	130	200	230	2	12
6	275	90	110	120	140	2	20
7	278	100	130	200	230	2	15
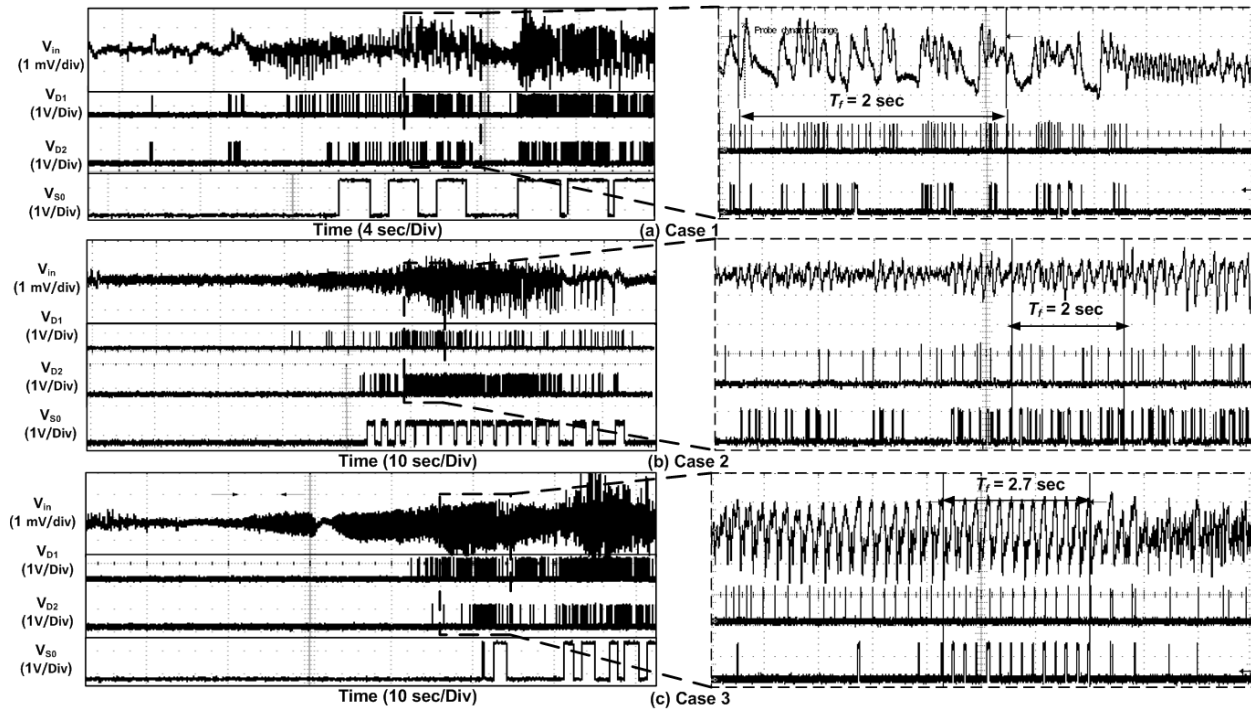
Figure 2-12: Measured seizure onset detection by the SOD chip, where V_{in} is the icEEG of seizure from EZ, $V_{D1} - V_{D2}$ are high frequency detections in the icEEG, and V_{SO} is seizure onset detection: (a) Case 1, (b) Case 2, and (c) Case 3.

2009) and (PATEL, 2009) do not have a neural signal amplifier, and corresponding results are based on circuits simulation. The seizure detector from (VERMA, 2010) was fully integrated in CMOS 0.18-µm technology, but seizure detection results shown are based on software simulation platform using scalp EEG and no experimental results on seizure detection were reported. The proposed detector in this paper is a fully integrated device and the experimental results were based on icEEG recordings from different locations in the human brain. Furthermore, the power consumption of the proposed detector is 7 times lower than one presented in (RAGHUNATHAN, 2009). The DTD is varied depending on the patient's specific ictal onset pattern. Although the average DTD of the proposed SOD is 5 sec higher than the detector described in (RAGHUNATHAN, 2009), the SXT and specificity of the proposed SOD are maximized 100% to prevent unwarranted stimulation; however SXT of ESD (RAGHUNATHAN, 2009), SESD (VERMA, 2010), and NLESD (PATEL, 2009) are 95.3%, 94.35%, and 93%, respectively. The DTD and SXT of other seizure detectors (BHAVARAJU, 2006; AZIZ, 2006; AZIZ, 2007) are unknown.

Table 2.5: Comparison with latest competitive results.

Reference		RAGHUNATHAN, 2009	PATEL, 2009	VERMA, 2010	This work
Electrodes		Depth	Subdural and depth	Ag/AgCl	Subdural and depth
Location		Hippocampus	Frontal, temporal, and parietal lobe	Scalp	Lateral temporal, mesial temporal (amygdala/ hippocampus), frontal lobe
Amplifier		Data acquisition system (TDT system Inc) interfaced to a desktop computer	Neurofile NT digital video EEG system	CMOS 0.18-µm	CMOS 0.18-µm
	Process				
	PC	N/A	N/A	72 µW (measured)	50 µW (measured)
Detector		Simulation on MIT 180 nm SOI process	C5510 DSP processor TSMC 0.13-µm CMOS	CMOS 0.18-µm	CMOS 0.18-µm
	Process				
	PC	350 nW (simulation)	DSP: 80 µW (simulation)	48.1 µW (measured)	44.85 nW (measured)

Further a comparative analysis on seizure detection performance is demonstrated using the same icEEG recordings of seven patients with several detection methods, such as ESD (RAGHUNATHAN, 2009), SESD (VERMA, 2010), and NLESD (PATEL, 2009). Detection parameters of these methods were tuned for each patient according to (RAGHUNATHAN, 2009; VERMA, 2010; PATEL, 2009). These detection methods were validated in Matlab and comparative results of the detection methods using the same data is shown in Figure 2-13. The result shows that the ESD, NLESD and SESD methods have lower SXT because the methods sometimes detected brief high frequency bursts as seizures, but did not detect the seizure onset characterized by low-voltage fast activity. If the detection parameters of ESD, NLESD and SESD methods were adjusted to low-voltage fast activity seizure onset, the methods detected low amplitude physiological rhythms and other similar activity. Therefore, the proposed algorithm is based on the time frequency and time amplitude analysis, and avoids false detections of interictal

spikes and polyspikes, movement artifacts, physiological rhythms (e.g. sleep spindles), and brief asymptomatic high frequency voltage activities or very brief electrical seizures. Average DTD of the proposed SOD is higher than the ones given by the other methods, but well before onset of clinical manifestations. Moreover, the external low-frequency instrumental noise may cause false detection. Thus the proposed algorithm is more focus on noise reduction; however the detection algorithm of RNS system (SCHACHTER, 2009) is intended for data reduction. Furthermore, the detection criteria of RNS system are based on high frequency tracking of amplitude variations in icEEG recording, but the proposed algorithm detects progressive increase of high-frequency signal in icEEG. In addition, total power dissipation and DTD of the RNS system are unknown.
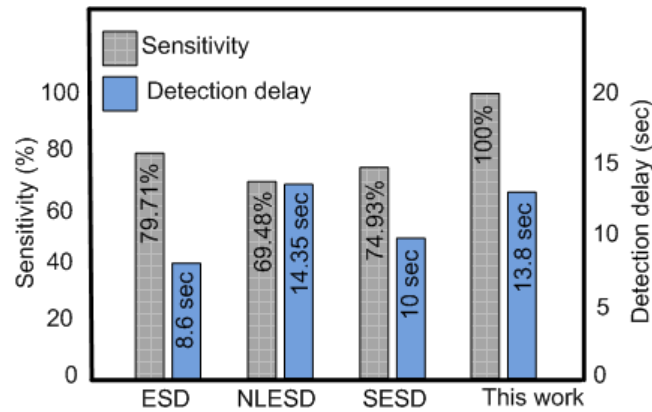
Figure 2-13: Comparative results of analyzing the same icEEG recordings with several detection methods (based on 7 patients).

2.7 CONCLUSION

We have described the design and implementation of a new implantable SOD chip responsive to ictal low-voltage fast activity patterns, focusing on low power and on noise reduction of involved circuits. Experimental results, reported from seven patients with drug-resistant partial epilepsy, demonstrate that the early modulation and proper rectification of icEEG can identify the progressive increase in amplitude and high frequency of signal efficiently. The fabricated SOD chip modulates icEEG recordings, amplifies the desired amplitude level of signal, extracts fast activity information using VLDs, demodulates the signal to extract the original frequency using RC circuit and detects the seizure by evaluating the frequency of fast activities and the progressive increase in amplitude.

2.8   ACKNOWLEDGMENTS

CHAPTER 3   A RESPONSIVE ELECTRICAL STIMULATOR

As mentioned in chapter 1, responsive neurostimulation therapy is a promising alternative for the treatment of epilepsy; we were working towards building a low-power neurostimulator. Chapter 2 has shown the design, fabrication and validation of a seizure detector for a neurostimulator and in this chapter, we present a low-power circuit technique for a responsive electrical stimulator that detects seizure onsets and triggers an electrical stimulation to suppress an upcoming seizure. The simulation and experimental results of the implantable device were demonstrated using icEEG recordings from seven patients with medically refractory epilepsy. This paper will soon appear in "Journal of Low Power Electronics - American Scientific Publishers". This paper is reproduced as follow.

3.1   LOW-POWER CIRCUIT TECHNIQUES FOR EPILEPTIC SEIZURES DETECTION AND SUBSEQUENT NEUROSTIMULATION

Muhammad T. Salam[1], Fayçal Mounaïm[1], Dang K. Nguyen[2], and Mohamad Sawan[1]

[1]Polystim Neurotechnologies Laboratory, Polytechnique Montréal, Québec, Canada

[2]Notre-Dame Hospital, Centre Hospitalier de l'Université de Montréal (CHUM), Québec, Canada

Abstract — In this paper, we present low-power circuit techniques for implementing a closed-loop neurostimulator (CLNS) as an alternative treatment for medically refractory epilepsy. The proposed circuit has low-power dissipation with better detection sensitivity compared to the recently proposed circuit techniques for epileptic seizure detector. We demonstrate low-power circuit techniques for implementation of an implantable CLNS, individual functional testing, and

validation of the seizure detector on real intracerebral EEG (icEEG) recordings and testing of self-triggering electrical stimulation. The CLNS comprises a low-power icEEG acquisition front-end, epileptic seizure detector, and a widely programmable current stimulator. Moreover, the tuneable parameters of the detector and stimulator are designed to adjust wirelessly. The detection algorithm was validated with Matlab tools and the detection circuits were implemented in 2 mm^2 chip area using CMOS 0.18-μm process. The current-mode stimulator was assembled on two circular (Ø 20mm) shape blocks in a printed circuit board (PCB). The proposed CLNS was tested using icEEG recordings from seven patients with medically refractory epilepsy. The icEEG recordings were assessed by the proposed CLNS (offline) and the predefined seizure suppression biphasic electrical stimulations were triggered ~14.4 sec after electrographical seizure onsets.

Keywords — Low-power, Implantable device, Seizure detector, Electrical stimulator, CMOS, FPGA.

3.2   INTRODUCTION

The growing demand for low power dissipation has been driven by implantable battery-powered therapeutic systems that demand ever-increasing functionality and battery life. The implantable medical devices have been widely used to restore neurological disorders including Parkinson's disease, epilepsy, urinary bladder dysfunctions, and restoration of vision. Epilepsy is the second most common neurological disorder, affecting ~50 million people worldwide. Antiepileptic drugs are the mainstay of epilepsy treatment. Though close to two- thirds of patients are controlled by oral medications, many report side effects and the rest continue to suffer from disabling seizures (SALAM, 2010(a); SCHACHTER, 2009). Epilepsy surgery may be an option in the presence of a well delineated epileptogenic zone (EZ) located in an area that can be resected without harm (SALAM, 2010(a); JEROME, 2009, SPENCER, 2009). For those with a poorly defined epileptic focus, multifocal epilepsy, an EZ located in a highly functional/non-resectable area or those with persisting seizures despite attempted resective surgery, additional therapeutic options are needed.

Proof-of-concept experiments conducted in animals and humans have demonstrated the safety of successful chronic electrical stimulation for the treatment of epilepsy (KOSSOFF, 2004; SKARPAAS, 2009; NIRO, 2007). At first, the Vagus nerve stimulator was introduced for adjunctive treatment of patients with partial seizures with or without secondary generalization or generalized seizures that are refractory to antiepileptic medications (approved in 1997 by FDA) (REESE, 2009; SETHI, 2008). Efficacy of this scheduled (open-loop) stimulation device is, however, limited to a 3% rate of seizure-freedom and a 30-40% responder rate (i.e. showing more than 50% reduction in seizure frequency) (REESE, 2009; SETHI, 2008; RYCHLICKI, 2006). A more recent approach has been to look at closed-loop stimulation triggered upon detection of an electrographic seizure onset (REESE, 2009; SETHI, 2008). The RNS system (Neuropace Inc.) is a cranially implanted responsive neurostimulator designed to detect seizure activity in the brain and to deliver predefined electrical stimulation to suppress seizures before any seizure symptoms appear (SKARPAAS, 2009). A recent pivotal randomized double-blind sham stimulation controlled trial assessing the efficacy and safety of the RNS system showed moderate reduction in seizure frequency in patients with refractory partial onset epilepsy originating from one or two locations in the brain (SKARPAAS, 2009). Closed-loop stimulation (KOSSOFF, 2004; SKARPAAS, 2009; OSORIO, 2005; OSORIO, 2009) has some potential advantages over the open-loop method (REESE, 2009; SETHI, 2008; RYCHLICKI, 2006; FISHER, 2010): (i) lower number of treatments; (ii) fewer stimulation-related adverse events, (iii) high efficiency due to rapid access; and (iv) ability to review recordings to monitor seizure frequency. Any closed-loop system relies upon accurate seizure onset detection (without false alarms).

In the last decade, many mathematical models have been developed for seizure detection based on wavelet (BERDAKH, 2009), entropy-based approach (ZANDI, 2009), spectral feature extraction (Sukhi, 2005), and spectral instability (AKSENOVA, 2007). These models were developed using desktop computers for off-time data processing and cannot be employed in a low-power implantable microchip due to the heavy computation. However, several seizure detection algorithms have been proposed for low-power implantable device and hardware implementations have been shown feasible using CMOS 0.18-µm (SALAM, 2009(b), VERMA, 2010; SALAM, 2010(c); SALAM, 2010(f)), MIT 180 nm SOI (RAGHUNATHAN, 2010), and CMOS 0.13-µm (PATEL, 2009) process. These types of implementation in custom integrated circuits are sensitive enough to detect seizures early on but also specific enough to prevent

unwarrantedly triggered focal intervention. Therefore, the seizure detectors need complicated functionalities which result in higher power consumption. Power management is an important issue for medical devices. Although rechargeable wireless batteries may partially solve the problem, it is important to improve the implantable devices with new features/system design to minimize power dissipation while optimizing their performance.

Apart from the seizure detection performance, the other concerns are safety of chronic electrical stimulation and the determination of optimal stimulation parameters. Table 3.1 shows the parameters used in pilot trials. Osorio, demonstrated the feasibility and short-term safety of automated high-frequency electrical stimulation (100 – 500 Hz) in blocking seizures using an external prototype (OSORIO, 2005). Moreover, many promising advances have been made in the understanding of electrical stimulation parameters and locations of stimulation (KOSSOFF, 2004;

Table 3.1: Biphasic stimulation parameters

Stimulation	Location	Stimulation parameters		
		Frequency	On	Off
OLNS (FISHER, 2010)	ATN	145 Hz	1 min	5 min
CLNS (OSORIO, 2005)	EZ	100-500 Hz	1 sec	1 min
	ATN	100-200 Hz	2.5 sec	1 min

OLS: Open loop neurostimulation, CLNS: Closed-loop neurostimulation,
ATN: Anterior thalamic nucleus, and EZ: Epileptogenic zones

SKARPAAS, 2009; REESE, 2009; FISHER, 2010). Several low-power miniaturization implantable electrical stimulators have been reported for Urinary bladder dysfunctions (MOUNAIM, 2007; MOUNAIM, 2011; SAWAN, 2008) and restoration of vision (COULOMBE, 2007; SAWAN, 2005; NADEAU, 2006). However, several issues remain to be addressed for the electrical brain stimulation treatment for epilepsy, such as maximum charge density, stimulation mode, current distribution, shunting of injected current, impedance of cerebral tissue, and the region affected by stimulation.

In this paper, we present low-power circuit techniques for implementing responsive neurostimulator for the treatment of refractory partial onset epilepsy. This prosthetic device analyzes the intracerebral EEG (icEEG) recording, detects electrographic seizures at their onset,

and triggers focal electrical stimulation to the EZ (or a chosen target such as the anterior thalamic nucleus) to abort the seizure. The device comprises intracranial electrode contacts, the icEEG acquisition front-end, a seizure detector, and an electrical stimulator. The proposed seizure detection algorithm has enhanced sensitivity of detection for the patient-specific seizure pattern, while minimize power dissipation. Moreover, the algorithm reduces instrumentational low-frequency noises by manipulating the icEEG recording into high frequency and demodulating the signal to the original frequency band in the digital domain. The widely programmable electrical stimulator is suitable for the treatment of refractory epilepsy. The performance of the proposed CLNS is verified using icEEG recordings from seven patients with refractory partial epilepsy. The measured results of CLNS demonstrate the reliability of the system in an implantable device for neurostimulation therapies.

3.3   METHOD OF TREATMENT

The proposed CLNS is designed to deliver high frequency electrical stimulation (100 – 500 Hz) directly to the EZ at seizure onset prior to clinical manifestation. The CLNS is dedicated to the treatment of refractory partial epilepsy. The CLNS will be implanted within the skull and interfaced directly with the recording/stimulation sites (Figure 3-1(a)). The CLNS comprises subdural or depth electrodes, a seizure detector (SD) and an electrical stimulator (ES). Figure 3-1
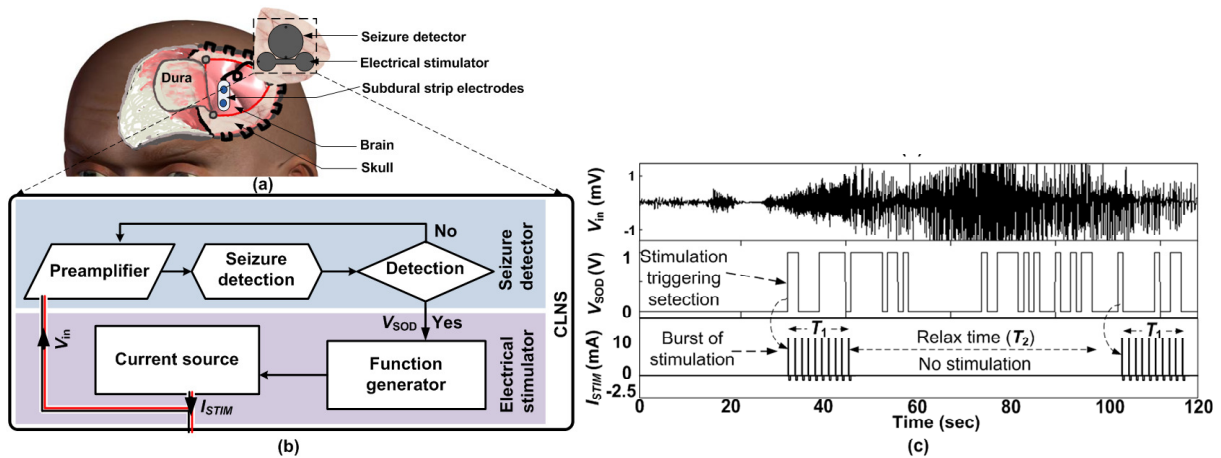
Figure 3-1: Overview of method of treatment: (a) proposed CLNS interfaces directly to the part of brain through subdural electrodes; (b) flow chart of CLNS; and (c) graphic representation of automatic triggering neurostimulation, where V_{in} is icEEG of seizure from epileptogenic zone, V_{SOD} is seizure onset detection, and I_{STIM} is bipolar biphasic electrical stimulation.

(b) illustrates the functional block diagram and flowchart of the CLNS. The corresponding graphic representation in Figure 3-1(c) demonstrates the real-time icEEG recording (V_{in}) acquisition, seizure detection (V_{SOD}) at their onset, and triggering of direct electrical stimulation (I_{STIM}) for T_1 period to the EZ to abort the seizure, while another seizure detection begins after T_2, if the seizure does not terminate. The SD and ES have different tuneable parameters designed to detect patient-specific seizure onset patterns and provide individualized effective bipolar biphasic stimulation to the brain tissue in order to disrupt seizures. The SD requires low-power, continuous, long-term icEEG monitoring to identify seizures online before the appearance of disabling clinical manifestations (e.g. altered consciousness, tonic or clonic movements). On the other hand, ES remains in sleep mode, unless SD triggers it to active (stimulation) mode.

After the implant procedure, patients need to have follow-up visits with the clinician to program the CLNS. The clinician uses external controller to program the CLNS. This programming session sets the optimal detection and stimulation parameters to best manage patient's seizures while minimizing side effects. Battery life of CLNS can vary depending upon the programmed stimulation parameters (e.g. amplitude, frequency, pulse width) and number of seizure detection. However, this battery can be recharged wirelessly through the skin; moreover, it will be automatically recharged during the programming session. The frequency of these follow-ups depends on the medical background of the patients and the individual circumstances.

3.3.1 Low-power accurate seizure detector design

The proposed seizure detector performs real-time icEEG analysis, of which output triggers a burst of electrical stimulation. This epileptic seizure detector is designed for lower power dissipation and instrumentational low-frequency noises isolation (e.g. flicker noise, dc offset voltage, and thermal noise) and also other sources of noise (e.g. 60 Hz noise). Mathematical model of the proposed seizure detector was introduced in our previous work (SALAM, 2008(b)) and here, we present a brief description of the model, and advantages and disadvantages of the model for real-time neurostimulation applications.

In this mathematical model, high sampling frequency modulates the input signal amplitude and passes through amplitude detectors with different threshold voltages to detect the specific features characterized by progressive amplitude increase. The detected amplitudes confined in a time frame pass through frequency analyzers for time-frequency analysis. Therefore, the algorithm determines

the high frequency as well as progressive increases in amplitude and declares an upcoming seizure.

The input icEEG is modulated into high frequency (F_s) for two reasons: (i) instrumentation low-frequency noise does not affect the seizure detection performance and (ii) the amplitude modulation converts negative signal amplitudes to positive amplitudes, thus, amplitude detectors are required only in positive comparators for time-amplitude analysis. Signal processing and demodulation are done in digital domain to reduce power dissipation and avoid addition ripple noise generated from a classical chopper preamplifier (GOSSELIN, 2004). Finally, an upcoming seizure is declared without influence of internal and external noises, if the filters and detection settings are adjusted correctly; otherwise high frequency sampling noise degrades the detection performance.

Apart from the noise effects in the seizure detection, there are others biological impacts that may degrade seizure detection performance. Clinically, seizures may be electrical (especially if they occur in non-eloquent cortex and remain very focal) or electroclinical (when the ictal discharge involves/propagates to a symptomatic zone). Seizure symptoms are obviously dependent on what area of the brain is involved and may range from subtle sensations to overt convulsions. Electrographically, there are several seizure onset patterns which can be seen in icEEG recording, such as low-voltage fast-activity, high-voltage fast-activity or rhythmic spiking (SPENCER, 2009). The proposed algorithm is designed to detect electroclinical seizures starting with low-voltage fast-activity, the most frequently encountered ictal pattern.

The ictal discharges generally contain high frequency components; however, not all high frequency discharges are seizures, as some are physiological rhythms. Therefore, the high frequency filtering from icEEG is not a sufficient criterion for detecting an epileptic seizure onset. Thus, the proposed detection algorithm incorporates both time-frequency and time-amplitude analysis of icEEG recordings. Figure 3-2 (a)-(c) show time-frequency F_{SZ} and time-amplitude V_{MA} (mean absolute) analysis of different icEEG recordings of a patient to demonstrate the seizure detection criteria.

The signal analysis of normal icEEG recordings V_{in} shows no abnormalities in F_{SZ} and V_{MA} (Figure 3-2(a)). A brief electrical seizure (BES) in V_{in} (Figure 3-2(b)) has high frequency contents in F_{SZ}, but it does not have progressive amplitude increase in V_{MA} and stay for a short period (e.g.

4/5 sec). However, the signal analysis of V_{in} at seizure onset (Figure 3-2(c)) demonstrates a sudden increase in F_{SZ} and progressive amplitude increase in V_{MA} (Figure 3-2(c)) leading to clinical manifestations. Therefore, the seizure detector proposes two detection criteria: patient-specific high frequency activity and progressive amplitude increase. Because the initial ictal electrical pattern may vary from patient to patient according to the underlying substrate, the type of intracerebral electrodes used, and their locations with respect to the EZ, the seizure detector has
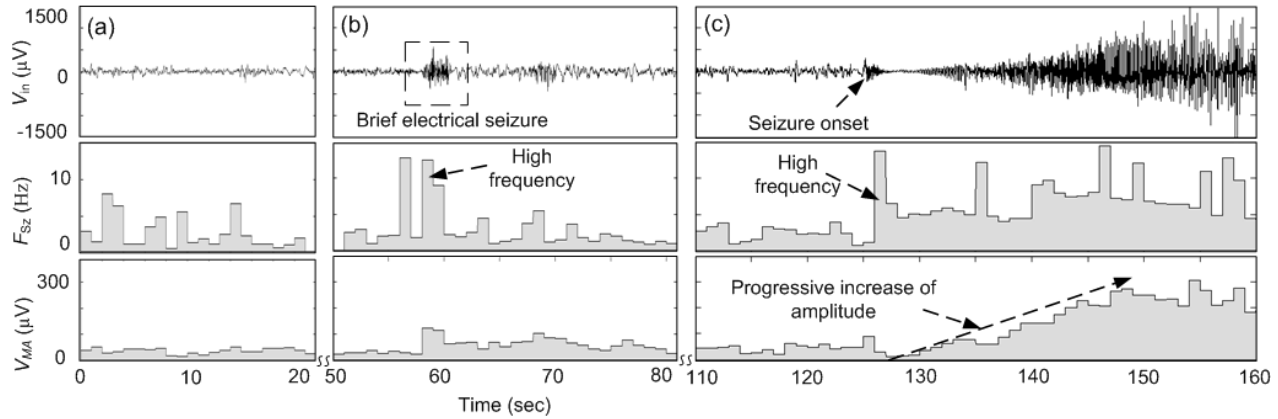
Figure 3-2: Time-frequency (F_{SZ}) and time-amplitude (V_{MA}) analysis of icEEG recording (V_{in}) in (a) normal signal, (b) BES, and (c) electroclinical seizure.

several adjustable parameters for optimizing sensitivity and specificity. Further details of the parameters are described in section 3.3.

3.3.2 Stimulation parameters

Chronic cortical electrical stimulation for the treatment of neurological conditions has been shown to be feasible, safe, tolerable and efficacious in humans (KOSSOFF, 2004; SKARPAAS, 2009; NIRO, 2007). There are two modes for the electrical stimulation: bipolar and unipolar stimulation. The unipolar mode tends to stimulate a wider region while the bipolar mode is effective in producing localized current flows (NATHAN, 1993). Moreover, electrode-tissue impedance varies over the time and a voltage controlled stimulator cannot stimulate the brain tissue with a fix current. Therefore, current controlled stimulation is always preferable because of Ohm's law and safety purpose. The current stimulator can deliver the desired quantity of charges into the brain tissue by keeping the current amplitude constant. Furthermore, charge-balanced asymmetric current biphasic stimulation (Figure 3-3(a)) can avoid damaging electrochemical

processes of the brain because the anodic pulse (I_{STIM1}) of the biphasic stimulation (Figure 3-3(a)) activates the neurons and the cathodic pulse ($I_{STIM2}=I_{STIM1}/4$) removes the delivered charges of I_{STIM1}. However, two subsequent opposite pulses could prevent the generation of an action potential. Thus, a short time delay (T_4) between the pulses is required to propagate the action potential away from the stimulation site before removing the injected charge. It is generally agreed that limiting the maximum charge density (σ_{MAX}) to 60 µC/cm^2 per phase can avoid tissue damage (SKARPAAS, 2009). Figure 3-3(b) illustrates the electrical brain stimulation safe region using standard subdural electrodes (diameter: 5mm and interelectrode spacing: 10 mm). The safety region is defined by Eq. (3.1).

$$I_{STIM} = \frac{\sigma_{MAX} \; A}{T_4} \tag{3.1}$$

where T_4 is pulse width, A is area of the electrode and I_{STIM} is injected current to brain tissue. During the biphasic stimulation using bipolar subdural electrodes, there is significant shunting of
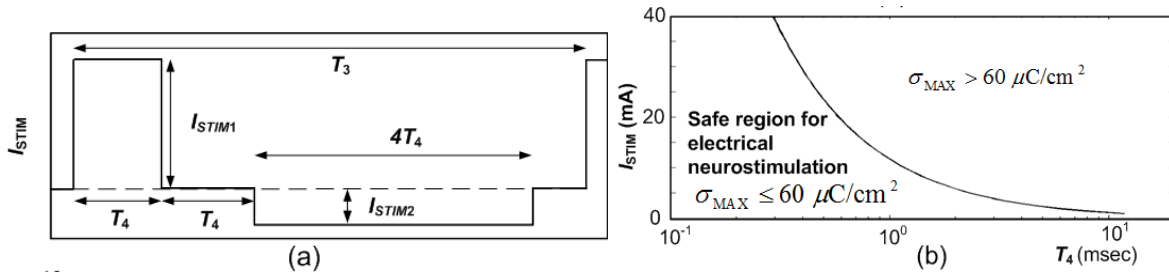
Figure 3-3: Biphasic stimulation parameters: (a) stimulation waveform profile; and (b) limitation of maximum pulse width with injected current of biphasic stimulation.

current through the cerebrospinal fluid (CSF) because of higher (approximately four times) current density in CSF than the gray matter (NATHAN, 1993). Therefore, the proposed CLNS has a wide range of output current I_{STIM}.

The proper stimulation parameters need to be individualized during the presurgical icEEG study for maximum efficacy prior to the implantation of a stimulation device. The stimulation is delivered at close proximity to the seizure onset, directly to (i) EZ by subdural electrodes, which is suitable for patients with one or two discrete EZ (SKARPAAS, 2009; OSORIO, 2005); or (ii) the anterior thalamic nucleus (ATN) by way of depth electrodes, which may be suitable for patients with large or more than two EZ (FISHER, 2010). Further details are described below.

3.4   LOW POWER SYSTEM DESIGN METHODOLOGY

Figure 3-4 illustrates the architecture of the CLNS. The proposed CLNS features advance icEEG monitoring and neurostimulation technology. We achieve low-power design goal in the closed-loop system by using power gating strategy. In the CLNS, SD provides continuous long-term monitoring of icEEG and ES delivers electrical stimulation in response to seizure detection. Thus, long-term energy dissipation in CLNS is dominated by SD. The field programmable gate array (FPGA) embedded ES stays in sleep mode and shuts down output stage, unless SD triggers it to active mode. The SD comprises two main blocks: detection core and controller of SD. Details of the CLNS are described below.
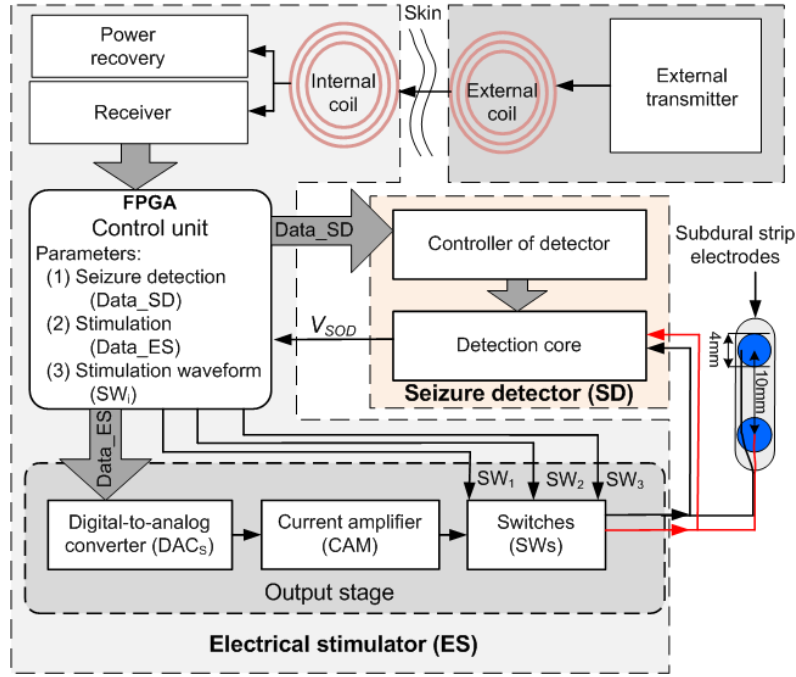
Figure 3-4: Block diagram of the proposed CLNS.

3.4.1   Seizure detector

A new seizure detector chip was introduced and measurements of the chip have been reported in our previous work (SALAM, 2010(f)). However, in this paper, the detector chip was integrated in a closed-loop system that monitor continuous long-term icEEG recording, adjust detection and stimulation parameters wirelessly, and able to trigger electrical stimulation on seizure detection. The detection core is responsible for icEEG acquisition front-end and epileptic seizure detection,

while the controller adjusts tuneable parameters of the detection core in order to optimize the sensitivity of detection (Figure 3-4). As mentioned before, the epileptic seizure detection criteria may vary from patient to patient and detection criteria for a patient may change from time to time. Thus, the controller is introduced in SD so that a clinician can always modify the criteria through wireless communication.

3.4.1.1 Low-power detection core design

The classical chopper preamplifier (GOSSELIN, 2004) is widely used for icEEG acquisition front-end. Figure 3-5(a) illustrates schematic diagram of a traditional detection core based on the classic preamplifier. The traditional system consumed 24.06μW. To improve power management technique, a new chopper preamplification method was integrated with the detection system (Figure 3-2(b)). The demodulator and low-pass filter of a classical chopper preamplifier (Figure 3-2(a)) were replaced by a rectifier and a digital demodulator (Figure 3-2(b)) to reduce addition noise (e.g. ripple noise) by demodulator and extra power consumption by a low-pass filter with sharp cutoff frequency. Moreover, the traditional design required four amplitude detectors (ADs) (positive and negative comparators) and four frequency detectors (FDs) to determine progressively increase low voltage fast activity in icEEG (figure 3-5(a)). But amplitude modulation in the low-power design converts the negative amplitude signal information into positive amplitudes. Therefore, two ADs (only positive comparators) and two FDs are required to determine an upcoming seizure (figure 3-5(b)).
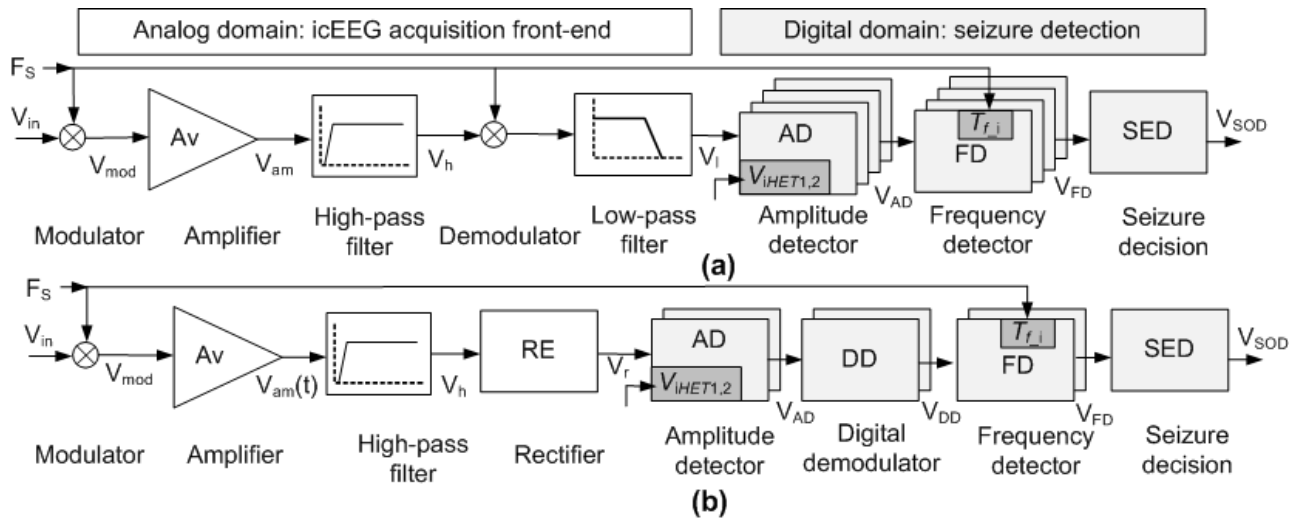
Figure 3-5: Schematic diagram of the detection core: (a) detection core based on the classic chopper preamplifier and (b) low-power detection core.

Table 3.2 show the comparison between a traditional and low-power detection core. Overall, the new preamplifier (Figure 3-5(b)) has lower power consumption (6.70 µW) and improved input-referred noise (6 µVrms) in 17 kHz (2 kHz to 19 kHz) bandwidth. The amplified modulated signal rectified the negative side of signal and passed through two ADs with variable threshold voltages $V_{iHET1,2}$. The digital demodulator translated the signal back to baseband and later, the FDs detected seizure frequency by measuring fast activities in time frame T_{f_i}. The T_{f_i} and $V_{iHET1,2}$ can be tuned to the specific seizure onset frequency of a patient so that no false alarms occur during signal monitoring.

Table 3.2: Comparison on simulated power consumption (PC) of traditional and low-power detection cores

Block	Power consumption (W)	
	Traditional	Low-power
Acquisition front-end	24 µ	6.70 µ
Amplitude detector	22.8n	11.4n
Frequency detector	25.2n	12.6n
Digital demodulator	0	12.6n
Seizure decision	10.96n	5.48n
Total system	24.06µ	6.74 µ

3.4.1.2 Controller of detector

The detection core has several tuneable parameters that are personalized in a specific manner to prevent false seizure detections. The controller of detector (Figure 3-4) provides digitally-controlled high precision signal to adjust SD. The controller comprises digital-to-analog converter ($DAC_{D,i}$), buffers ($BF_{D,i}$), and oscillator (OLT_1). Figure 3-4 shows that the controller receives 48 bits serial input Data_SD to adjust 6 tuneable parameters (6 x 8 bit) of the detection core.

3.4.2 Electrical stimulator

The ES has two operating modes: sleep and active mode. During the icEEG monitoring period, the ES stays in sleep mode to improve power management techniques. The detection signal of SD (V_{SOD}) interrupts control unit to active mode and generates predefined stimulation waveforms (Figure 3-6). Figure 4 shows that the entire ES is partitioned into several parts. Control unit of the ES reduces the switching on clock networks and saves power consumption. Optimization of the

clock routing power allows to enable those portions of the clock network that are required to feed downstream registers. Furthermore, power is reduced by gating clocks when they are not needed. Moreover, discrete components of the output stage have shutdown mode that reduce further power dissipation. The output stage maintains constant current amplitude and delivers a burst of electrical stimulations to the brain tissue. A miniaturized ES with wireless system was introduced in our previous work for dysfunctions of the lower urinary tract (MOUNAIM, 2007). In this paper, internal structure of the ES has been modified to adapt in the CLNS and the ranges of stimulation parameters of ES were changed to Table 3.1 for the treatment of epilepsy. Further details of the control unit and output stage are described below.

3.4.2.1 Control unit

The control unit of the CLNS is based on a commercially available FPGA and the achieved prototype of ES has been made using one of latest FPGA (Ex256). The miniaturized FPGA facilitates low-power multi-function features. Moreover, external controller provides energy and transmits data to the implanted CLNS by means of inductive coupling of spiral antennas. The power recovery module rectifies and filters the carrier signal to provide different regulated power supplies for the implant. The receiver demodulates and sends the Manchester-coded data to the control unit. Details of the power recovery and receiver are described in our previous works (FAYCAL, 2009). The flow chart of the control unit (Figure 3-6) shows that the control unit remains idle unless the data entry or seizure detection signal interrupts it. The control unit is
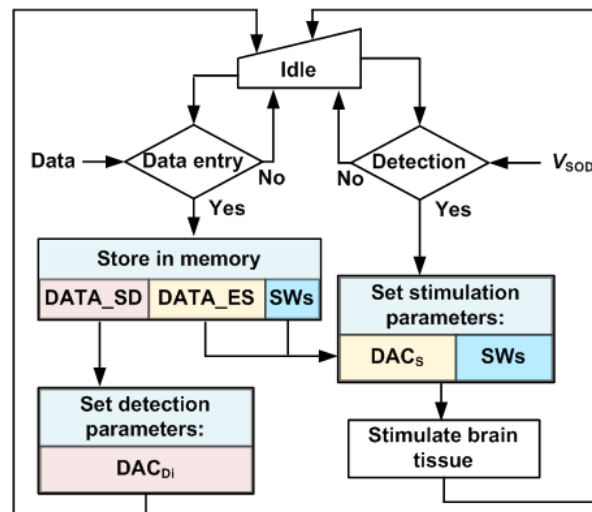
Figure 3-6: Flow chart of electrical stimulator

responsible for receiving input parameter values for seizure detections (Data_SD) and electrical stimulations (Data_SD and SWs). The control unit stores the parameters in memory and loads into the detector and stimulator. There are five variable parameters in ES: stimulation duration (T_1), relax time (T_2), stimulation frequency ($F_{ES} = 1/ T_3$), pulse width (T_4), and stimulation current (I_{STIM}). Figure 3-7 shows the time process of electrical stimulation with variable parameters. The stimulation duration is defined with the number of stimulation pulses N_T and $T_1 = N_T \times T_3$, where $T_3 \geq 6 T_4$.
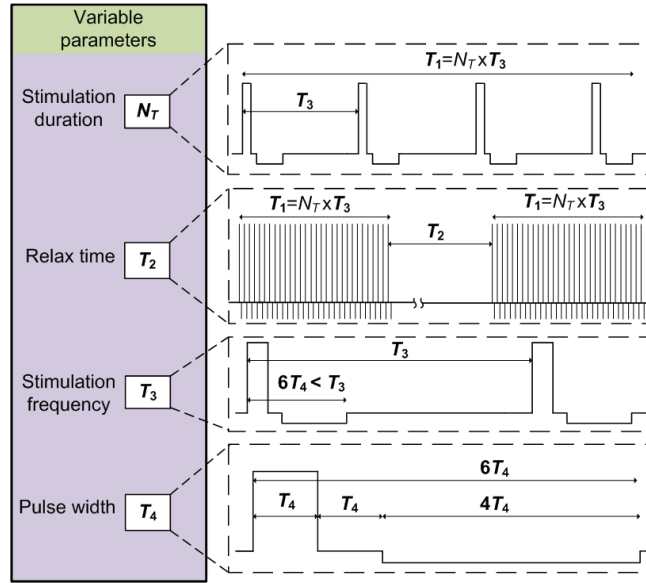
Figure 3-7: Timing process of electrical stimulation waveform using variable parameters

3.4.2.2 Output stage

The output stage retrieves stimulation parameters from the FPGA (stored in Data_ES and SWs), generates biphasic stimulation waveform, and injects to the EZ through the subdural electrodes or to the anterior thalamic nucleus (ATN) by way of depth electrodes. The output stage includes a digital-to-analog converter (DAC$_S$) and a current amplifier (CAM) and three sets of synchronous CMOS analog switches to direct the stimuli (Figure 3-8(a)). At first, the V_{SOD} signal interrupts the FPGA to send the amplitude code stored in Data_ES to DAC$_S$. The output voltage of DAC$_S$ is converted into a proportional current (I_{STIM}) by the CAM and R$_1$ resistance. The injected current I_{STIM} is limited by the R$_1$. Figure 3-8(b) shows that the analog switches manipulate constant current ($I_{STIM1} = I_{STIM}$ and $I_{STIM2} = I_{STIM}/4$) and generate biphasic stimulation waveform I_{STIM} across the two electrodes. Switches SW$_1$ and SW$_2$ set the stimulation current direction and SW$_3$

bypasses high transient current (glitch) of the biphasic stimulation. Moreover, SW_3 switch shunts the CAM output with its negative input before SW_1 and SW_2 activation and confirms the appearance of appropriate stimulation parameter on both electrodes before releasing the SW_3 switch.
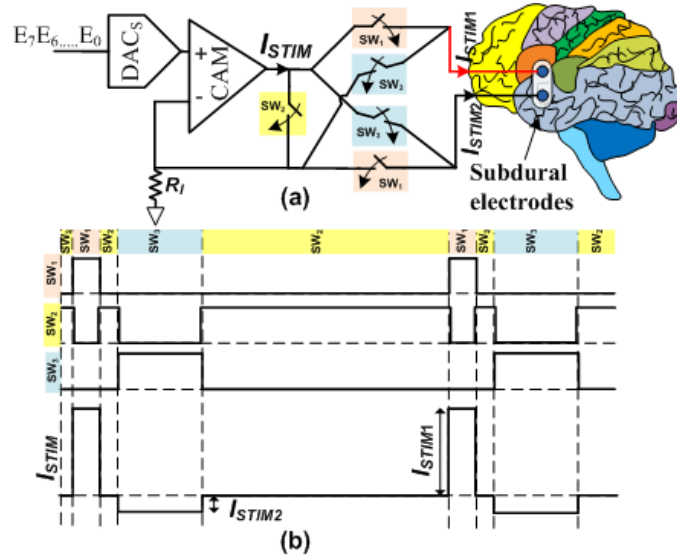
Figure 3-8: Output stage of the CLNS: (a) block diagram of output stage and (b) control signals sequence of switches to generate biphasic stimulation waveform.

3.5   EXPERIMENTAL AND CLINICAL RESULTS

The CLNS is assembled into two PCBs (Figures 3-9(a) and (b)). The ES is designed in two 20mm diameter circular shape blocks in a PCB. The top part of the ES PCB (Figure 3-9(a)) contains a spiral antenna, the power and data recovery stages described in (MOUNAIM, 2007). The bottom part of the ES PCB shows the output stage and its opposite side is the control unit of the ES. On the other hand, the SD is designed in 60mm diameter PCB. The controller of detection is shown in Figure 3-9(b) and the zoom inset shows the detection core, located on the opposite side of Figure 3-9(b). The detection core was fabricated in a CMOS 0.18-µm process and occupied 2 mm^2 of silicon area. Figure 3-9(c) shows photographs of the fabricated chip assembled in a package and zoom inset of the figure shows the fabricated detection core. Details of the measurement and validations are described below.
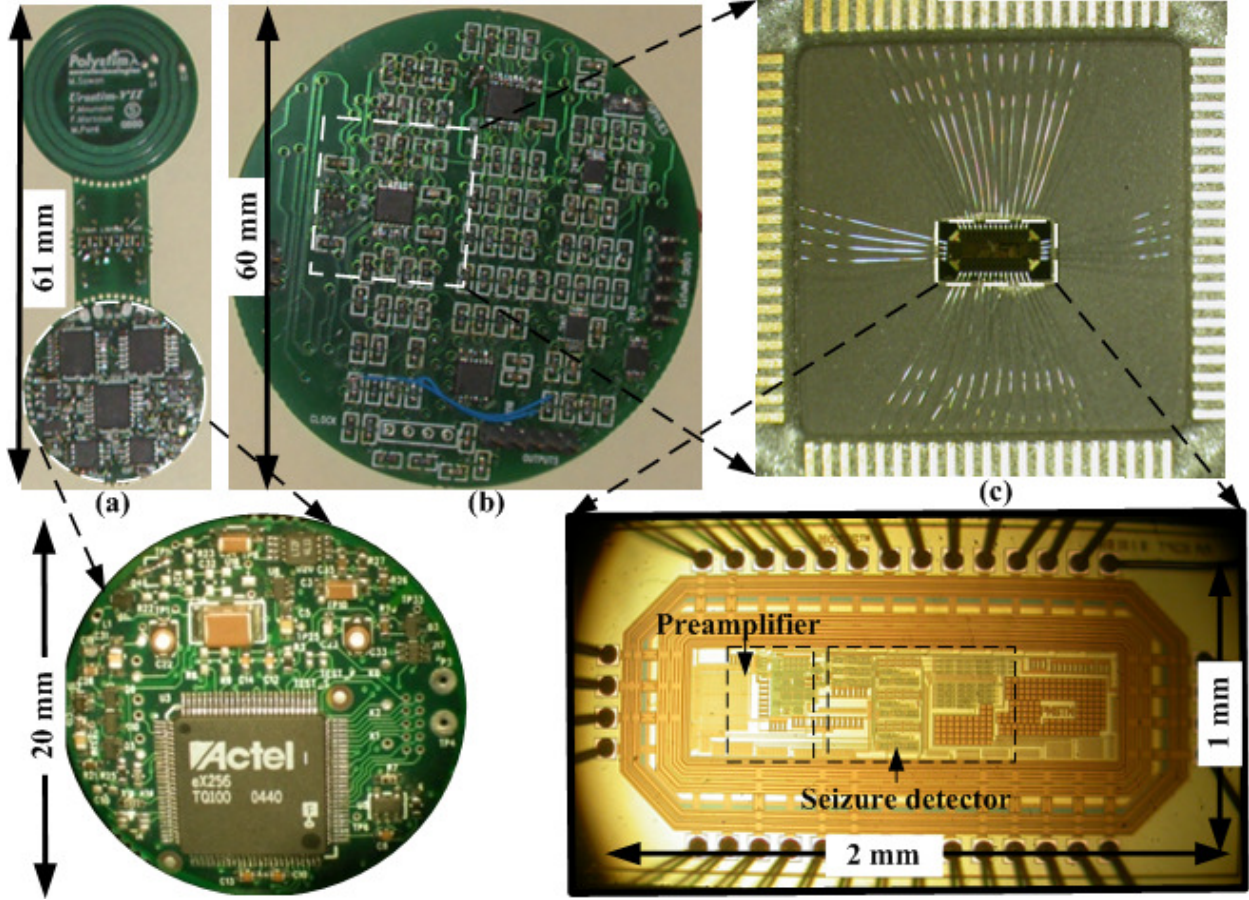
Figure 3-9: The proposed CLNS device: (a) is ES PCB and zoom inset shows opposite side; (b) is SD PCB; and (c) is detection core attached in opposite side of (b); and zoom inset of (c) shows photograph of detection core chip.

3.5.1 Circuit Measured Performance

Measurements on each block of the CLNS were done separately. The detection core of the SD was tested on ten samples of the fabricated chip and provided consistent results. Figure 3-10 shows measured digitally controlled waveforms of T_{f_i}, F_S, and $V_{iHET1,2}$. Figure 3-10(a) illustrates the variation of F_S from 985 Hz to 5.12 kHz and the corresponding generation of T_{f_i} from 1.6 sec to 16.63 sec. Figure 3-10(b) shows that the value of $V_{iHET1,2}$ can be controlled from 18 mV to 588 mV. On the other hand, in the ES, stimulation current was delivered to a 1 kΩ load and Figure 3-10(c) demonstrates the range of I_{STIM} (17 µA to 42 mA) with 164 µA resolution. The detailed measured power consumption of the CLNS is shown in Table 3.3. Table 3.4 presents measurements of widely variable stimulation parameters (I_{STIM}, T_1, T_2, T_3, and T_4).
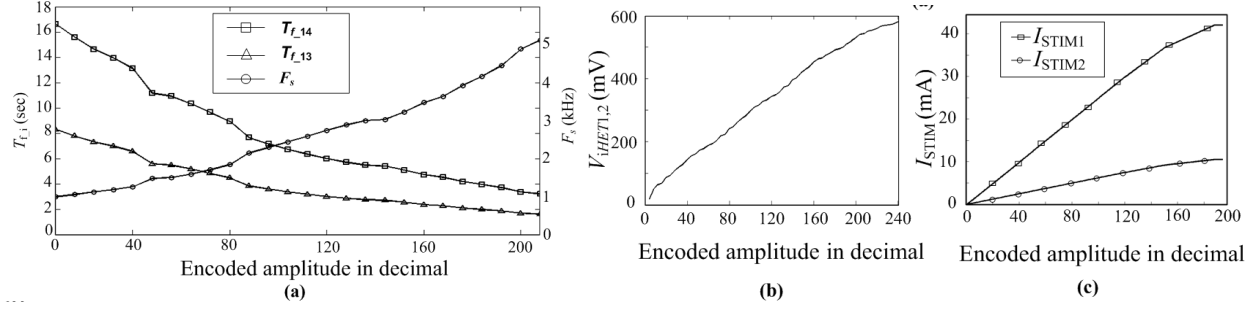
Figure 3-10: Digitally controlled measured results: (a) time frame T_{f_i} generation using sampling frequency F_S; (b) threshold voltage $V_{i,HET1,2}$; and (c) output stimulation current I_{STIM}.

Table 3.3:Measured power consumption (PC) of CLNS

System	Blocks	PS[a] (V)	Component Name	Commercial name	PC (mW)	
SD[b]	Detector core	1.8	Preamplifier Seizure activity detector High frequency detector Others		0.05	
	Controller	3.3	$DAC_{D,i}$ $BF_{D,i}$ OLT_1	DAC0845 LM324 LTC6900	1.5	
ES[c]	Control unit	3.3	FPGA	Ex 256	(Sleep)	(Active)
			DAC_S	MAX550		
	Output stage		SW	MAX4678	2	20
			OLT_2	LTC6900		
			CAM	LT1806		
CLNS[d]	IcEEG monitoring (sleep) mode				4	
	Stimulation (active) mode				22	

[a]PS: Power supply, [b]SD: Seizure detector, [c]ES: Electrical stimulator, and [d]CLNS: Closed-loop neurostimulator.

Table 3.4: Measured stimulation parameters of the electrical stimulator.

Parameter	Variable	Variable size (bit)	Values	
			Min	Max
Number of stimulation	N_T	10	1	1023
Duration of stimulation	T_1	-	1 ms	1min 54 sec
Relax time	T_2	18	1 s	4.36 min
Stimulation Frequency	T_3	4	1ms	15 ms
Pulse width	T_4	10	12 µs	12 ms
Stimulation current	I_{STIM}	8	7 µA	42 mA

3.5.2 Method of case studies and validation

This study was conducted at Notre-Dame Hospital, Centre Hospitalier de l'Université de Montréal (CHUM) with approval from the CHUM ethical committee and research ethics committee of Ecole Polytechnique. This study included seven patients (age: 15 to 49) with refractory epilepsy who underwent an intracranial study to better delineate the EZ. Through a craniotomy window, a combination of depth and subdural (strip and/or grid) electrodes were implanted over suspected areas of epileptogenicity. Following the implantation of intracranial electrodes, the patients underwent long-term (~3 weeks) video-icEEG monitoring (using Stellate's EEG system) in the epilepsy monitoring unit waiting for spontaneous seizures to occur. A post-implantation MRI was used to reconstruct a 3-D representation of electrode positions (using Stellate's gridview software) (Figures 3-11(a)-(c)). Recorded seizures were carefully analyzed to delineate the EZ. For each seizure, onset was marked by an epileptologist (DKN) (yellow marker shown in Figure 3-11(d)). The recordings from the contacts (Figure 3-11(c)) showing earliest ictal changes were fed into the CLNS. Figure 3-11(e) shows the validation procedure. The icEEG recordings from the two contacts positioned over the EZ (Figure 3-11(c)) were selected, transferred to the signal conditioner and then to the CLNS for detection and triggering of a predefined electrical stimulation.
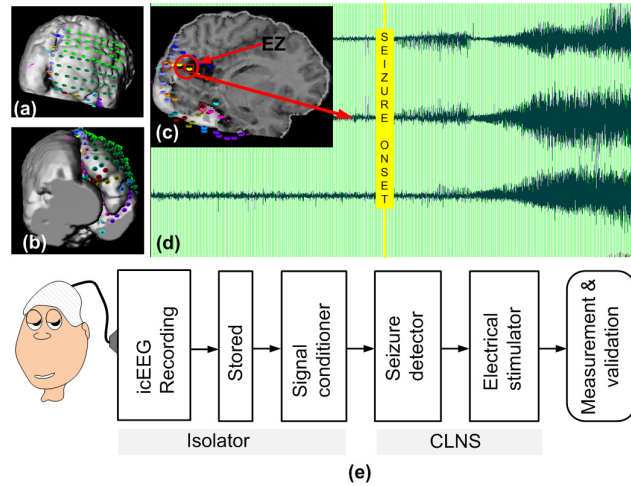
Figure 3-11: Case study and validation method: (a) - (b) 3-D reconstruct images of implanted electrodes using Stellate's gridview software; (c) identify epileptogenic zones; (d) icEEG recordings from the zone; and (e) the icEEG recording from the epileptogenic zone of patients were used to test the proposed seizure detector and the triggering of predefined electrical stimulation was validated.

3.5.3 Validation of the closed-loop neurostimulator

For each patient, the icEEG recording was fed into the CLNS. Input signals were sampled and modulated at F_S, amplified, filtered and analyzed in time-frequency and time-amplitude domain in order to detect seizure. The CLNS was tested on an average of six seizures per patient and results are shown in Table 3.5. The CLNS detected the electroclinical seizures of the seven

Table 3.5: Seizure detection performance on seven patients and average seizure detection delay (T_{DET})

Case No.	Age /Gender	Epileptogenic zone	Average T_{DET} (sec)
1	36/M	Left lateral temporal	15
2	44/M	Left premotor cortex	15
3	41/M	Right amygdala/ hippocampus	21
4	49/F	Left hippocampus	12
5	32/M	Left hippocampus	12
6	15/M	Right lingual gyrus	20
7	24/M	Right hippocampus	6

patients an average of 14.4 sec after seizure onset, well before visible clinical manifestation. Figure 3- 12 shows the seizure detection on icEEG recordings (V_{in}) from a patient (cases 1 in Table 3.5) and the seizure detection delay T_{DET} = 6.4 sec on $V_{SOD,}$ well before clinical manifestation onset. In this study, the CLNS was set to ignore the many BES as the clinician judged them to be too short and frequent, and not always leading to clinical manifestations. In response to the early detection of seizure development V_{SOD}, a burst (T_1 = 1.3 sec) of 198.4 Hz bipolar biphasic stimulation was administered and no stimulation period V_{NS} began right after the stimulation period (Figure 3-12). However, the proper stimulation parameters need to be individualized during the presurgical icEEG study for maximum efficacy prior to the implantation of a stimulation device. Power consumption of the CLNS was dominated by the stimulation current and waveforms; however 4 mW power was continuously dissipated by the CLNS in sleep mode. Power dissipation densities (δ_P) of the seizure detector and electrical stimulator were under maximum safety level (δ_{Pmax} = 6mW/cm^2 that may cause enough heat to damage surrounding tissue) (HARRISON, 2008). Figure 3-13 (a) – (b) illustrate devices operation modes in icEEG recording and corresponding average δ_P.
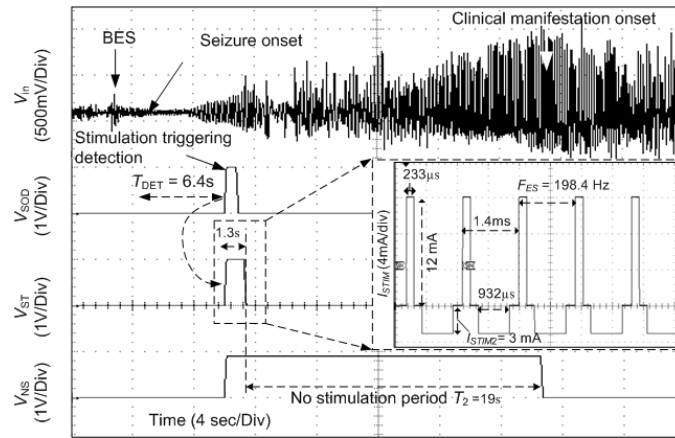
Figure 3-12: Measured electrical stimulation process triggered by seizure onset detection, where V_{in} is icEEG of seizure from epileptogenic zone, V_{SOD} is seizure onset detection, V_{ST} is electrical stimulation period (offline), zoom inset shows stimulation waveforms, and V_{NS} is no stimulation period.
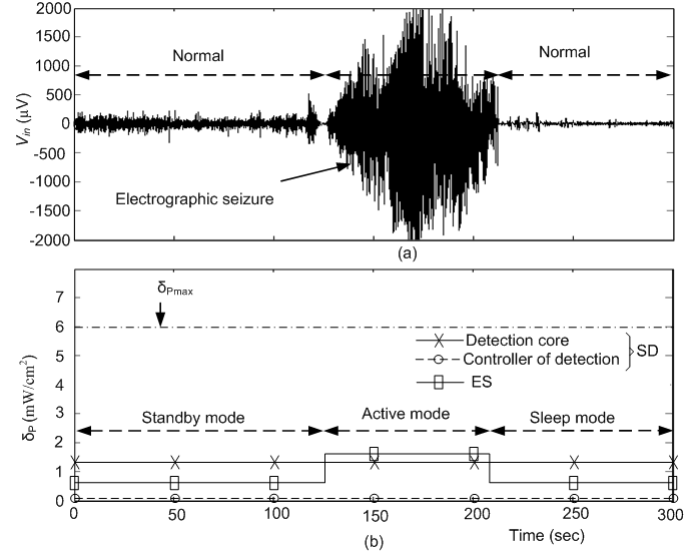
Figure 3-13: Demonstration of power dissipation of proposed CLNS: (a) Electrographic seizure in icEEG recording and (b) Power dissipation densities δ_P of the devices.

3.5.4 Performance analysis of the proposed CLNS

Detection performance of the proposed detector based on seven patients with refractory epilepsy and all the detection performed before clinical manifestation. This performance was evaluated in terms of power consumption and sensitivity of the detector. This detector has performed better than feature extraction process (FEP) (VERMA, 2010), dual-path detector (DPD) (SAFI-HARB, 2011), event-based seizure detector (ESD) (RAGHUNATHAN, 2009), cascaded two-stage seizure detector (CSD) (RAGHUNATHAN, 2011), and linear discriminant analysis classifier (LDA) (PATEL, 2009). Figure 3-14 illustrates the comparative analysis and it shows that the power consumption of the proposed detector is lower and sensitivity of the detector is higher than (VERMA, 2010; SAFI-HARB, 2011; RAGHUNATHAN, 2009; RAGHUNATHAN, 2011; PATEL, 2009). Moreover, the proposed detector demonstrates the use of different effective detection parameters for creating several decision boundaries and reduces the number of false detections for the patient's specific seizure onset pattern while enhanced the sensitivity. The detector can categorize different electrographic icEEG patterns (e.g. normal neural activity, low-voltage fast activity, slow spike wave, brief electrical seizure, artifact, and progressive amplitude increase signal) and identify the specific electrographic pattern at the seizure onset without having false detection.

There has been very few electrical stimulator reported for suppressing upcoming seizure. The pilot study (KOSSOFF, 2004; OSORIO, 2005) was done using a large constant current stimulator (S-12; Grass Instruments). Neuropace Inc. (Mountain View, California, US) has a responsive neurostimulator (RNS) system and investigation on the device is evaluated in clinical trials (SKARPAAS, 2009). The detection algorithm of RNS system is based on data reduction (line length function and area under the curve) and feature extraction (half wave analysis). However, the proposed seizure detection is based on noise reduction (modulation), feature extraction (progressively increasing low-voltage fast activity), and data reduction (digitally demodulation).
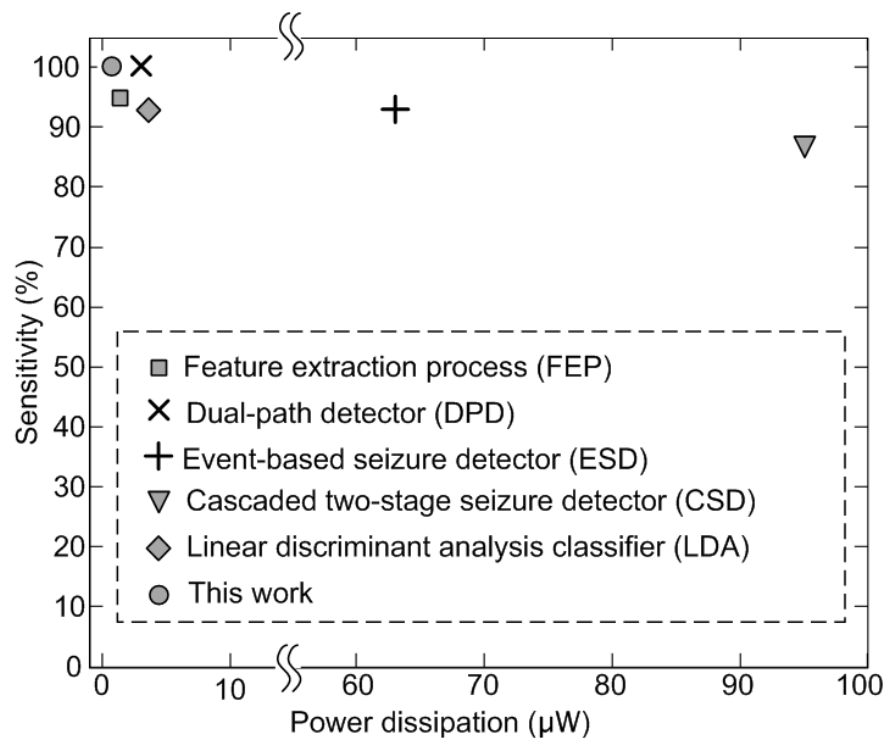
Figure 3-14: A comparative analysis of the proposed results (based on 7 patients) from different detectors.

The detection criteria of RNS system are based on high frequency tracking of amplitude variations in icEEG recording, but the proposed algorithm detects progressively increase signal amplitude as well as high-frequency signal in icEEG. Furthermore, Neuropace Inc. has not yet to publish the hardware description, detection performances and power consumption of their RNS system. A microcontroller based stimulator (NIRO, 2007) has been proposed for brain stimulation, but its power consumption is also unknown. Power consumption of the proposed ES is dominated by the stimulation parameters and would vary from patient to patient.

3.6   CONCLUSION

In this paper, we present an implantable low-power closed-loop neurostimulator for the treatment of epilepsy. This device records icEEG activity, analyzes the signal in time-frequency and time-amplitude domains, and triggers a predefined seizure suppression biphasic electrical stimulation. The proposed CLNS uses low-power management technique. The neural signal amplifier and seizure detector consumes 6.74 µW, while power consumption of ES mainly depends on electrical stimulation parameters. The tuneable patient-specific parameters of SD and ES can be adjusted wirelessly. The performance of the CLNS was tested in seven patients with refractory epilepsy and the early detection of seizure was able to trigger subsequent responsive electrical stimulation.

CHAPTER 4   IMPLANTABLE CLOSED-LOOP EPILEPSY PROSTHESIS

We presented a responsive neurostimulator for the treatment of epilepsy in chapter 3 and this chapter concerns another neurostimulator which has lower power consumption, wider range of features, better precision, and larger memory. This chapter also demonstrates effect of focal bipolar electrical stimulation and corresponding spatial voltage distribution in an *in vitro* morphologic electrical model. The experimental results show the optimum stimulation parameters for efficiently affecting the suspected epileptic focus. This work will be appeared in "ACM Journal on Emerging Technologies in Computing Systems" as reproduced in the following papers.

4.1   IMPLANTABLE CLOSED-LOOP EPILEPSY PROSTHESIS: MODELING, IMPLEMENTATION AND VALIDATION

Muhammad T. Salam[1], Mohamad Sawan[1], and Dang K. Nguyen[2]

[1]Polystim Neurotechnologies Laboratory, Polytechnique Montréal, Québec, Canada

[2]Notre-Dame Hospital, Centre Hospitalier de l'Université de Montréal (CHUM), Québec, Canada

Abstract - In this paper, we present an implantable closed-loop epilepsy prosthesis, which is dedicated to automatically detect seizure onsets based on intracerebral electroencephalographic (icEEG) recordings from intracranial electrode contacts and provide an electrical stimulation feedback to the same contacts in order to disrupt these seizures. A novel epileptic seizure detector and a dedicated electrical stimulator were assembled together with common recording electrodes to complete the proposed prosthesis. The seizure detector was implemented in CMOS

0.18-μm by incorporating a new seizure detection algorithm that models time-amplitude and -frequency relationship in icEEG. The detector was validated offline on ten patients with refractory epilepsy and showed excellent performance for early detection of seizures. The electrical stimulator, used for suppressing the developing seizure, is composed of two biphasic channels and was assembled with embedded FPGA in a miniature PCB. The stimulator efficiency was evaluated on cadaveric animal brain tissue in an in vitro morphologic electrical model. Spatial characteristics of the voltage distribution in cortex were assessed in an attempt to identify optimal stimulation parameters required to affect the suspected epileptic focus. The experimental results suggest that lower frequency stimulation parameters cause significant amount of shunting of current through the cerebrospinal fluid; however higher frequency stimulation parameters produce effective spatial voltage distribution with lower stimulation charge.

4.2 INTRODUCTION

Over the last 20 years, there have been many advances in the treatment of epilepsy. Antiepileptic drugs remain the first line of treatment albeit with side effects in a significant number of patients. Furthermore, approximately a third of 'refractory' patients fail to be controlled despite several antiepileptic drug trials. These patients with pharmacoresistant epilepsy can sometimes be helped by resective epilepsy surgery. Unfortunately, not all are good candidates for epilepsy surgery such as patients with a poorly delineated epileptogenic zone, multiple epileptic foci or an epileptogenic zone overlying eloquent areas (language, motor, visual) which cannot be removed (JEROME, 2009; SPENCER, 2009).

Recently, there has been a growing interest to fill the gap between antiepileptic drug therapy and epilepsy surgery. Several research groups have explored treating conventionally untreatable epilepsies with non-resective therapeutic alternatives (e.g. vagus or trigeminal nerve stimulation (RYCHLICKI, 2006; SETHI, 2008; REESE, 2009); focal cooling (GUERRA, 2005), focal drug delivery (STEIN, 2000) or electrical stimulation (FISHER, 2010)). Recent studies have shown that electrical stimulation is effective in reducing seizure frequency (FISHER, 2010; OSORIO, 2005; SKARPAAS, 2009; NIRO, 2007; KOSSOFF, 2004). There are two main approaches to brain stimulation: open loop (FISHER, 2010; SETHI, 2008; REESE, 2009; RYCHLICKI, 2006) and closed-loop neurostimulation (OSORIO, 2009; SKARPAAS, 2009; NIRO, 2007). The open loop

system consists in scheduled delivery of stimulation. Whereas in a closed-loop system, stimulation is only triggered upon detection of a seizure. Closed-loop stimulation has several potential advantages over the open-loop method such as lower number of stimulations, higher efficiency because of rapid access, and ability to review intracerebral electroencephalographic (icEEG) recordings to monitor seizure frequency (OSORIO, 2009; SKARPAAS, 2009; SCHACHTER, 2009; SUN, 2008). A closed-loop system requires an efficient seizure detector to identify seizures at their onset and trigger an abortive stimulation before clinical manifestations occur. Although many seizure detection algorithms have so far been proposed (ZANDI, 2009; NANDAN, 2009; POLYCHRONAKI, 2010), these have mainly been developed for high-speed desktop computers and short-term applications which cannot be employed in a low-power implantable microchip (SALAM, 2010(a)). Further development in epileptic prosthetic devices would benefit from an epileptic seizure detection algorithm for low-power integrated circuits that could provide high-detection accuracy and reduce instrumentational low-frequency noises (SALAM, 2009(a); RAGHUNATHAN, 2009; PATEL, 2009; SALAM, 2010(b); VERMA, 2010).

In addition to the seizure detection performance of such a closed-loop system, the safety of focal electrical stimulation and choice of electrical stimulation parameters are also important issues. Proof-of-concept experiments conducted in animals and humans have demonstrated that limiting the maximum charge density to 60 $\mu C/cm^2$ per phase can avoid tissue damage (SKARPAAS, 2009; GORDON, 1990). It remains unclear however how selected parameters at specific anatomical locations affect the electric field strength and modulate pathological neural activity. Traditionally, stimulation parameters have been determined empirically: tune the parameters (i.e. current, pulse width and frequency) in order to achieve best possible seizure suppression parameters (SUN, 2008; OSORIO, 2009; FISHER, 2010). But these parameters vary from patient to patient possibly due to the variability of the epileptogenic zone localization: depth of sulcus, superficial cortex, deep hippocampal focus etc. In other words, the optimal parameters may depend on the location of epileptogenic zone being stimulated (SRAMKA, 1990). Electric field distribution is difficult to predict (i.e. which area is directly affected by the stimulation). Several simulation models of cerebral cortex and subcortical structures (thalamus and subthalamic nucleus) have been proposed to estimate the charge density (CHRISTOPHER, 2008; NATHAN, 1993; AGARWAL, 1994; RAYPORT, 1969; BUTSON, 2008) and voltage distribution (MIOCINOVIC, 2009; CAMERON, 2004; RAYPORT, 1969). The subcortical

structure model for the treatment of Parkinson's disease is well established and validated *in vitro* and *in vivo* (LESTER, 2009; BLAD, 2007; BUTSONA, 2006; KUNCEL, 2006; MCINTYRE, 2004). However, a cerebral cortex structure model for the treatment of epilepsy is not well established. Lack of model validation is a drawback for choosing effective seizure suppression stimulation parameters. Moreover, several others aspect need to be addressed, such as stimulation mode, current distribution, shunting of injected current, and impedance of cerebral tissue.

In this paper, we present an implantable epilepsy prosthesis that identifies electrographic seizure onsets and triggers focal electrical stimulation to disrupt seizure progression. We also demonstrate spatial characteristics of voltage distribution in cerebral cortex generated by the electrical stimulation. The proposed device includes intracranial electrodes, a data acquisition system, a digital signal processor for real-time seizure detection, and a programmable electrical stimulator. The integrated seizure detection algorithm has high detection sensitivity for patients' specific seizure patterns, and low false detections. The seizure detector was validated on different platforms (Matlab, Cadence post-layout CMOS 0.18-µm circuit simulation and fabricated chip). The electrical stimulator was built around an FPGA platform and allows tuning all parameters of the employed biphasic stimulus. The proposed device was validated using recorded icEEG from ten patients with refractory partial epilepsy. Furthermore, the electrical stimulator was tested on cadaveric animal brain tissue in an *in vitro* morphologic electrical model. The experimental data showed that high frequency stimulation parameters provided optimal spatial voltage distribution in gray matter.

The remaining of this paper includes Methods and Materials in section 2. Results are reported in section 3, and Conclusions are the subject of section 4.

4.3 METHODS AND MATERIALS

4.3.1 Patient selection and device validation method

More than half of epilepsy patients suffer from partial (focal) seizures and a non-negligible percentage of them are drug resistant. In a partial seizure, the ictal discharge originates from a seizure onset zone which frequently will not lead to any overt clinical manifestations unless it builds up to involve a larger area (the symptomatic zone). Further propagation ipsilaterally and

controlaterally may lead to the most commonly known and most bothersome ictal manifestation: tonic-clonic convulsions.

Patients with intractable non-lesional partial epilepsy who are candidate for epilepsy surgery may sometimes require an intracranial study to better delineate their epileptogenic zone. Through a craniotomy window, a combination of depth and subdural (strip and/or grid) electrodes are implanted over suspected areas of epileptogenicity. Following the implantation of intracranial electrodes, patients are then transferred to the epilepsy monitoring unit for long-term (~2-3 weeks) video-icEEG recording of spontaneous seizures. Once the epileptogenic zone is adequately delineated, the patient returns to the operating room for the removal of electrodes and resection of the identified epileptogenic zone. During this evaluation with intracranial electrodes, 128 channel-icEEG recordings are performed using amplifiers (PRO-36 amplifiers, Stellate Harmonie System) at 200 Hz and 2000 Hz sampling frequency.

The icEEG seizure recordings used for the validation of the proposed closed-loop epilepsy prosthesis came from such patients undergoing an invasive EEG study. Offline recordings from two contacts positioned over the epileptogenic zone are selected, uploaded onto a signal conditioner (arbitrary signal waveform generator) for reproducing icEEG recording and fed into the closed-loop epilepsy prosthesis for detection by the seizure detector which is supposed to trigger a burst of electrical stimulation on a cadaveric animal brain tissue *in vitro* model (Figure 4-1). During the stimulation, voltage recording is performed in the vicinity of the active subdural electrodes implanted on the cerebral cortex.
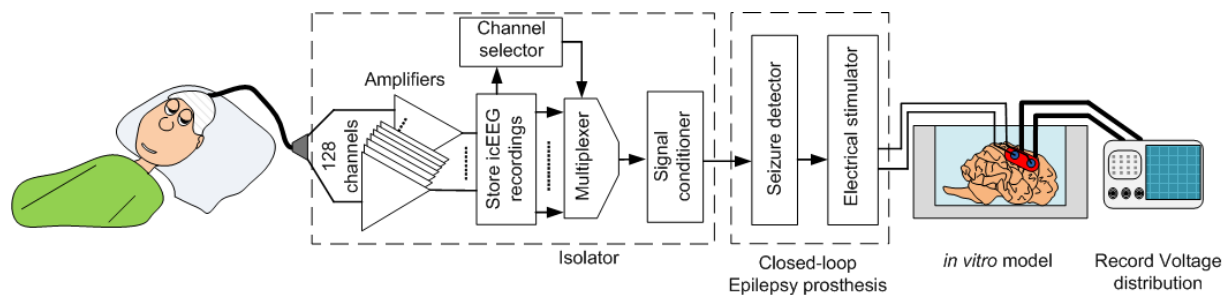
Figure 4-1: The closed-loop epilepsy prosthesis: icEEG recorded from patients with medically refractory epilepsy were used to test our seizure detection algorithm and the triggering of an electrical stimulation to cadaveric animal brain tissue.

4.3.2 Proposed closed-loop Epilepsy prosthesis

The proposed implantable closed-loop epilepsy prosthesis provides continuous long-term monitoring from epileptogenic zone. Figure 4-2 illustrates the implant configuration. The device is intended to be implanted within the skull and interface directly with the recording/stimulation sites. This device is composed of two main parts: 1) a seizure detector, and 2) an electrical stimulator.
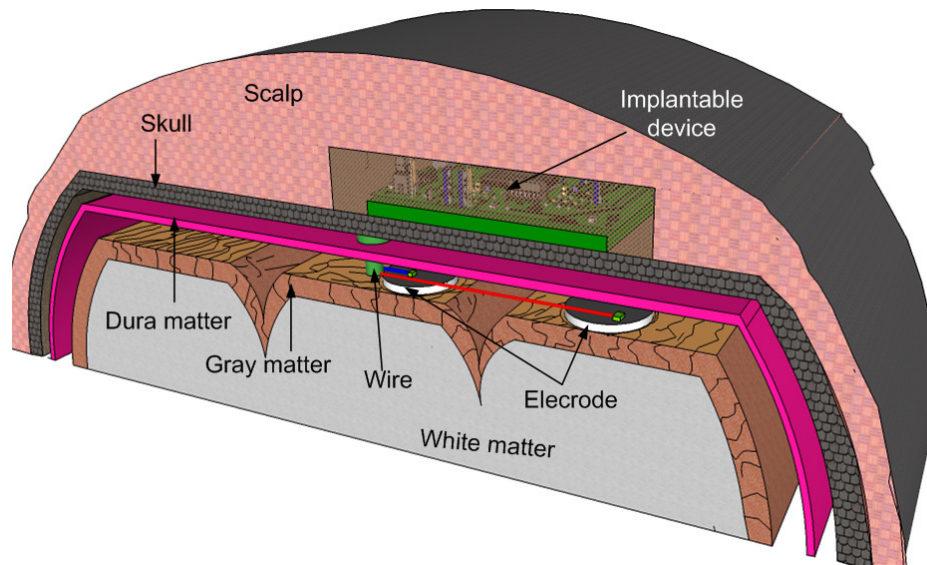
Figure 4-2: Illustration of the proposed implantable closed-loop epilepsy prosthesis.

4.3.2.1 The Seizure Detector

The seizure detector is based on a detection algorithm first validated in Matlab, followed by circuit validation using CMOS 0.18-µm technology under Cadence environment and chip fabrication by TSMC through CMC Microsystems. Features of the device are described below.

The implemented algorithm detects seizure onsets before first clinical manifestations. Electrographically, several patterns can be seen at seizure onset such as low-voltage fast-activity, high-voltage fast-activity or rhythmic spiking (SPENCER, 2009). The proposed epileptic seizure detection algorithm is designed to detect partial seizures characterized by a progressive increase of low-voltage fast-activity on icEEG recordings. This detection algorithm is illustrated in Figure 4-3. At first, the recorded icEEG is modulated into high frequency ($F_s = 1/T_s$) and the discrete

modulated signal (V_{mod}) is confined to a time frame (T_f). Later, V_{mod} passes through several voltage level detectors (VLD) to detect the progressive increases of signal amplitude. The threshold voltages of VLD ($V_{iHET1,2}$) are adjusted to the amplitude levels of interest for each individual patient. The outputs of VLD (V_{SDi}) are demodulated to the original frequency band and analyzed in frequency domain. The real-time signal frequencies f_{si} in different amplitude level are compared to the specific seizure onset frequency (f_{SZ}) of a patient to declare the start of a seizure. The sensitivity and specificity of the algorithm is dependent on the optimal values of $V_{iHET1,2}$ and T_f (SALAM, 2009(b)).
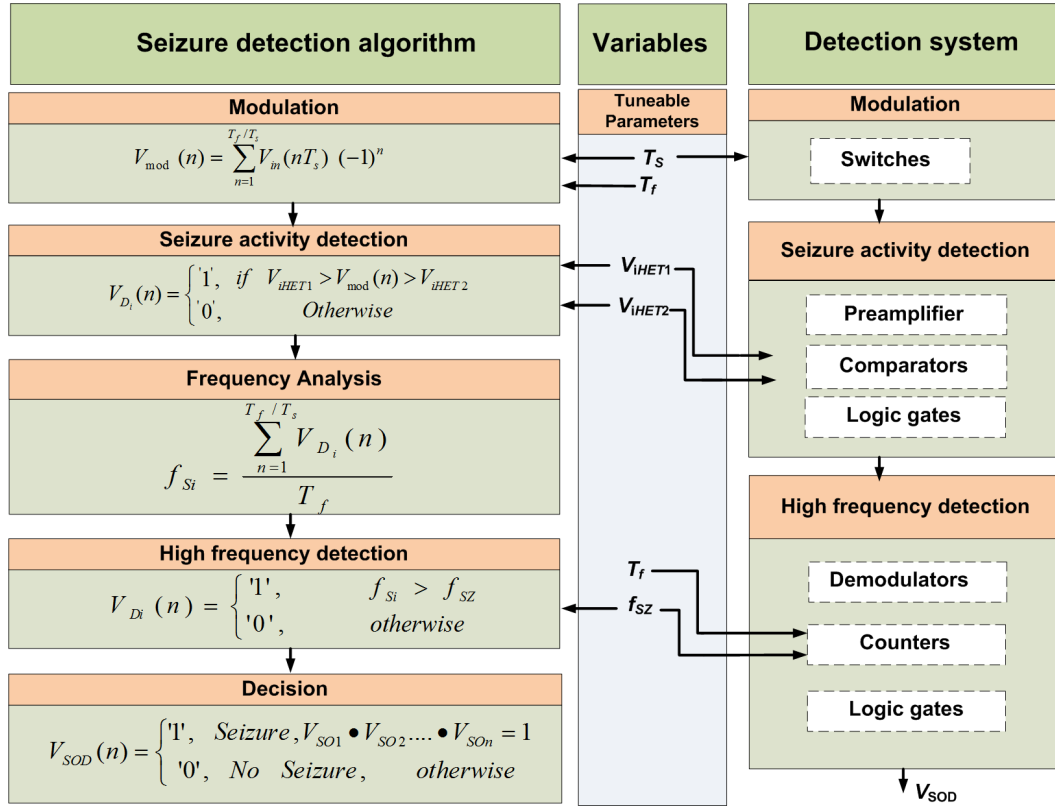
Figure 4-3: Flowchart of the proposed epileptic seizure detection algorithm, tuneable parameters, and block diagram of the proposed detection system.

The functional block diagram of the implemented detector is shown in Figure 4-3 (detection system). This detector consists of a modulator, a seizure activity detector, and a high frequency detector. Several variable parameters (T_s, $V_{iHET1,2}$ and T_f) are introduced to facilitate high accuracy in real-time seizure onset detection (SALAM, 2009(b)).

For the modulator, four synchronous switches modulate the icEEG signal and translate the signal into high frequency (F_s). Therefore, signal processing of icEEG in circuits is not effected by flicker noise, thermal noise and DC offset.

The seizure activity detector contains a preamplifier, comparators, and logic gates. The preamplifier consists of a low-power low-noise amplifier and a high-pass filter. The preamplifier has a 80 dB midband gain and 17 kHz (2 kHz to 19 kHz) bandwidth with 6μVrms input-referred noise. Moreover, the gain of the preamplifier is variable and a certain amplitude range of the input signal can be amplified. Two comparator and logic gates are used to construct a voltage level detector (VLD) that detects the progressive increase of signal amplitude.

The high frequency detector (HFD) consists of a demodulator, counters and logic gates. The demodulator comprises RC circuits and a VLD that digitally demodulate the signal to the original frequency band. The frequency detector is composed of counters and logic gates that could declare the start of a seizure by detecting the high frequency signal on icEEG.

4.3.2.2 The Electrical Stimulator

Several versions of a dedicated electrical stimulator were introduced in our laboratory for the treatment of epilepsy (SALAM, 2010(c); SALAM, 2011(d)). The closed-loop stimulator (SALAM, 2010(a)) was simulated on CMOS 0.18μm and only simulation results were reported. A FPGA based stimulator was implemented in an Actel EX256 embedded system (SALAM, 2011(d)), which was replaced by a low-power FPGA device, the Actel igloo AGL125. In addition to small dimensions and low-power consumption, the Igloo devices have larger memory and higher number of logic gates. Therefore, the stimulator integrated in the proposed device has a wide range of parameters, higher precision and more flexibility in data manipulation.

Concerning the stimulation parameters, different cortical electrical stimulation strategies employing several types of stimuli have been shown feasible, safe, tolerable, and efficient (FISHER, 2010; OSORIO, 2005; SKARPAAS, 2009; NIRO, 2007; KOSSOFF, 2004). The proposed stimulator generates charge-balanced asymmetric biphasic stimulation through bipolar platinum electrodes; thus it reduces electrochemical processes and avoids damaging brain tissues (MERRILL, 2005; OSORIO, 2005). Moreover, the bipolar stimulation can effectively produce localized current flows (NATHAN, 1993) in specific region. Table 4-1 shows main parameters and their values for the proposed stimulator.

Table 4.1: Available parameters in the proposed electrical stimulator

Parameter	Variable	Value Min	Max	Parameter	Variable	Value Min	Max
Number of stimulation	N	1	1023	Duration of stimulation	T_1	2 msec	10 sec
Off time	T_2	1 min	4.26 min	Stimulation Frequency	T_3	2 msec	10 msec
Pulse width	T_4	10 µsec	12 msec	Current	I_{STIM}	10 µA	40 mA

Figures 4-4 (a) – 4(d) demonstrate the timing process of the stimulator in the response to seizure detections V_{SOD}. The duration of current stimulation (I_{STIM}) is T_1; if the stimulation does not terminate the seizure another stimulation is triggered by the detector after T_2. Repetition of stimulation is subject to a safety constraint of no more than five stimulations per detection (OSORIO, 2005; SKARPAAS, 2009). Figure 4-4(d) shows that the cathodic pulse (I_{S1}) of the biphasic stimulation activates the neural cells and the anodic stimulus ($I_{S2}=I_{S1}/4$) removes the delivered charges of I_{S1}. However, two subsequent opposite stimuli could prevent the generation of an action potential. Thus, a short time delay (T_4) in between the pulses is required to propagate the action potential away from the stimulation site before removing the injected charge (RUBINSTEIN, 2001; CONSTANDINOU, 2008).
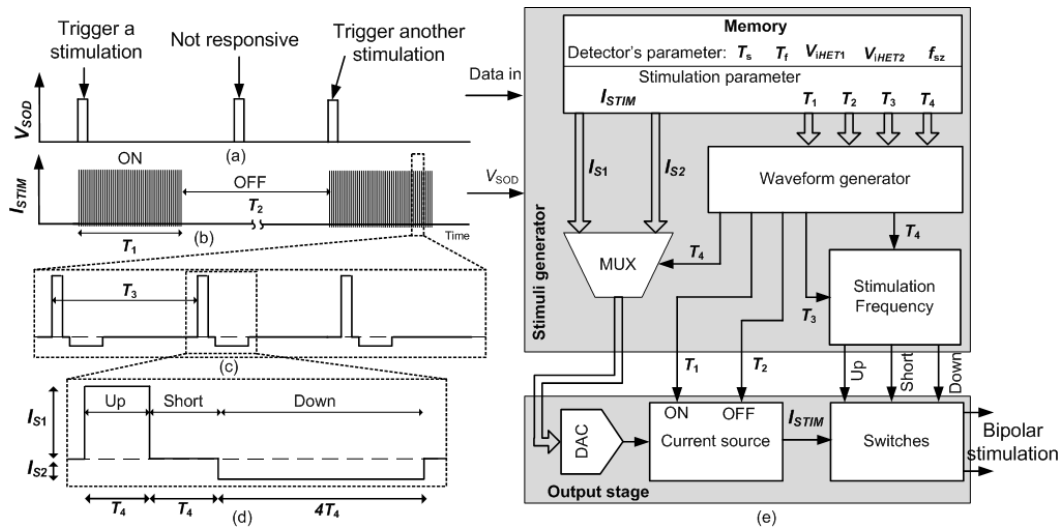
Figure 4-4: Proposed electrical stimulator: (a) seizure detections V_{SOD} (b) two subsequent bursts of biphasic stimulations, (c) the biphasic stimulation, (d) the stimulation waveform profile, and (e) block diagram of the stimulator.

The stimulator also includes a stimuli generator, which is composed of a memory, a waveform generator, a frequency controller, and a digital multiplexor (MUX) (Figure 4-4(e)). The memory is used to store all parameters for the seizure detector and electrical stimulator. The waveform generator controls the stimulation duration (T_1), rest time (T_2), stimulation frequency (T_3), pulse width (T_4), and stimulation current (I_{stim}). The stimuli generator remains in standby mode unless data entry or a seizure detection signal interrupts it. The memory receives the input data by serial protocol interface.

Finally, the output stage includes a digital-to-analog converter (DAC), a current source, and several switches. The DAC receives 8-bit data of I_{stim} from the stimuli generator and outputs the stimulation current (I_{s1} or I_{s2}). The switches generate biphasic simulation waveforms across the bipolar electrodes. Moreover, the stimuli generator controls the stimulation duration (T_1) and the rest time (T_2).

4.3.2.3 Circuits and devices implementation

The detection algorithm was tested in Matlab tools and post-layout circuit simulation (PLCS). Then, the seizure detector was fabricated in a CMOS 0.18-µm process, occupying a 2 mm x 1 mm silicon area. The electrical stimulator was assembled on 20-mm diameter circular printed circuit board (PCB). Photographs of the chip layout, the fabricated chip and electrical stimulator are shown in Figures 4-5 (a), (b), and (c), respectively.
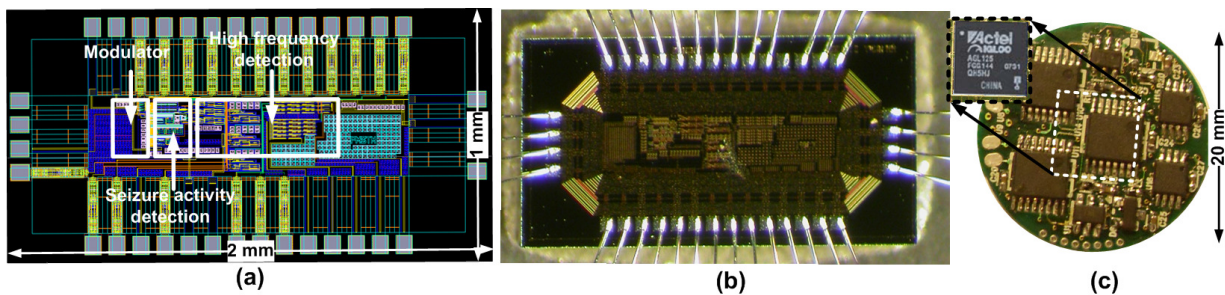
Figure 4-5: Photographs of main parts of the system: (a) Layout of chip, (b) Fabricated chip, and (c) Electrical stimulator and zoom inset shows FPGA in the opposite side.

4.3.3 Seizure detection from icEEG recordings

Ten patients (age: 15 to 49) with intractable nonlesional partial epilepsy candidate for epilepsy surgery underwent an intracranial study (Figures 4-6(a) – (b)) to better delineate the epileptogenic zone. A combination of depth, subdural grid and strip electrodes were implanted in various suspected areas of epileptogenicity. Following the implantation, patients underwent a magnetic resonance imaging (MRI) study to verify the location of implanted electrodes (Figures 4-6 (c) – (d)). All icEEG recordings were reviewed by an epileptologist (DKN) who marked the onset of electrical and electroclinical seizures (e.g. yellow mark 'Seizure' shown in Figure 4-6(e)). The recorded seizure was electrically characterized by a diffuse slow wave followed by desynchronization (Figure 4-6(e)) and regional low-voltage high-frequency activity over temporal neocortical contacts (Figure 4-6(d)). The electroclinical seizures could be preceded by low-frequency preictal spiking, high-frequency preictal spiking or even a brief electrical seizure (BES). The recordings from the contacts showing the earliest ictal changes were fed into the proposed seizure detection algorithm (Matlab software) and seizure onset detector (CMOS 0.18 μm process). The detection performances of Matlab analysis, PLCS and fabricated chip measured results are presented.
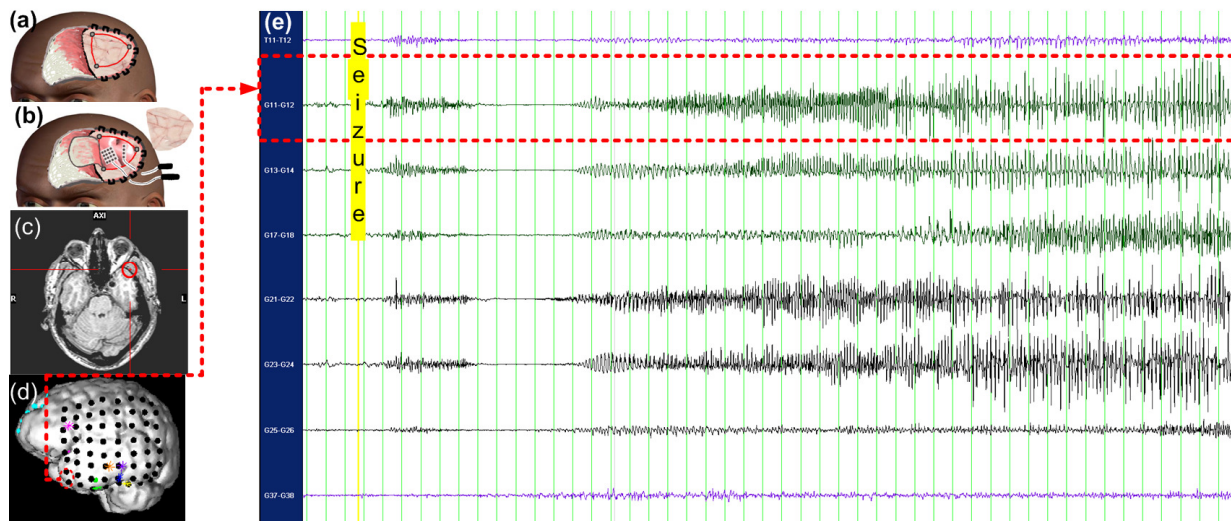
Figure 4-6: Method of case studies: (a)-(b) is an intracranial study for better delineate the epileptogenic zone, (c) is axial MRI image and (d) is 3-D reconstruction of implanted electrodes, and (e) electrical seizure onset was marked ('Seizure') on icEEG.

4.3.4 *In Vitro* Experiments

The in vitro experiments were performed by suspending a subdural strip electrode (Ad-tech, Inc.) on a cadaveric animal brain tissue in saline solution (Figure 4-7(a)). The conductivity of saline solution is 17 mS/cm, which is similar to conductivity of cerebrospinal fluid (CSF) (MANOLA, 2005). The conductivity of the gray matter of the cadaveric animal brain tissue varies from 1.4 mS/cm to 4 mS/cm. Figure 4-7(a) shows the interface between brain tissue (i.e. gray matter) and the subdural electrodes (i.e. platinum electrode, medical grade Polydimethylsiloxane (PDMS) and stainless steel wire). The equivalent electrical equivalent circuit model for Figure 4-7(a) is shown in Figure 4-7(b), where R_{wi} is wire resistance, R_{pi} is polarized resistance of electrolyte; C_{pi} is double layer capacitance, R_{CSF} is resistance of saline solution, R_{GM} is resistance of gray matter, and C_{GM} is capacitance through gray matter. Resistance of CSF is 3 to 12 times lower than the gray matter (NATHAN, 1993; AGARWAL, 1994; MANOLA, 2005). Thus a bipolar stimulation causes significant shunting of current through the CSF at low frequency stimulation. However, stimulation at high frequency reduces impedance ($R_{GM} \parallel C_{GM}$) through the gray matter and decreases the shunting of current.
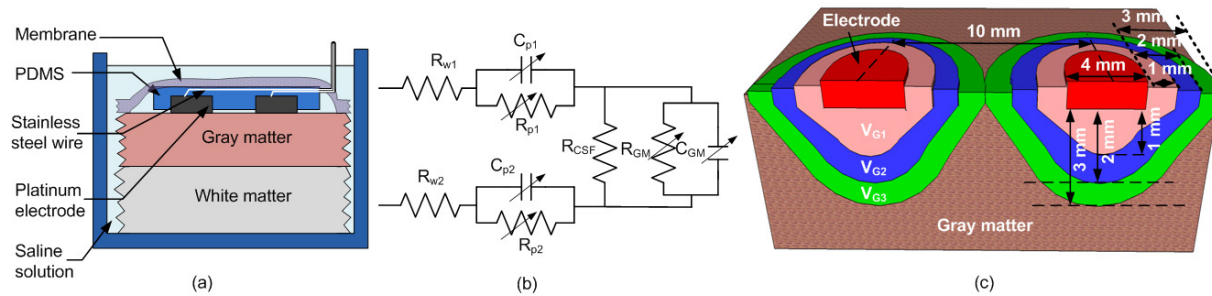
Figure 4-7: *in vitro* voltage recordings using a cadaveric animal brain tissue in saline solution: (a) Experimental setup, (b) Equivalent electrical circuit model of (a), and (c) spatial voltage distribution were recorded in 1 mm (V_{G1}), 2 mm (V_{G2}) and 3 mm (V_{G3}) distance.

Biphasic constant-current pulse trains were applied through the subdural electrodes and voltages generated in gray matter of brain were recorded with commercial microelectrodes (FHC Company). The microelectrodes were positioned at 1 mm, 2 mm and 3 mm outer radius of the stimulating electrodes and similarly underneath, 1 mm distance interval up to 3 mm (Figure 4-

7(c)). During the stimulation with different parameters, voltage distribution at 1 mm (V_{G1}), 2 mm (V_{G2}) and 3 mm (V_{G3}) were recorded to characterize the stimulations effect on different areas.

4.4 RESULTS

4.4.1 Power dissipation of the proposed device

Measured power consumption of the proposed system is shown in Table 4-2. Power measurements in simulation platform were undertaken separately on each block. The core seizure detector consumed 6.71 µW in PLCS, whereas fabricated detector chip assembled in the closed-loop device consumed 51 µW due to the loading of electrical stimulator, adjustable circuits of the detection parameters and parasitic effects. The detection core was always in active mode due to the continuous icEEG monitoring (Table 4-2). The achieved prototype of stimulator has been made using one of the latest FPGA (AGL125). Power consumption of the stimulator was dominated by the stimulation current; however 2 mW power was continuously dissipated by the FPGA in standby mode. Power dissipation densities (δ_P) of the seizure detector and electrical stimulator were under maximum safety level (δ_{Pmax} = 6mW/cm^2 that may cause enough heat to damage surrounding tissue) (HARRISON, 2008). Figures 4-8 (a) – (b) illustrate devices operation modes in icEEG recording and corresponding average δ_P.

Table 4.2: Measured power consumption of proposed closed-loop epilepsy prosthesis

System	Block	Power supply	Power consumption (W)	
			Standby mode	Active mode
Seizure detector	Preamplifier	1.8 V	50 µ	50 µ
	Detector		45.8 n	45.8 n
Electrical stimulation	Stimuli generator	3.3 V	2 m	10 m
	Output stage	5 V	10 n	5 m
Total power consumption of the proposed system			~2 m	~16 m
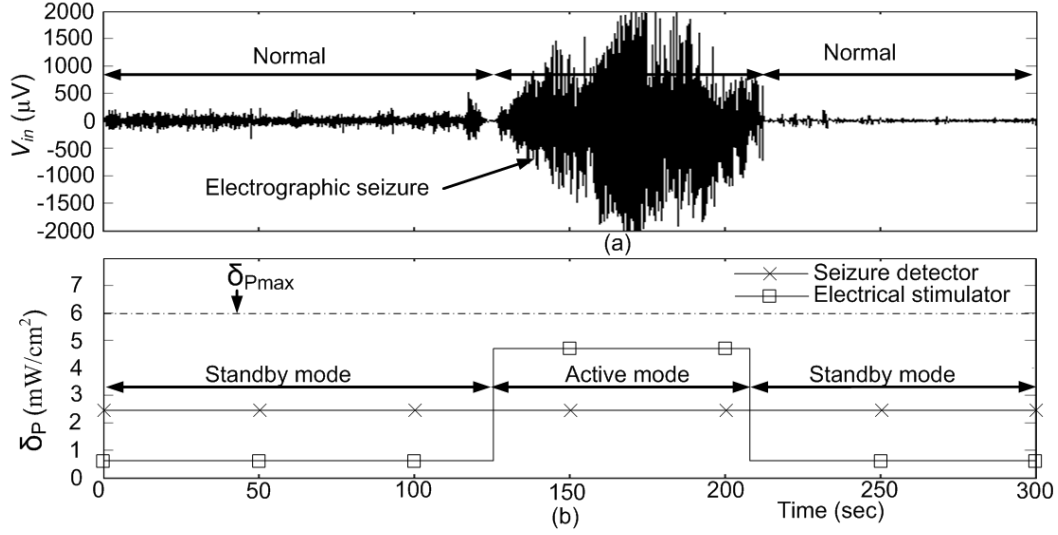
Figure 4-8: Demonstration of power dissipation of proposed system: (a) Electrographic seizure in icEEG recording and (b) Power dissipation densities δ_P of the devices.

4.4.2 Validation of seizure detection

The achieved validation was performed on three incremental steps: 1) Algorithm under Matlab simulation, 2) Post-layout circuit simulation (PLCS) under Cadence environment, and 3) Measurement through the fabricated chip. The details of these results are the following:

The signal recorded from two contacts located in the epileptogenic zone during a normal state (Figure 4-9(a)), a BES (Figure 4-9(b)), and an electroclinical seizure (Figure 4-9(c)) were fed into Matlab to test the seizure detection algorithm. Figure 4-9(a) shows that there was no abnormalities detected in VLDs ($V_{D1,2}$ in Figure 4-9(a)) and no false alarms (V_{SOD}) during the normal state. The algorithm ignored the BES (V_{SOD} in Figure 4-9(b)) in this example (as specified by the clinician because in this particular patient, BES signals were very frequent and did frequently lead to an electroclinical seizure). However, it would have been possible to modify detection parameters so that these BES be detected. The algorithm detected the electroclinical seizure onset after 8 sec (V_{SOD} in Figure 4-9(c)).
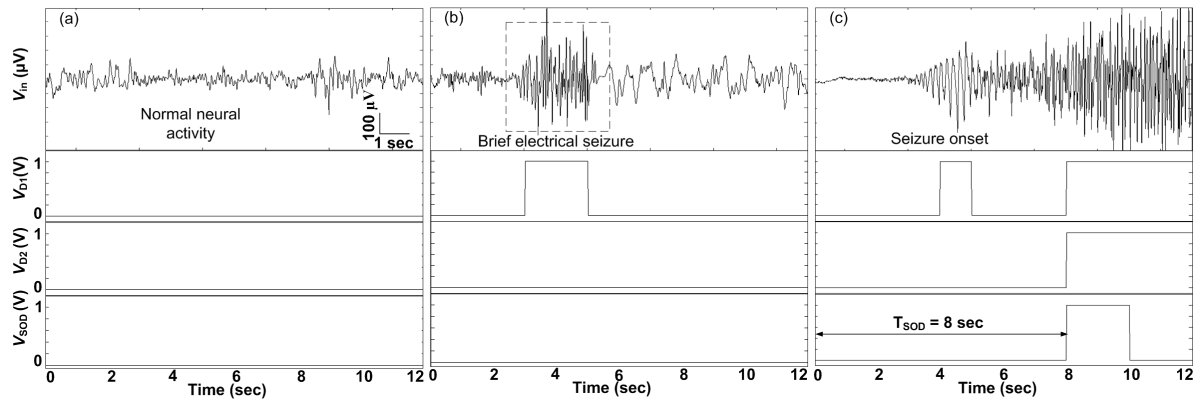
Figure 4-9: The seizure detection algorithm is validated in (a) normal signal, (b) a BES, and (c) an electroclinical seizure: V_{in} is icEEG recording from the two contacts positioned over epileptogenic zone, $V_{D1} - V_{D2}$ are abnormalities detection in VLD, and V_{SOD} is seizure detection.

Following the testing of the algorithm in Matlab, the detection circuits were constructed in Cadence software (CMOS 0.18-µm technology) and tested using the seizure recordings containing an electrical seizure quickly followed by an electroclinical seizure. Similarly, the PLCS ignored the BES (as specified by the clinician) and detected the electrographic seizure onset after 7 sec (V_{SOD} in Figure 4-10(a)).

After the testing of the seizure detection in PLCS, the detection circuits were fabricated in a microchip and tested using the same seizure recordings (Figure 4-10(b)). For this particular seizure, the microchip detected the electroclinical seizure onset after 15 sec (V_{SOD} in Figure 4-10(b)). Overt clinical manifestations for this seizure occurred approximately 30 sec after the electrographic seizure onset. Table 4-3 shows operating frequency F_s of the detector is 5 kHz to reduce the lower-frequency noises. The tunable detection parameters values and the seizure detection delays of the seizure detector are shown in Table 4-3. The seizure detection performances in Matlab, PLCS and fabricated chip differed due to the various surrounding environment. The Matlab and PLCS provide idle environment without noises effect. However, real-time test in fabricated chip includes other sources of noise (e.g. 60 Hz noise). Therefore, the threshold voltages of VLDs of a chip were always kept higher in real-time test compared to the simulation platform (Table 4-3). Moreover, PLCS and fabricated chip had 100mV dc offset in the amplified icEEG recording, thus the threshold voltages of VLDs were different from Matlab simulation.

The detectors were validated on ten more patients: no false alarm and 100% sensitivity were obtained. Overall for all patients, the device detected the electroclinical seizures after a mean delay of ~16 sec after seizure onset and before onset of overt clinical manifestations.
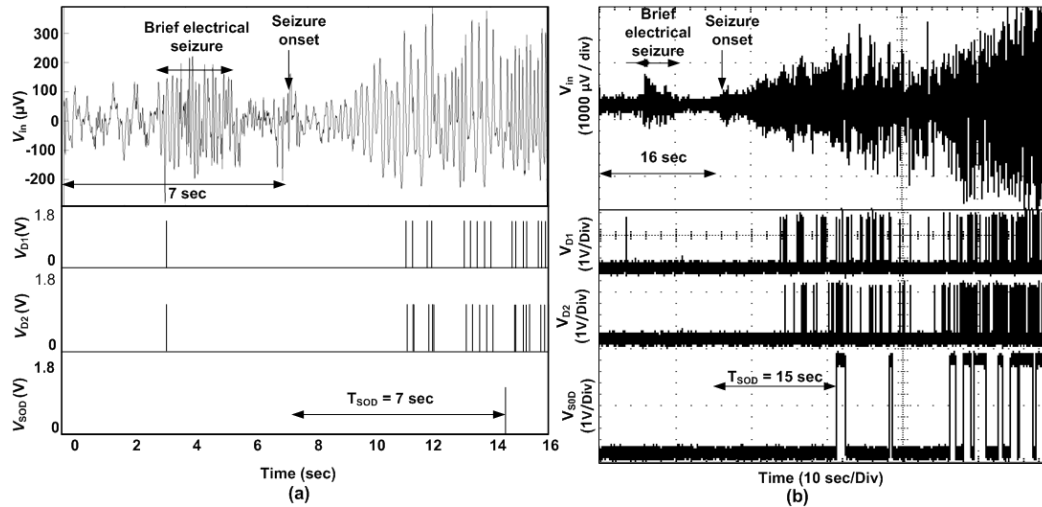
Figure 4-10: The seizure detection performance: (a) post-layout circuit simulation results and (b) fabricated chip measured results.

Table 4.3: Average tuneable parameters and detection delay (T_{SOD}) of seizure detector

Method	F_s (kHz)	$V_{1HET1,2}$ (mV)	$V_{2HET1,2}$ (mV)	T_f (sec)	T_{SOD} (sec)
Matlab	5	80, 100	100,130	3	10
PLCS*	5	197, 233	233, 270	2	9
Chip	5	210, 240	270, 300	2.5	16

*PLCS: Post-layout circuit simulation

The detection performances are compared with published different types of seizure detectors based on wavelet artificial neural network (WANN) (AZIZ, 2006), events (ESD) (RAGHUNATHAN, 2009), nonlinear Energy (NED) (PATEL, 2009), and spectral energy (SED) (VERMA, 2010) in Table 4-4. Results presented in ESD and NED are based on circuits simulation, but WANN and SED were fully integrated and results were based on animals, human and scalp EEG. The proposed detector is a fully integrated device and the experimental results

were based on icEEG recordings from different locations in the human brain. The proposed detector has maximum sensitivity and lower power consumption, and higher average detection delay, but well before overt clinical manifestations in all patients. Moreover, proposed detector shows promising improvement in hardware cost. Table 4-4 shows comparison of normalized hardware cost of the competitive detectors. The normalized hardware cost is defined by Eq. (4.1).

$$Normalized \ Hardware \ \cos t \ = \ \frac{1}{2} \left(\frac{PC_D}{PC_{max}} \ + \ \frac{A_D}{A_{max}} \right) \qquad (4.1)$$

where, PC_D and PC_{max} are power consumption of a detector and maximum consumption of the compared detector, respectively. A_D and A_{max} are area on a detector and maximum area on the compared detector, respectively. The algorithm ESD, NED and SED had lower sensitivity because the algorithms often detected brief high frequency bursts as seizures, but did not detect the seizure onset characterized by progressively increases low-voltage fast activity. Moreover, if the detection parameters of ESD, NED and SED methods were adjusted to low-voltage fast activity seizure onset, the methods detected low amplitude physiological rhythms and other similar activity. These algorithms do not have specific boundaries to distinguish an electrographic seizure onset from brief electrical seizures or other physiological rhythms. Therefore, the proposed algorithm were introduced several effective detection parameters that create several decision boundaries and reduce the number of false detections for the patient's specific seizure onset pattern while enhanced the sensitivity. Figures 4-11 (a) – (c) show time-amplitude (V_{MA}) and time-frequency (f_{Si}) analysis of a train data V_{in} that extract patient's specific detection parameters ($V_{iHET1,2}$ and f_{SZ}) and draw several detection boundaries (Figure 4-11(d)) such as normal neural activity, low-voltage fast activity, slow spike wave, brief electrical seizure, artifact, and progressive amplitude increase. Later, continuous icEEG recording with other five seizures was fed into the detector and Figure 4-11(d) shows that all seizure onsets were located inside the detection boundaries without having false detection. Therefore, the proposed algorithm has high detection sensitivity and avoids false detections of interictal spikes and polyspikes, movement artifacts, physiological rhythms (e.g. sleep spindles), and brief asymptomatic high frequency voltage activities or very brief electrical seizures.

Table 4.4: A competitive comparison of different types of seizure detectors

Reference	AZIZ, 2007	RAGHUNATHAN, 2009	PATEL, 2009	VERMA, 2010	This work
# of subject	1(animal)	6 (animal)	13 (Human)	16 (Human)	10 (Human)
Sensitivity	N/A	95% (sim[a])	94% (sim[a])	93% (sim[a])	100% (mea[b])
Detection delay	N/A	8.5 sec	N/A	8.2 sec	16 sec
Chip area (cm^2)	351μ	N/A	N/A	62.5m	20m
Power consumption	23 μW	350nW	2.7 μW	63 μW	44.8 nW
Normalized Hardware Cost	0.18	N/A	N/A	1	0.16
Process	0.35-μm	180-nm	0.13-μm	0.18-μm	0.18-μm

[a]sim: Simulation results and [b]mea: Measured results
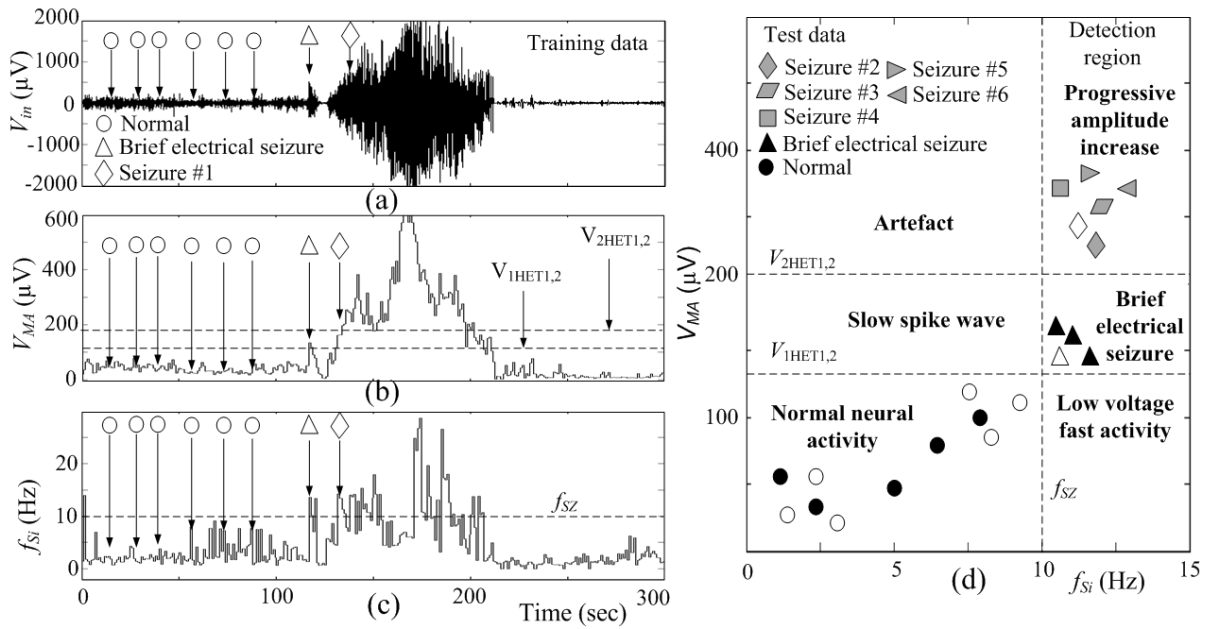
Figure 4-11: Illustration of proposed seizure detection performance: (a) – (c): Analysis on training data V_{in} and detection parameters ($V_{iHET1,2}$ and f_{SZ}) setting from patients' specific seizure patterns, and (d) Decision boundaries formation using $V_{iHET1,2}$ and f_{SZ} and test detection performance using other 5 seizures, 3 brief electrical seizures and 5 normal activities.

Neuropace Inc. has seizure detection in responsive neurostimulator (RNS) system. The detection algorithm of RNS system is based on data reduction (line length function and area under

the curve) and feature extraction (half wave analysis). However, the proposed seizure detection is based on noise reduction (modulation), feature extraction (amplitude levels detection), and data reduction (demodulation). The detection criteria of RNS system are based on high frequency tracking of amplitude variations in icEEG recording, but the proposed algorithm detects progressive increase of high-frequency signal in icEEG. In addition, hardware description, total power dissipation and detection performance of the RNS system are unknown.

4.4.3 Validation of electrical stimulation

The effective bipolar stimulation was administered to cadaveric animal brain tissue in response to the early detection of seizure development. The stimulation parameters (I_{STIM}, T_1, T_2, T_3, and T_4) are widely programmable. Figure 4-12(a) shows that the range of stimulation current in spice simulation platform and experiment. Figure 4-12(b) shows self-triggering of a burst of biphasic stimulation in response to the detection of a seizure and illustrates the corresponding individualized parameters.
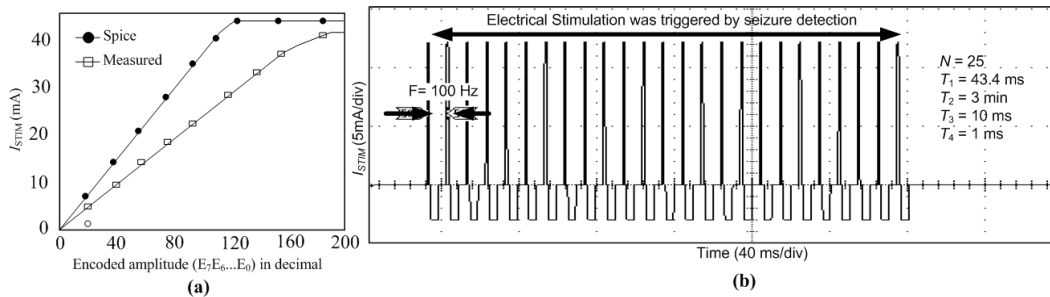
Figure 4-12: Measured and simulation results of electrical stimulator: (a) Output current of the stimulator for binary encoded amplitude and (b) Measured electrical stimulation triggered by seizure detector.

4.4.4 *In vitro* voltage distribution

The goal of this study was to quantify the electric field in the surrounding tissue during biphasic current stimulation using different parameters. In vitro experiments, the seizure detector triggered bipolar stimulation on brain tissue that generated spatial voltage distribution around the subdural electrodes. The maximum voltages were recorded under the active electrode (V_{Elect}) and the voltage distributions decayed non-linearly as a function of distance from the active electrode.

Figure 4-13 demonstrates a substantial voltage drop across the electrode–brain interface due to the double-layer phenomenon. The V_{Elect} was increased with the stimulation current and the voltages generated in the surrounding medium varied as function stimulation parameters.
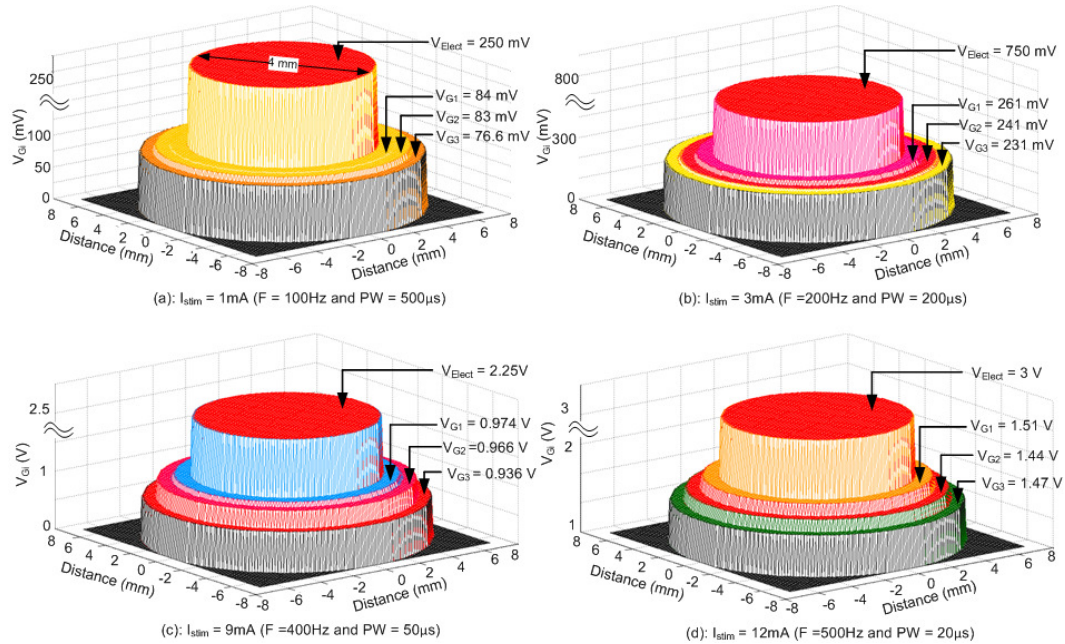
Figure 4-13: Current-controlled stimulus waveforms (1 – 12 mA, 100 – 500 Hz, and 100-500 μsec pulse width) were applied on the brain tissue and individual voltage recordings plotted against the distance from the microelectrode tips around the active subdural strip electrodes: (a) – (d) Spatial maps of the voltage distribution in brain when stimulated by 1 – 12 mA

The spatial voltage distribution, as a function of different stimulation parameter settings (i.e. frequency, pulse width and current amplitude), was recorded from the cortical surface and underneath. Figures 4-14 (a)-(c) show the spatial maps as a function of stimulation pulse width and frequency. The spatial voltage distributions remained constant for low amplitude current stimulation (Figure 4-14(a)), but the distributions were inversely proportional to pulse width for high amplitude current stimulation (Figure 4-14(b)). However, the distributions at high amplitude stimulation increased progressively with frequency (Figure 4-14(c)) while the distributions resulting from low current stimulation remained almost constant (not shown in this figure).
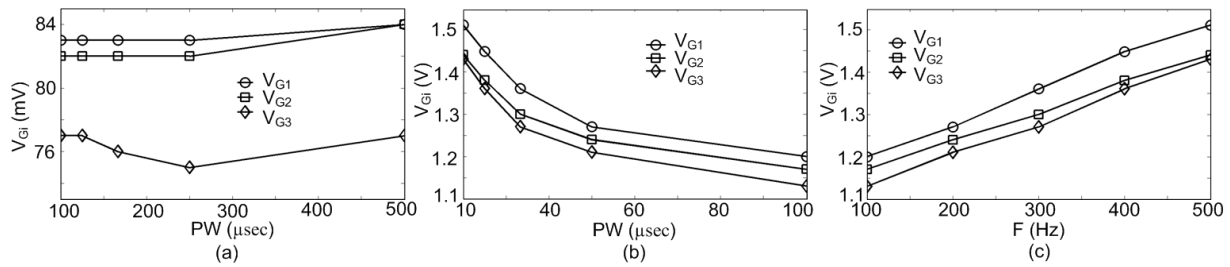
Figure 4-14: Voltage distribution resulting from biphasic current stimulation: (a) Low-amplitude current (1mA) at 100 – 500 µsec pulse width, and high-amplitude current (12mA) at 10 – 100 µsec pulse width (b) and 100 – 500 Hz frequency (c).

Constant-current stimulation generated various voltage distributions as a function of the stimulation parameters. Thus, an electric field can be predicted to desynchronize a group of neurons process at variable distance. Figure 4-15(a) shows variation V_{G3} with different stimulation parameters. The V_{G3} increased slowly resulting from low frequency stimulation parameters (high pulse width and low frequency). However, V_{G3} increased linearly with stimulation current at high-frequency stimulation parameters (low-pulse width and high frequency). The bipolar stimulation at low frequency parameters increased impedance of gray matter (R_{GM} and C_{GM} in Figure 4-7(b)) that causes significant shunting of current through the CSF and voltage distribution (V_{G3} did not increase linearly with stimulation current). On the other hand, high-frequency stimulation parameters decreased impedance of gray matter and reduced shunting of current through the CSF. Therefore, V_{G3} increased linearly with stimulation current at high frequency. Figure 4-15(b) illustrates applied stimulating charge density ($\delta_C = I_{stim} \times T_4$ / Area of electrode) per phase due to the stimulation parameters used in Figure 4- 15(a). The high-frequency stimulation parameters required a lower stimulating charge compared to low-frequency stimulation parameters (Figure 4-15(b)). At the higher frequency stimulation, most of the applied charge went through the gray mater and only a small amount of the charge was shunted through the CSF. Thus, the higher frequency stimulation parameters generated higher voltage distribution with lower applied charges. Intuitively, the high frequency stimulation parameters appear more suitable for affecting an epileptogenic zone at least in a radius of 3 mm.
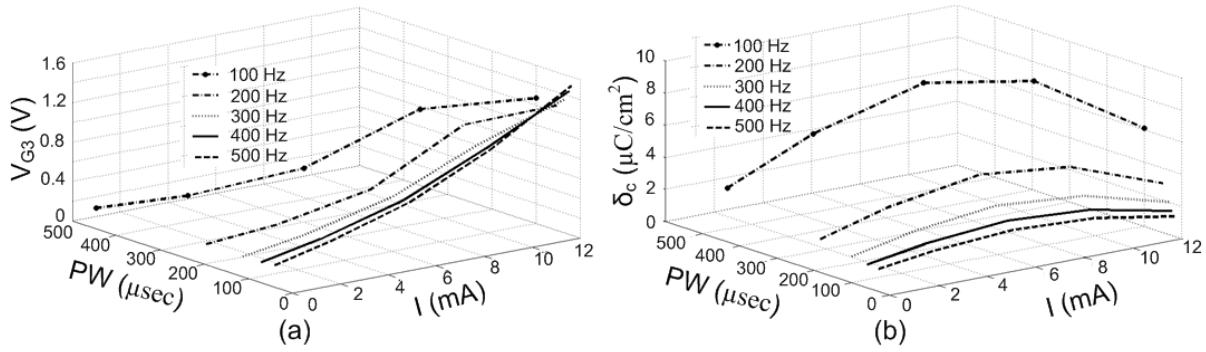
Figure 4-15: 3D plot of voltage distribution at 3 mm distance and charge density per phase resulting from current-controlled bipolar stimulation settings.

4.5   CONCLUSION

In this article, we describe a close-loop seizure detector and neurostimulation device, which records signal from cortical regions, modulates recorded icEEG, amplifies the signal till the desired amplitude level, extracts abnormal activity information using voltage level detectors, demodulates the signal to the original frequency, detects seizure frequency by dedicated circuits and administrates individualized electrical stimulations. Most of signal processing is done in the digital domain, while analog signal processing is accomplished by imposing the signal in high frequency in order to isolate the instrumentational low-frequency noise. Analysis and comparison of the seizure detection performances in different platforms were presented. The overall test performance using seizure icEEG recording from ten patients with refractory epilepsy showed early detection of electroclinical seizure onsets. Efficiency of the stimulator has demonstrated on cadaveric animal brain tissue, and spatial voltage distribution was depicted as a function of electrical stimulation parameters.

4.6   ACKNOWLEDGMENTS

CHAPTER 5   IMPLANTABLE DRUG DELIVERY SYSTEM

Following the discussion on the closed-loop electrical stimulator in chapters 3 and 4, this chapter presents another alternative promising implantable device therapy: direct drug injection. A new power saving strategy is employed to design a direct drug delivery device. This chapter presents a new preamplifier, an asynchronous seizure onset detector, a drug delivery system, and hybrid subdural electrodes. The experimental results demonstrate the efficiency of the device and wide range of drug dosing capabilities at seizure onset. The content of this chapter is an manuscript that will appear in the "IEEE Transactions on Neural Systems and Rehabilitation Engineering" and it is reproduced in following pages.

5.1   AN IMPLANTABLE CLOSED-LOOP ASYNCHRONOUS DRUG DELIVERY SYSTEM FOR THE TREATMENT OF REFRACTORY EPILEPSY

Muhammad Tariqus Salam[1], Marjan Mirzaei[1], My Sandra Ly[1], Dang Khoa Nguyen[2], and Mohamad Sawan[1]

[1]Polystim Neurotechnologies Laboratory, École Polytechnique de Montréal, Québec, Canada

[2]Notre-Dame Hospital, Centre Hospitalier de l'Université de Montréal (CHUM), Québec, Canada

Abstract – In this paper, we present an implantable device for intra-cerebral electroencephalography (icEEG) data acquisition and real-time epileptic seizure detection with simultaneous focal antiepileptic drug injection feedback. This implantable device includes a neural signal amplifier, an asynchronous seizure detector, a drug delivery system (DDS) including a micropump, and a hybrid subdural electrode (HSE). The asynchronous detection

algorithm is based on data-dependent analysis and validated with Matlab tools. The detector and DDS have a power saving mode. The HSE contacts are made of Platinum (Pt) encapsulated with polydimethylsiloxane (PDMS). Given the heterogeneity of electrographic seizure signals and seizure suppression threshold, the implantable device provides tunable parameters facility through an external transmitter to adapt to each individual's neurophysiology prior to clinical deployment. The proposed detector and DDS were assembled in Ø 50 mm and Ø 30 mm circular printed circuit boards, respectively. The detector was validated using icEEG recordings of 7 patients who had previously undergone an intracranial investigation for epilepsy surgery. The triggering of the DDS was tested and a predefined seizure suppression dose was delivered ~16 sec after electrographical seizure onsets. The device's power consumption was reduced by 12% in active mode and 49% in power saving mode compared to similar seizure detection algorithms implemented with synchronous architecture.

Index terms – Epilepsy, seizure detection, focal drug delivery.

5.2 INTRODUCTION

Interest has grown recently in emerging prosthetic therapies for conventionally-untreatable neurological conditions, such as epilepsy (TERRY, 2009), Parkinson's disease (SARMA, 2010), depression (PENESCU, 2005), and motor impairments (CELIK, 2010). Researchers are exploring the brain-machine interface to translate physiological activity and neuromodulation into machine language for therapeutic purposes. Brain signal monitoring, clinical state analysis and low-power dissipation in prosthetic devices for long-term treatment are key challenges for emerging prosthetic therapies. Epilepsy, which affects approximately 60 million people worldwide, is the second most common chronic neurological condition. It is characterized by a predisposition to unprovoked recurrent seizures. Despite the existence of a number of anticonvulsants, ~30% of patients continue to have disabling seizures. Half of them may benefit from epilepsy surgery if the epileptogenic zone (EZ) can be identified and resected without harm. Others, however, are not good surgical candidates. Due to the limited spatial or temporal resolution of currently available non-invasive localization techniques, accurate delineation of the EZ may sometimes be arduous, particularly in patients with non-lesional refractory epilepsy (JEROME, 2009; SPENCER, 2009). Moreover, many patients have an extensive area of

epileptogenicity, multifocal epileptic foci, or an EZ overlying eloquent areas (language, primary motor or visual regions) that cannot be resected without permanent sequelae (SPENCER, 2009). Hence, there is a need for alternative treatment modalities.

Proof-of-principle experiments conducted in animals and humans with epilepsy have demonstrated the safety of successful chronic electrical stimulation (RYCHLICKI, 2006; THEODORE, 2004; BOON, 2009), focal pharmacological manipulations (GOOD, 2004; STEIN, 2000), and thermal cooling (GUERRA, 2005) for the treatment of epilepsy. Much progress has been made with focal electrical stimulation therapy methods. Neuropace Inc. has developed a closed-loop-responsive neurostimulator (RNS) that records intra-cerebral electroencephalographic (icEEG) signals, analyzes them and triggers electrical stimulation only upon seizure detection. Preliminary results of electrical stimulation therapy are acceptable, but many patients do not respond to the stimulation and continue have disabling seizures (SUN, 2008; SKARPAAS, 2009; SALAM, 2010(a)).

Focal drug delivery has shown promising seizure suppression results (BOON, 2009; STEIN, 2000). Direct drug injection onto the epileptogenic zone could enhance the efficacy of medication while limiting side effects to a minimum. Table 5-1 shows drugs and doses used in pilot trials. Maximum safe tolerated dose was 150 µL per 20 min for a rat (STEIN, 2000). Two main approaches have been described for focal drug delivery: open-loop and closed-loop. The open-loop approach has been used to increase seizure threshold through continuous drug release while the closed-loop drug delivery system (DDS) is meant to release the drug only upon a seizure detection (STEIN, 2000). The advantages of closed-loop drug delivery over the open-loop method are (i) lower drug dose injection, (ii) potentially less adverse effects, and (iii) rapid focal drug injection. However, several issues of closed-loop systems remain to be addressed, such as

Table 5.1: Pilot studies on focal drug delivery therapy

Drug	Therapy	Dose	Result
Diazepam (STEIN, 2000)	Closed-loop	35-50 µL	Seizure supression
pH-balenced vehicle (STEIN, 2000)	Closed-loop	35-50 µL	Seizure number reduction
Adenosian (ANSCHEL, 2004)	Open-loop	750 µL	Seizure prevention
Lidocaine (SMITH, 1993)	Open-loop	5 µL	Seizure severity reduction
Gabapentine (OOMMEN, 2007)	Open-loop	N/A	Seizure threshold increment

the sensitivity and specificity of seizure detection and device power consumption.

Good quality icEEG recording and effective automated seizure detection are obviously necessary for any closed-loop system. Over the past few decades, several seizure detection mathematical models have been developed, with support vectors (MEIER, 2008), artificial neural networks (GHOSH-DASTIDAR, 2008), wavelet transformation (ZANDI, 2010), wavelet decomposition (SAAB, 2005), nonlinear time series analysis (LEHNERTZ, 1995), and mean nonlinear decision function (TITO, 2009). These complex mathematical models are meant to be run on high-speed desktop computers for off-line, long-term data processing to help clinicians find seizures but can hardly be employed in low-power implantable devices. Later, several implantable seizure detectors have been described in the literature on closed-loop epilepsy prostheses (SALAM, 2009(a); RAGHUNATHAN, 2009; SALAM, 2009(b); PATEL, 2009; SALAM, 2010 (b); VERMA, 2010; SALAM, 2010(c); SALAM; 2011(c)). Power management is an important issue for these detectors. Power consumption is mainly dependent on signal transitions in a device, such as charging and discharging of parasitic capacitances in transistors and short-circuit currents during switching (NIELSEN, 1999). Thus, power consumption can be reduced by avoiding unnecessary signal transitions (NIELSEN, 1999). With synchronous designs (SALAM, 2009(a); RAGHUNATHAN, 2009; SALAM, 2009(b); PATEL, 2009; SALAM, 2010 (b); VERMA, 2010; SALAM, 2010(c); SALAM; 2011(c)), all components share a common clock signal distributed throughout the circuit, and unnecessary signal transitions arise from clock gating. Because of these limitations in conventional synchronous circuit design, the asynchronous design technique is likely to become more popular. An asynchronous device is fundamentally different, and device transistors do not change their transient state unless an event happens. This device does not use or share a common clock; thus, it has no clock skew and no clock tree.

In the following parts, we will describe methods and materials in Section II and results in Section III. Conclusions are summarized in the last section of this paper.

5.3   METHODS AND MATERIALS

5.3.1 Proposed closed-loop epilepsy prosthesis

The proposed closed-loop epilepsy prosthesis would benefit the patients with focal epilepsy with or without secondary generalization who are not controlled and report significant side effects with oral antiepileptic drugs, especially those whose epileptic focus cannot be removed because it overlies an important functional area (motor, sensory, visual, language areas). This epilepsy prosthesis requires low-power, continuous, long-term icEEG monitoring to identify seizures online before the appearance of disabling clinical manifestations (e.g. altered consciousness, tonic or clonic movements). An asynchronous device has inherent properties that work locally and activate all modules, if needed. Therefore, an asynchronous design holds significant promise in icEEG recording extraction applications, where complex analyses are
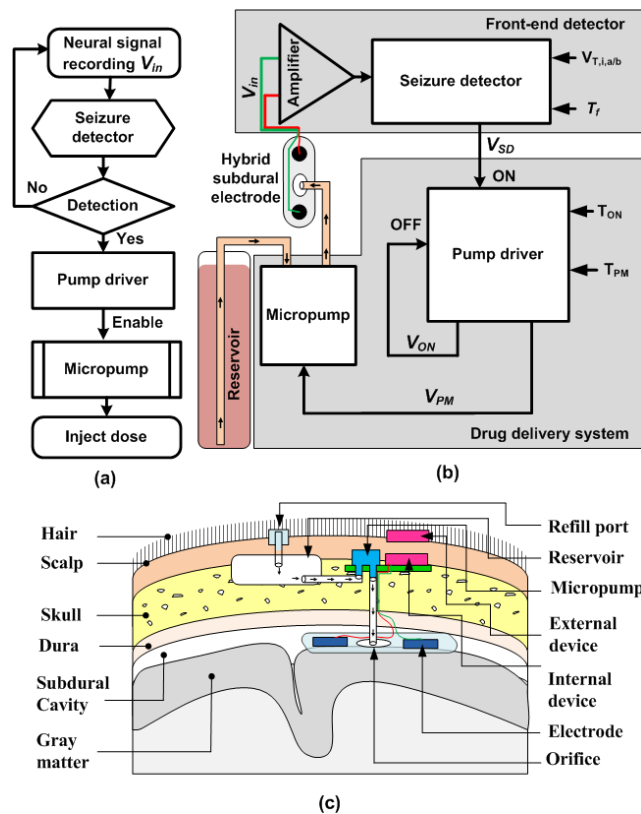
Figure 5-1: Proposed closed-loop drug delivery system: (a) Flow chart, (b) Block diagram, and (c) Implant configuration.
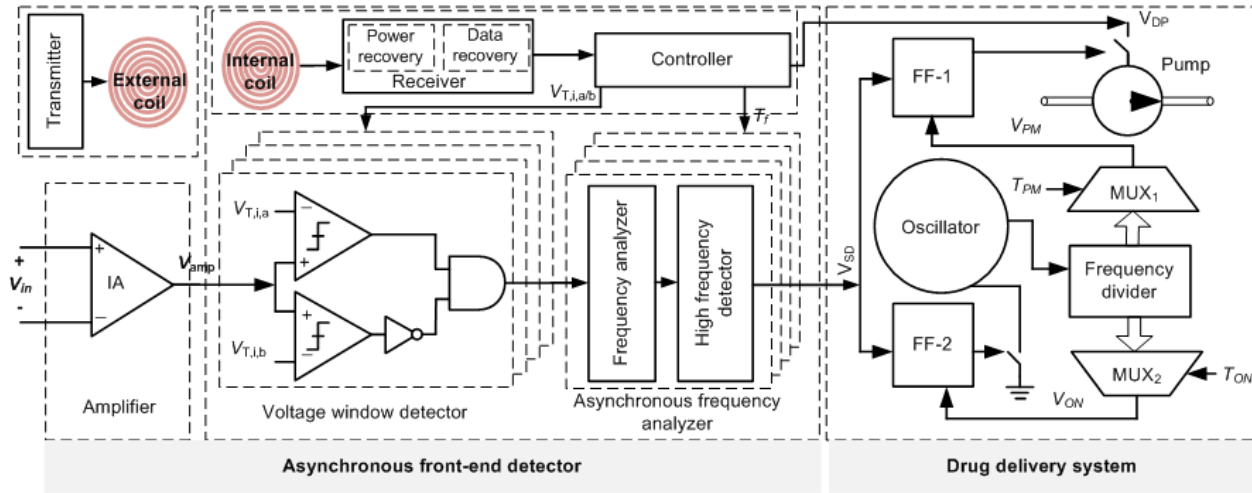
Figure 5-2: Block diagram of closed-loop asynchronous drug delivery system.

needed for a short period (e.g. seizure onset). Therefore, power management pleads in favor of an asynchronous design. In this paper, an asynchronous device is designed and implemented to improve data-dependent computation and power management.

Figure 5-1 illustrates flowchart, block diagram, and implant configuration of the proposed closed-loop drug delivery system. The refilling port is made of a microtube (Ø 1.93 mm) coated with PDMS and sealed the entry port with PDMS so that a syringe easily goes through the PDMS to fill the reservoir without having a bacteria entry point. The functional block diagram in Figure 5-2 presents the architecture of the closed-loop DDS that includes total 11 modules, such as 1 amplifier, 4 voltage level detectors, 4 asynchronous frequency analyzers, 1 receiver- controller, and 1 DDS. First, the icEEG recording V_{in} is amplified and decomposed by seizure detectors. The extracted activities define an upcoming seizure. The responsive DDS must be adjusted by setting voltages ($V_{T,i,a/b}$), time windows (T_f), and dose (drug injection period T_{PM} and micropump control voltage V_{DP}) labeled as corresponding to seizures and non-seizures. Optimum parameters are measured from time-amplitude and time-frequency analysis of 1 seizure from the EZ and normal signal activity. Clinical studies have shown that several electrographic patterns (e.g. low-voltage and high-voltage fast activities or rhythmic spiking) can be seen in EZ at seizure onset, depending on such factors as etiology, location, position of intracerebral electrodes (SPENCER, 2009; SALAM, 2010(a)). Generally, same patient-specific pattern and seizure frequency can also be

seen in EZ which lead to a clinical seizure (SALAM, 2010(a); SALAM, 2010(b), SALAM, 2010(c), SALAM, 2011(a)).

5.3.1.1 Front-end seizure detector

Synchronous epileptic seizure detection algorithms have been suggested in our previous works (SALAM, 2010(b), SALAM, 2009(b), SALAM, 2010(c)). In this paper, an asynchronous seizure detection algorithm is proposed for better power management. Table 5-2 compares the synchronous and asynchronous algorithms. Details of asynchronous front-end seizure detector are described below.

Table 5.2: Comparison of synchronous and asynchronous epileptic seizure detection algorithms

Synchronous (SALAM, 2010(b))	Asynchronous (this work)
Modulates input signals before analysis	Directly analyzes input signals without modulation
Window detection in positive amplitude	Window detection in positive and negative amplitude
Signal analysis in high frequency band	Signal analysis in original frequency band
Demodulates to original frequency band	No demodulation
Frequency divider generates time frames	External[a] device generates time frames
Clock controls frequency analysis	External device controls frequency analysis

[a]External: On top of the skin

5.3.1.2 Asynchronous epileptic seizure detection algorithm

Amplified input signal (V_{amp}) passes through voltage window detectors (VWDs), and outputs $V_{w,i}$ define the strength of neural signal activities in different amplitude windows (Eq. 5.1).

$$V_{wi} = \begin{cases} \text{'1'}, & for \quad \left| V_{T,i,a} \right| > V_{amp} > \left| V_{T,i,b} \right| \\ \text{'0'}, & for \quad otherwise \end{cases}$$

(5.1)

where i = 1, 2, 3…N. $V_{T,i,a\text{-}b}$ are the threshold voltage of VWDs.

Frequency analyzers extract $V_{w,i}$ and measure the signal frequency ($F_{S,i}$), as shown in Eq. (5.2).

$$F_{S,i} = \frac{\sum\limits_{t=0}^{t=T_f} V_{W,i}}{T_f} \tag{5.2}$$

If $F_{S,i}$ is greater than a specific seizure onset frequency (F_{SZ}), the output of each channel $V_{D,i}$ is considered fast activity (Eq. 5.3).

$$V_{D,i}(n) = \begin{cases} \text{'1'}, & for \quad F_{S,i} \geq F_{SZ} \\ \text{'0'}, & for \quad otherwise \end{cases} \tag{5.3}$$

Seizure detection logic analyzes $V_{D,i}$ and quantifies specific features characterized by a progressive increase in amplitude and signal frequency. Thus, a seizure onset is declared on the basis of the following conditions (Eq. 5.4).
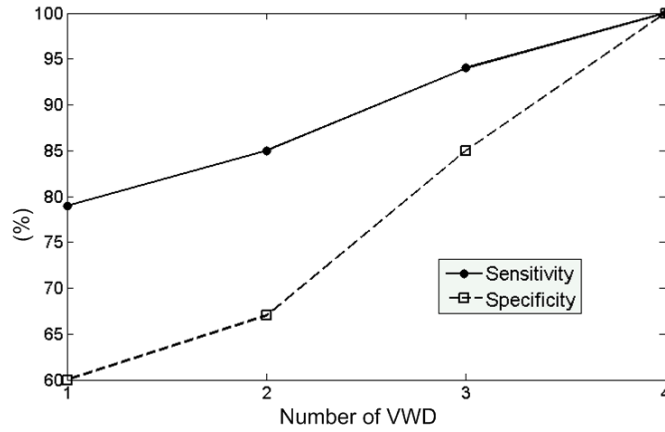
Figure 5-3: Asynchronous seizure detection performance analysis using optimum parameters of different VWDs based on 5 seizures and long normal icEEG of the test patient.

$$V_{SD} = \begin{cases} \text{'1'}, & for \quad V_{D,1}. \; V_{D,2}. \; V_{D,3}... \; V_{D,N} = 1 \\ \text{'0'}, & for \qquad\qquad otherwise \end{cases} \tag{5.4}$$

$V_{T,i,a\text{-}b}$ and T_f are tuned to the patient's specific F_{SZ} to minimize false alarms. The parameters can optimize the decision boundary and enhance sensitivity and specificity. Figure 5-3 shows maximum detection performance using 4 VWDs (2 VWDs monitor basal activities and the other 2 VWDs detect epileptic activities).

5.3.1.3 Asynchronous front-end detector

Figure 6-2 shows block diagram of the asynchronous front-end detector (AFED). The detector contains a neural signal amplifier, an asynchronous seizure detector, a controller and a receiver. Details are described below.

5.3.1.3.1 Amplifier

The icEEG recording is generally characterized by low-amplitude signal (microvolts) and low-frequency bandwidth. Moreover, the instrumentation amplifier has relatively poor noise performance for amplifying the low spectral microvolt-level signal due to the flicker and thermal noise. Thus, icEEG signal must be amplified very carefully before further analysis (e.g. detection, digitization). The proposed neural signal amplifier has 3 stages for amplification and noise reduction (Figure 5-4(a)) (SALAM, 2011(a)). A feedback noise reduction circuit reduces DC offset V_{OS} (Figure 5-4(b)). Furthermore, flicker noise V_{nF} and thermal noise V_{nT} are reduced by high- and low-pass filters (Figure 5-4(b)). The amplifier features high-amplification gain: 60 dB and 48 Hz (3 Hz to 51 Hz) bandwidth (Figure 5-4(c)) with 6 µVrms input-referred voltage noise. Figure 5-4(d) shows measured input-referred noise voltage spectral densities of the proposed and commercial amplifier.

5.3.1.3.2 Asynchronous seizure detector

The detector comprises 4 VWDs and 4 asynchronous frequency analyzers. The VWDs have 8 tunable parameters to adjust their threshold voltages ($V_{T,i,a-b}$). Asynchronous frequency analyzers detect high-frequency events by analyzing neural activities in T_f, which can be tuned externally and configured to the specific seizure onset frequency (F_{SZ}) of a patient to reduce false alarms during icEEG monitoring.

5.3.1.3.3 Controller

The proposed seizure detector allows to tune several parameters that are personalized in a specific manner to prevent false seizure detection. The controller includes 8 digital-to-analog
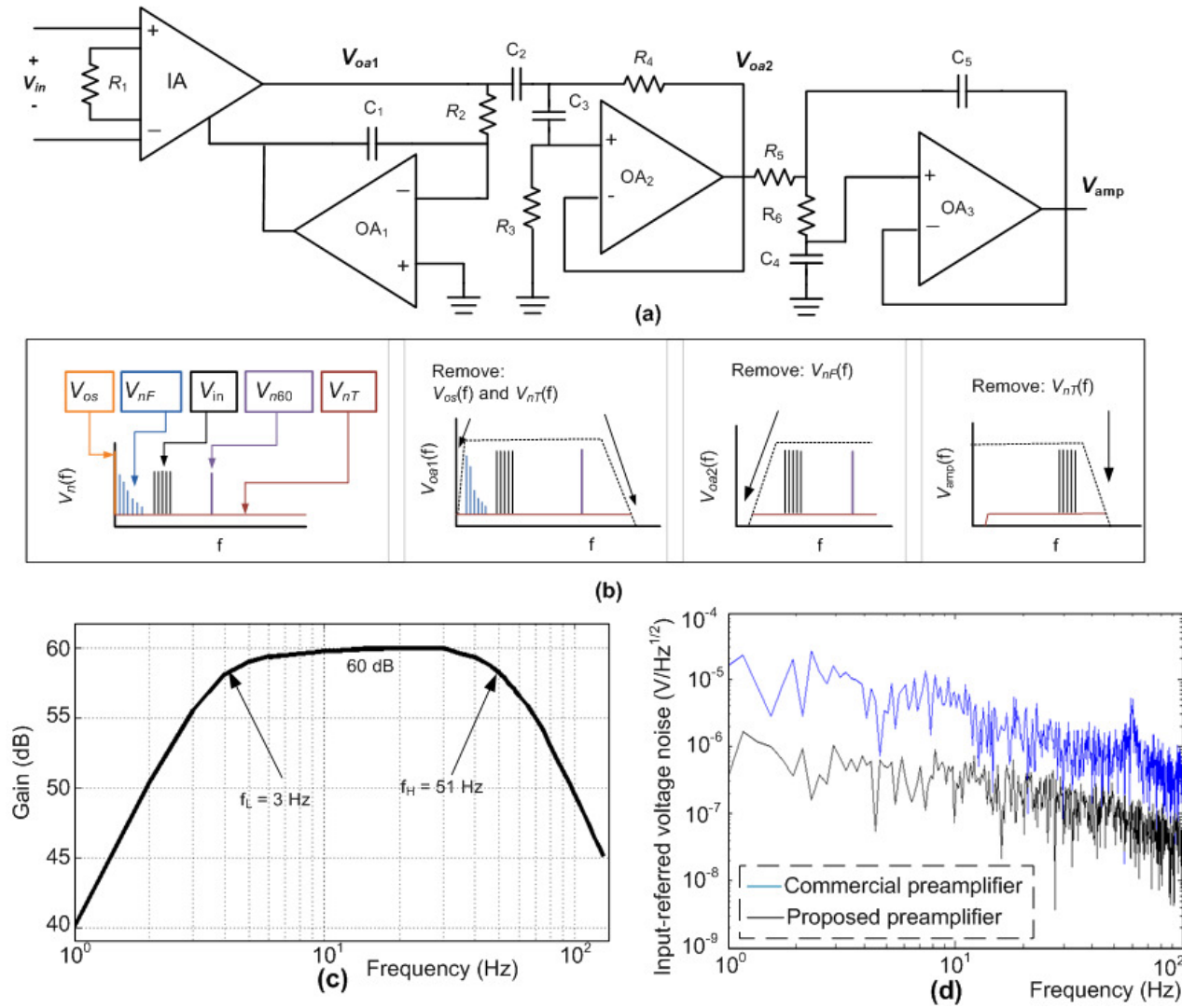
Figure 5-4: Neural signal amplifier: (a) Schematic diagram of amplifier, (b) Noise reduction method and corresponding frequency analysis of signals in different nodes, (c) Frequency response, and (d) Measured input-referred noise voltage spectral densities of the proposed and commercial amplifier.

converters, and 8 buffers. This controller can provide digitally-controlled, high-precision voltage $V_{T,i,a/b}$ and V_{DP}.

5.3.1.3.4 Receiver

The receiver is responsible for power and data (e.g. T_f) recovery. The power recovery circuit was introduced in our previous work [35] and Figure 5-5(a) shows a schematic diagram of the data recovery. The external transmitter generates and transmits predefined T_f with inductive communication. A parallel LC network of the internal device receives T_f and controls the seizure

detector. Graphic representation of the time-frame generation in Figures 5-5 (b)-(c) shows transmitted signal pattern V_{ER} and T_f recovered from V_{RST}.
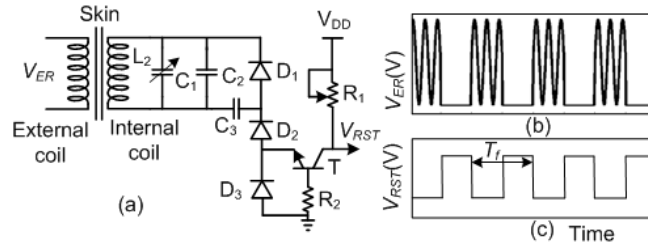
Figure 5-5: Time frame generation: (a) Schematic diagram of receiver, (b) Transmitted signal pattern V_{ER} from external coil, and (c) Recovered time frame V_{RST}.

5.3.1.4 Drug delivery system

Figures 5-6(a)–(d) illustrate the operation of the DDS and demonstrate its timing process in response to seizure detections V_{SD}. The duration of drug delivery (V_{PM}) is T_{PM}; if the injection does not terminate the seizure another dose is triggered by the detector after T_{ON}. V_{PM} generates
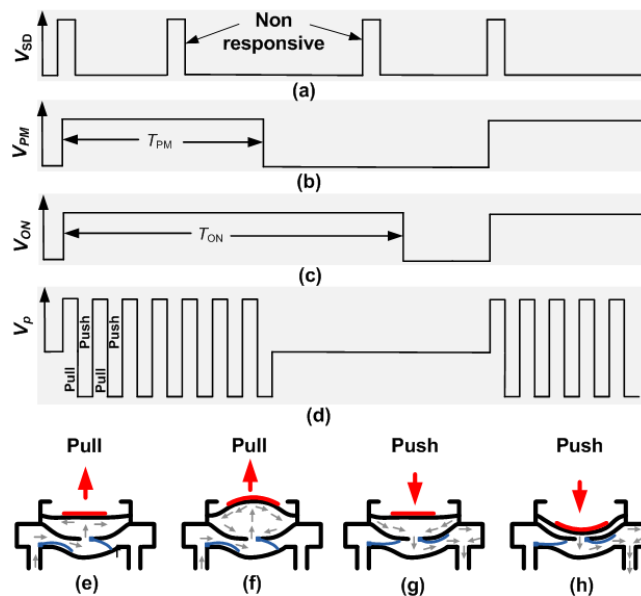
Figure 5-6: Proposed drug delivery system: (a) Seizure detections V_{SD} (b) Drug injection period T_{PM}, (c) Focal treatment duration T_{ON}, (d) Two subsequent drug injections, and (e) – (h): Operation of micropump.
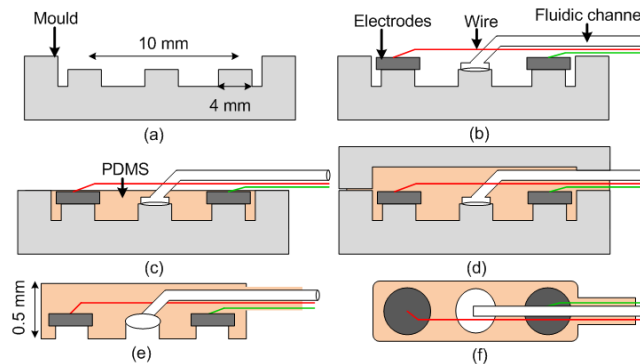
Figure 5-7: Hybrid subdural electrodes fabrication process: (a) Dimension of mould; (b) Electrode, wire and fluidic channel assembly on mould; (c) Pour PDMS; (d) Cover up and heating with 110°C; (e) Side view of the released subdural electrodes; and (f) Top view of the electrodes.

V_P push-pull signal in the micropump (13 x 13 x 5 mm^3) (Microbase technology Corporation) to drive the drug.

5.3.1.5 Hybrid subdural electrodes

The electrodes fabrication process includes mould fabrication, electrodes assembly, and biomedical grade polydimethylsiloxane (PDMS) encapsulation. The mould was fabricated on an Aluminum substrate (Figure 5-7(a)) using a computer numerically controlled machine. Electrodes (Platinum), wires (Platinum) and fluidic channel (Micro-tube: Ø 0.5 mm) were assembled on the mould (Figure 5-7(b)). PDMS is poured (Figure 5-7(c)) and the covered mould was heated to 110°C for 20 minutes (Figure 5-7(d)). Once subdural electrode arrays become encapsulated with a thin PDMS substrate, they are released from the mould (Figures 5-7 (e) – (f)).

5.3.2 Circuits and devices implementation

The closed-loop DDS was assembled with discrete commercial components on circular shape printed circuit boards (PCB). Figures 5-8 (a) – (c) show photographs of the asynchronous front-end detector. Photographs of the drug delivery system and hybrid subdural electrodes are presented in Figures 5-8 (d) – (f).
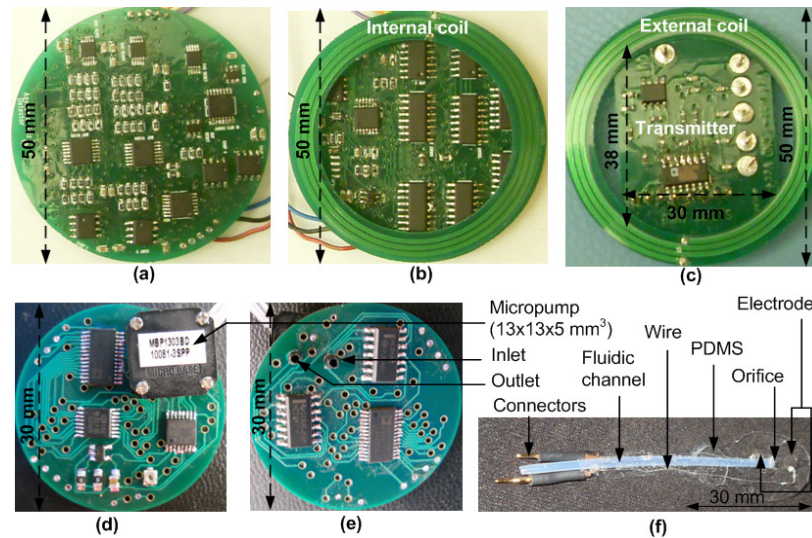
Figure 5-8: Proposed closed-loop drug delivery system: (a) – b) Top and bottom views of asynchronous front-end detector, (c) External transmitter, (d)–(e) Top and bottom views of drug delivery system, and (f) hybrid subdural electrodes.

5.3.3 Patients description

This study was conducted at Notre-Dame Hospital, Centre Hospitalier de l'Université de Montréal (CHUM). Seven patients with refractory focal epilepsy (age 15 to 49 years) were qualified for these studies based on electrographic seizure onset. The selected patients had previously undergone a comprehensive noninvasive assessment of brain. These complementary non-invasive studies failed to adequately localize the epileptogenic zone and invasive intracranial electrode studies were required to delineate with more precision the EZ. The seizure signals of cases 1, 4, 5, 6 and 7 were recorded using depth electrodes and the signals of cases 2 and 3 were recorded using subdural strip electrodes. These patients had seizure onsets characterized by progressive increase of low-voltage fast-activity in icEEG recordings. These patients also had frequent electrical seizures on the EZ. There is no consensus on what constitutes an appropriate definition of electrical seizure apart from the fact that they do not generate any clinical manifestations (BABB, 1984; GOTMAN, 1985). Some electrical seizures are simply very brief (a few seconds), focal (without spread) high-frequency discharges which do not evolve significantly in time or frequency, and are hence clinically silent. Others are longer (several seconds) with some evolution.

5.3.4 Device validation method

The proposed implantable device was tested offline using icEEG recordings obtained from the 7 patients. The experimental procedure was approved by the University of Montreal's Hospital Center (CHUM) and Polytechnique Montreal research ethics committees. Figure 5-9 shows the proposed device validation procedure. These icEEG studies consist in implanting electrodes into or on the surface of the brain through a craniotomy or burr holes under general anaesthesia. After intracranial electrode implantation, patients are transferred to the Epilepsy Monitoring Unit for continuous video-EEG telemetry to record seizures. 128 channel icEEG recordings were performed using amplifiers (PRO-36 amplifiers, Stellate Harmonie System) at 200 Hz and 2000 Hz sampling frequency.
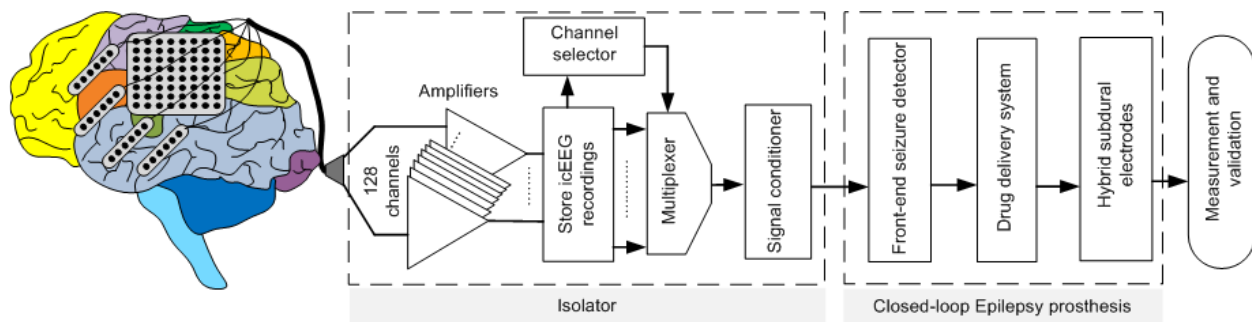
Figure 5-9: The closed-loop epilepsy prosthesis: icEEG recorded from patients with medically refractory epilepsy were used to test the proposed seizure detector and the triggering of predefined drug dose was validated.

Post-implantation MRI served to reconstruct 3-D representation of electrode positioning (via Stellate's Gridview software) (Figure 5-10). During the invasive study, several brief electrical seizures and electroclinical seizures were recorded and marked by an epileptologist (DKN). All the seizures were found to originate from the red circle-marked electrodes in Figure 5-10 with subsequent rapid spread to square-marked electrodes and then propagation to triangle-marked electrodes. Figure 5-9 illustrates that the icEEG recordings from the two contacts positioned over the epileptogenic zone (Figure 5-10) were selected, transferred to the signal conditioner (arbitrary signal waveform generator) for reproducing icEEG recording and fed into the closed-loop epilepsy prosthesis. The reproduced microvolt-level icEEG recordings were amplified by the amplifier of

the AFED and processed for the seizure detection. The AFED detected seizure onset and triggered the DDS to deliver a predefined drug dose through the hybrid subdural electrodes. During the drug injection, the delivered drug was measured to validate the seizure suppression doses (Table 5-1).
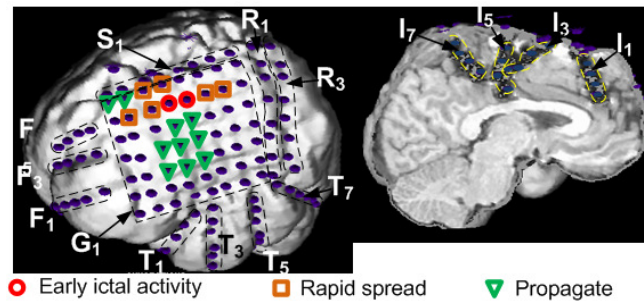
Figure 5-10: Invasive study: 3-D images of implanted electrodes reconstructed with Stellate's Gridview software and identification of epileptogenic zones.

In order to justify the effectiveness of the proposed responsive device, all the seizures were observed during the experiments and analyzed all channels to determine seizure progression and propagation. Figure 5-11 shows typical electrographic seizures as recorded from the electrode contacts in the epileptogenic zone as well as nearest adjacent functional regions. Based on video-EEG analysis of this seizure, the epileptiform discharges propagated slowly to the nearest functional region (22 sec) and patient reported feeling an aura 33 sec after the electrographic seizure onset. Altered consciousness occurred a few seconds later. This propagation time varied from patient to patient. In this experiment, the minimum propagation time is 22 sec in case 1
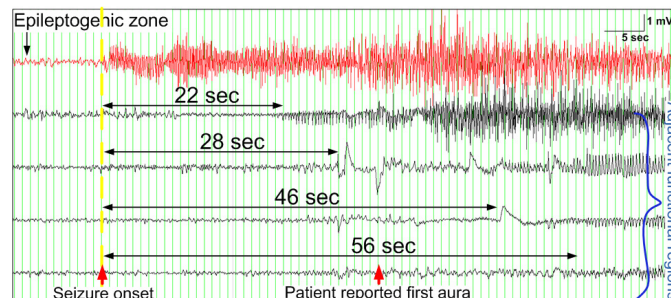
Figure 5-11: The icEEG recordings from the epileptogenic zone as well as adjacent functional regions and the corresponding behavioural relation with the electro-graphical signals.

(worst case scenario) and the maximum time is 110 sec in case 7 (worst case scenario). Furthermore, the pilot studies have shown epileptiform activities suppression within 5 sec due to the 35-50 µL Diazepam drug injection on epileptogenic zone during an electrographic seizure (STEIN, 2000). Therefore, the key challenges for an automated drug delivery system are to detect seizure onset and deliver drug on epileptogenic zone before the epileptiform discharges propagating to others adjacent functional areas.

5.3.5 Prosthesis pre-implantation procedure

A prosthesis pre-implantation procedure was introduced to observe patients' specific neurophysiology properties and configure the AFED and DDS. Ictal discharges from patients generally contained high-frequency activities, but not all high frequency discharges were seizures (i.e. some were physiological rhythms). Moreover, patients presented frequent, brief, low-voltage, high-frequency discharges without clinical manifestations (reminiscent of very Brief electrical seizures - BES) which our clinician choose to ignore. As these discharges did not frequently evolve into longer electro-clinical seizure, they were overlooked to prevent the triggering of non-clinically useful responsive drug deliveries that could rapidly deplete battery life and drug reserve. Hence, it was decided to configure the AFED to ignore these brief discharges. For proper AFED configuration, a normal signal, 2 BESs and an electro-clinical seizure from a patient were analyzed in the time-amplitude V_{MA} (root mean square) and time-frequency F_S domain. The obtained detection parameters from these training signals were used to adjust the AFED and consequently it detected the other seizures of the patient.

Figure 5-12 depicts the analysis of 30 minutes of icEEG recording to demonstrate optimum selection of the seizure detection parameters (i.e. F_{SZ} in Figure 5-12(b) and $V_{T,\text{i,a/b}}$ in Figure 5-12(c)). Signal analysis of normal icEEG recordings V_{in} revealed no abnormalities in F_S and V_{MA} which define basal activity ($|V_{T,2/3,\text{a}}|$). Brief high-frequency discharges or BES had high frequency contents in F_S with limited amplitude increase ($|V_{T,2/3,\text{b}}|$) in V_{MA}. Analysis of an electro-clinical seizure onset demonstrated a sudden increment in F_S with a progressive amplitude rise ($|V_{T,1/4,\text{a/b}}|$) in V_{MA} leading to clinical manifestations. Clinicians could set these parameters by visual inspection, but the pre-implantation procedure optimizes the tradeoff between detection delay and performance (i.e. sensitivity and specificity).
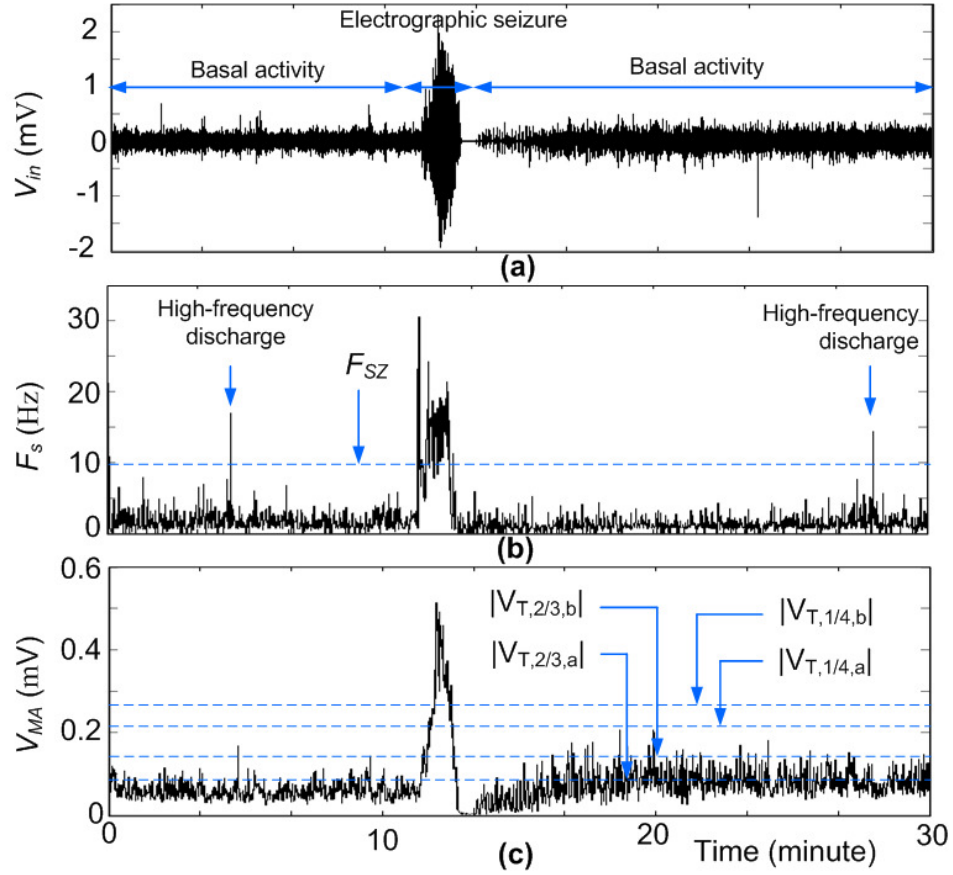
Figure 5-12: Prosthesis pre-implantation settings: (a) Training data V_{in} and (b) – (c): adjustment detection parameters F_{SZ} and $V_{T,i,a/b}$ from time-frequency (F_S) and time-amplitude (V_{MA}) analysis of V_{in}.

5.4   EXPERIMENTAL AND CLINICAL RESULTS

Measurements were undertaken separately on each block of the proposed asynchronous device and were compared with the synchronous system (SALAM, 2010(c)) assembled with discrete commercial components. Table 5-3 shows power dissipation of these devices in both active and power saving modes. These prototyped devices have been made using latest low-power discrete components. However, recently developed FPGA operated in freeze standby mode, discrete components or custom integrated circuits could reduce the power consumption to microwatts. These prototyped devices have demonstrated smart operation to reduce power dissipation.

Table 5.3: Measured power consumption of synchronous and asynchronous prototyped devices at 3.3 V power supply

Block	Comp[a]	Synch Device[b]			Asynch Device[c]		
		Qt[d]	PC[e] (mW)		Qt[d]	PC[e] (mW)	
			AM[f]	PSM[g]		AM[f]	PSM[g]
Amplifier	IA[h]	1	2	2	1	2	2
Detector	VWD[i]	3	13.1	13.1	4	17.4	8.0
	DFF[j]	3	6	6	0	0	0
	FD[k]	3	19.3	19.3	4	25.7	12.1
Clock	Osc[l]	1	1.5	1.5	0	0	0
Modulator &	SWs[m]	4	0.1	0.1	0	0	0
Demodulator	CP[n]	3	5	5	0	0	0
	VWD[i]	3	13.1	13.1	0	0	0
TFG[o]	FD[k]	3	19.3	19.3	0	0	0
Receiver		0	0	0	1	6	6
DDS[p]		1	0	5	1	10	5
Total power consumption[q]			70.1	65.1		61.2	33.1

[a]Comp: Component, [b]Synch Dev: Synchronous device, [c]Asynch Dev: Asynchronous device, [d]Qt: Quantity, [e]PC: Power consumption, [f]AM: Active mode, [g]PSM: Power saving Mode, [h]IA: Instrumentational amplifier, [i]VWD: Voltage window detector, [j]DFF: Mater-salve D flip-flop, [k]FD: Frequency divider, [l]Osc: Oscillator, [m]SWs: Switches, [n]CP: charge pump, [o]TFG: Time frame generator, and [p]DDS: drug delivery system, and [q]power dissipated by prototyped device based discrete components.

The asynchronous prototyped device turned OFF 6 modules during the icEEG monitoring period and turned ON all 11 modules at seizure onset. With the synchronous device, the clock would have kept all modules running during the monitoring period. As a result, measured power consumption in the asynchronous detector was reduced by 49% in icEEG monitoring period (power saving mode) and 12% in active mode compared to the synchronous detector. The power dissipation densities were under maximum safety level ($\delta_{Pmax} = 6mW/cm^2$ which may cause enough heat to damage surrounding tissue) (HARRISON, 2008). Figures 5-13 illustrate devices' operation modes and their corresponding average power dissipation (P_T) and power consumption densities (δ_p).

Impedances of the proposed hybrid electrodes were electrically characterized *in vitro* using electrochemical impedance spectroscopy (Impedance analyzer HIOKI 3522 LCR) in standard physiological saline solution (0.9% NaCl). Figures 5-14(a) shows scanning electron microscope
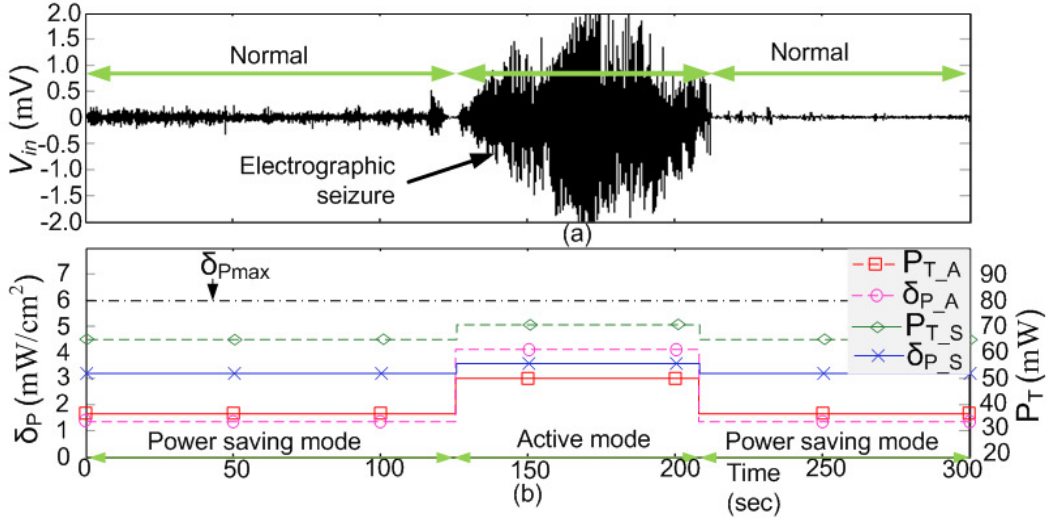
Figure 5-13: Demonstration of power dissipation of proposed system: (a) Electrographic seizure in icEEG recording and (b) Average power dissipation P_T and densities δ_P of the devices, where P_{T_A} and P_{T_S} are power dissipation in asynchronous and synchronous devices, and δ_{P_A} and δ_{P_s} are power consumption densities, respectively.

(SEM) images of the Pt electrodes and Figures 5-14(b) illustrates comparative studies on impedance magnitude of commercial electrode (AdTech Medical Instruments, WI, USA) and the proposed electrode. The proposed electrodes have significantly lower impedance and better recording performances (SALAM, 2011(b)).
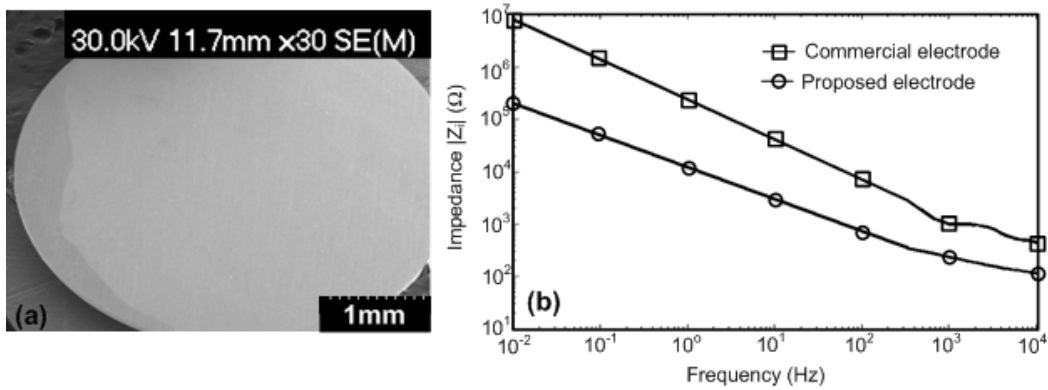
Figure 5-14: Electrical properties of the hybrid electrode: (a) SEM image of the proposed electrode contact and (b) Measured impedance sweep of the commercial and proposed electrodes.

5.4.1 Validation of asynchronous front-end detector

IcEEG recordings from two electrode contacts (Figure 5-10) located in the EZ from 7 patients were fed into the proposed algorithm and device. The AFED was tested on an average of 6 electro-clinical seizures, 15 brief electrical seizures and 10 long normal signals (30 min randomly chosen) per patient. Figure 5-15 shows validation of the proposed detection algorithm using Matlab tools. The recorded icEEG V_{in} from case 1 was uploaded in Matlab simulation platform, and analyzed in time-amplitude and time-frequency domain, and detected seizure onset. Figure 5-16 illustrates measured seizure detection of the proposed device on icEEG recordings (V_{in}) from case 1 and the seizure detection delay T_{DET} of V_{SD}. The simulation and experimental results of synchronous and asynchronous detectors are presented in Table 5.4. The AFED detected the electro-clinical seizures of all 7 patients in an average of 16 sec after seizure onset. Sensitivity of
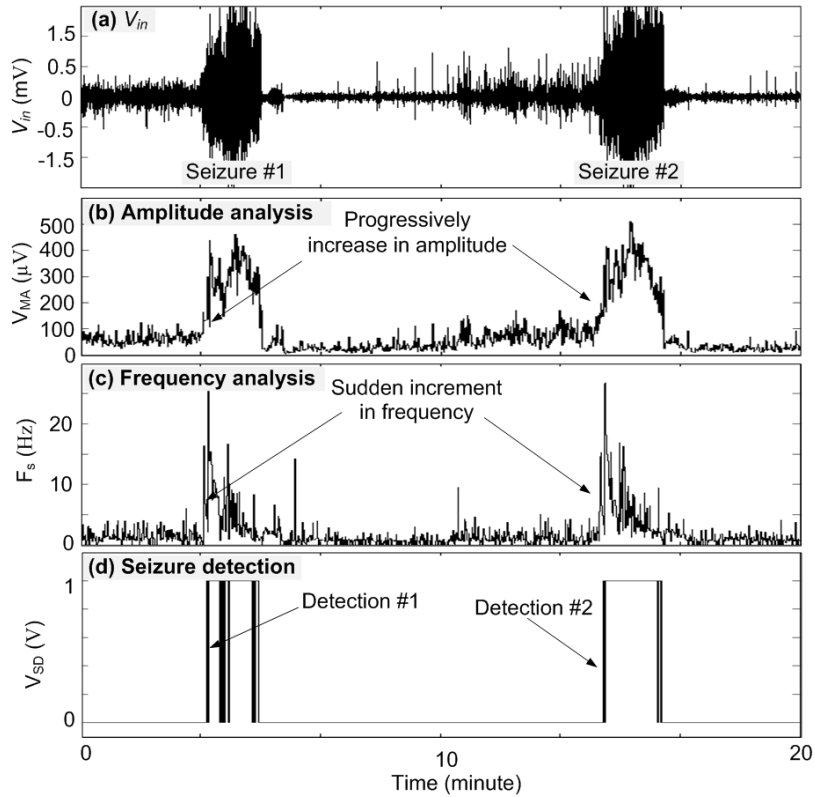
Figure 5-15: Validation of proposed algorithm: (a) icEEG recordings V_{in}, (b) seizure onset activity is characterized by progressive amplitude increase, (c) rapid fast-activity, and (d) seizure onset detections.
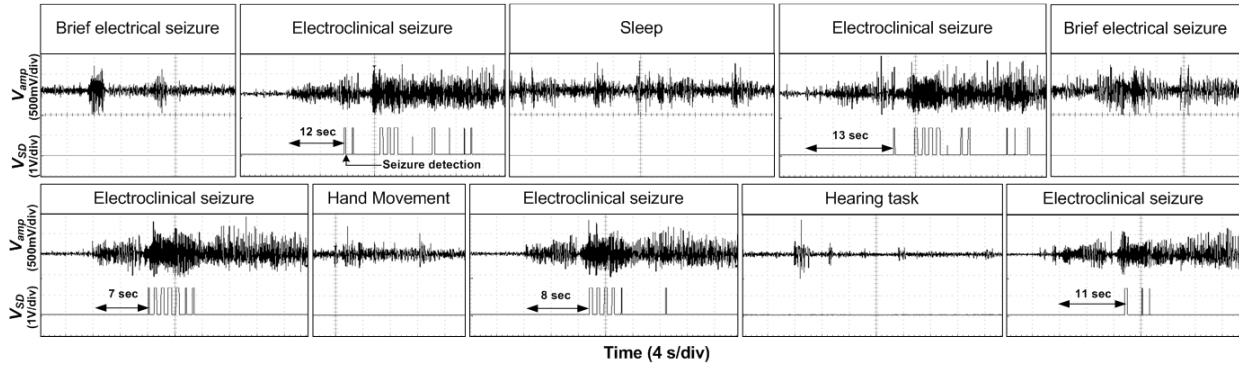
Figure 5-16: Measured seizure onset detection by AFED, where V_{amp} is icEEG of seizure from the epileptogenic zone, and V_{SD} is seizure onset detection of case 1.

the detectors has been defined according to (PANG, 2003) and both patient-specific seizure detectors had 100% sensitivity. The mean seizure detection delay was slightly longer than the one of the synchronous detector which took on average of 13 sec to detect seizures due to a lower noise effect in the device.

5.4.2 Validation of drug delivery system

The predefined drug dose was administrated in response to the early detection of seizure development. Figure 5-17 shows 3 self-triggered drug injections in response to the seizure

Table 5.4: Average seizure detection delay (T_{DET}) of synchronous and asynchronous detectors.

| Case no. | Age /Gender | Epileptogenic zone | Average T_{DET} (s) | | | |
| | | | Synch[a] | | Asynch[b] | |
			Sim[c]	Exp[d]	Sim[c]	Exp[d]
1	24/M	Right hippocampus	7	6	7	9
2	36/M	Left lateral temporal neocortex	12	15	10	16
3	44/M	Left pre-motor cortex	7	15	7	18
4	41/M	Right amygdala/ hippocampus	10	21	12	22
5	49/F	Left hippocampus	24	12	18	15
6	32/M	Left hippocampus	12	12	11	13
7	15/M	Right lingual gyrus	25	20	19	22

[a]Synch: Synchronous, [b]Asynch: Asynchronous, [c]Sim: Simulation results with Matlab, and [d]Exp: Experimental results .
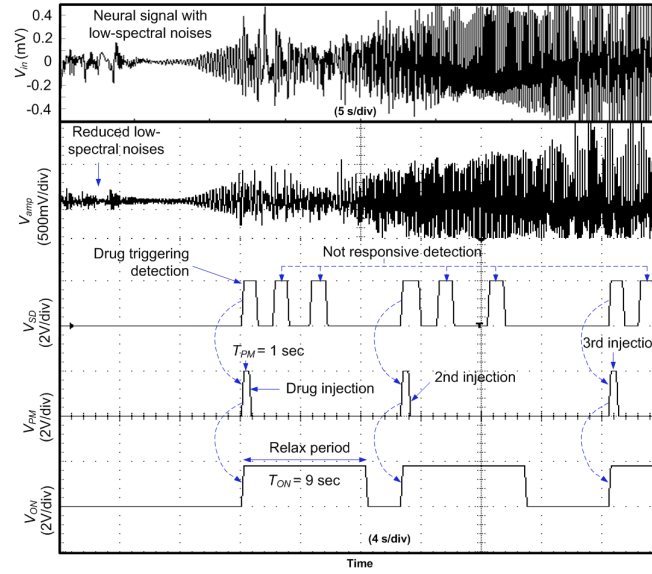
Figure 5-17: Monitored drug delivery process triggered by seizure detector, where V_{in} is neural signal, V_{amp} is amplified neural signal, V_{SD} is seizure detection, V_{PM} is drug injection period T_{PM}, and V_{ON} is focal treatment duration T_{ON}.

detection by the proposed system and illustrates the corresponding individualized dose. The doses are widely programmable by T_{PM} and micropump control voltage V_{DP}. Figure 5-18 shows range of drug dose for different variables. The desired seizure suppression dose (Table 5-1) was obtained by regulation T_{PM} (Figure 5-18(a)), however, more precise was achieved with different combinations of V_{DP} and T_{PM} (Figure 5-18(b)).

5.5   DISCUSSION

The proposed closed-loop epilepsy prosthesis offers promises of lower power dissipation, better data-dependent computation and higher detection performances compared to a synchronous design. Current commercially-implantable epilepsy devices (SUN, 2008) and seizure detectors (SALAM, 2009(a); RAGHUNATHAN, 2009; SALAM, 2009(b); PATEL, 2009; SALAM, 2010 (b); VERMA, 2010; SALAM, 2010(c); SALAM; 2011(c)) are based on a traditional synchronous design. Thus, these devices continuously dissipate battery power for clock gating which ultimately shortens the interval for battery replacement or recharging. Open loop devices, such as the VNS or anterior thalamic stimulators, stimulate in a periodic manner with a built-in clock which defines the periodic action (TERRY, 2009; SALAM, 2010(a); RYCHLICKI; 2006). These devices do not

require a change from traditional synchronous technology owing to the isolation of clock gating from the rest of the device in sleep mode. However, the RNS system (SUN, 2008) requires continuous long-term icEEG monitoring. Therefore, this system should replace traditional technology with asynchronous technology and improve data-dependent computation. Furthermore, the sensitivity of the proposed AFED are maximized 100% to prevent unwarranted drug delivery; however, sensitivity of (VERMA, 2010; RAGHUNATH, 2009; PATEL, 2009) are 94.35%, 95.3%, and 93%, respectively. Although the average detection of the proposed AFED is 8 sec (max) higher than the other detectors described in (VERMA, 2010; RAGHUNATH, 2009; PATEL, 2009); but the proposed device have showed well capability to detect seizure onset and deliver the antiepileptic drug well before the onset of clinical manifestations. For example, Figure 5-11 shows minimum seizure progression time (~22 sec) for case 1 and subsequent aura reported at 33 sec; however, the proposed system detected this seizure at 8 sec (2nd row, 3rd column of Figure 5-16) and delivered sufficient amount of drug in a short duration (Figure 5-18), and consequently seizure may suppress within 5 sec (STEIN, 2000). The average detection delay of the detector is 16 sec, thus all the detections have sufficient time to inject drugs and block seizure progression. The direct drug delivery experiments for the seizure suppression in Table 5- 1 were demonstrated using external prototypes (e.g. desktop computer and syringe pump); however, the proposed prototyped device is implemented on two PCB boards and expected to be reliable in an implantable device without risking false detections.

Figure 5-18: Controlled widely programmable measured drug dose by: (a) injection period T_{PM} and (b) microchip needed voltage V_{DP} with different T_{PM}.

5.6 CONCLUSION

We have described the design and implementation of an asynchronous closed-loop drug delivery system that paves the way for improved power management of currently-available technologies. The proposed asynchronous seizure detector was validated using icEEG recordings of 7 patients, and detection performance was as accurate as that obtained with synchronous devices, but reduced power consumption by 49% in power saving mode. Data-dependent analysis of this asynchronous design kept 6 modules (out of 11) OFF in icEEG monitoring mode unless abnormal activity interrupted it. The AFED integrates a multiple feature-based algorithm for the detection of epileptic seizures. Due to the heterogeneity of seizure onset patterns, an individualized method is the best solution among general feature-based approaches. Furthermore,

this method reduced device complexity. A computerized prosthesis pre-implantation procedure optimized individualized settings for adequate detection performance. Focusing on low-power dissipation, the proposed asynchronous detector is designed for progressively increasing low-voltage, fast-activity, seizure-onset patterns. Experimental results have demonstrated the feasibility of asynchronous design in a low-power, reliable, implantable device. Further validation in an animal model of epilepsy is warranted.

5.7 ACKNOWLEDGMENTS

CHAPTER 6   NOVEL INTRACRANIAL RECORDING SYSTEM

Performance of the closed-loop brain stimulator (chapters 3, 4 and 5) is dependent on high quality icEEG recording. In this chapter, we present new electrodes for better quality icEEG recording. Also, we propose a new intracerebral recording system for epilepsy presurgical evaluation. The new subdural mini grid electrode has a new shape and several attributes to overcome currently encountered drawbacks with current intracranial electrodes. We present in the design of novel electrodes, the method of their fabrication, the architecture of a wireless EEG recording system, and *in vitro* and *in vivo* experimental results. This work was submitted for publication in the "IEEE Transactions on Biomedical Circuits and Systems" and it is reproduced in the following pages.

6.1   SUBDURAL POROUS AND NOTCHED MINI GRID ELECTRODES FOR WIRELESS INTRACRANIAL ELECTROENCEPHALOGRAPHIC RECORDINGS

Muhammad Tariqus Salam[1], Sebastien Gelinas[1], Sébastien Desgent[2], Sandra Duss[2], Lionel Carmant[2], Mohamad Sawan[1], and Dang Khoa Nguyen[3]

[1]Polystim Neurotechnologies Laboratory, École Polytechnique de Montréal, Québec, Canada

[2]Research center, Sainte- Justine University Hospital Center (CHU Sainte- Justine), Université de Montréal, Québec, Canada

[3]Notre-Dame Hospital, Centre Hospitalier de l'Université de Montréal (CHUM), Québec, Canada

Abstract –In this paper, we present novel subdural electrodes in an attempt to improve localization of the epileptogenic zone with less morbidity. The new subdural mini grid electrode has a new shape and several attributes to address some of the problems encountered with currently used subdural electrodes. We demonstrate here the design of the novel electrodes, method of fabrication, in vitro and in vivo results. The mini grid electrodes contains 4 × 4

platinum/gold electrodes arrays on a thin polydimethylsiloxane (PDMS) substrate which is engineered to improve molding to the brain surface for better electrode tissue contact. Several mini grid electrodes are electrically connected as required to form a larger grid electrode. All the cables are routed internally and connected to the wireless recording device that is meant to be implanted on the skull under the skin. Up to 32-channel intracranial electroencephalo-graphic (icEEG) signals are recorded through intracerebral electrodes and transmitted wirelessly to a remote base station. The wireless system operates in the Medical Implant Communication Service (MICS) 400 MHz band. Results of in vitro experiment have shown minimum impedances for optimum choice of pure gold materials for electrodes and wire. The in vivo icEEG recordings in adult Sprague Dawley rats were performed for three weeks for basal activities and ~40 min for seizure activities recordings. The wirelessly icEEG recording system demonstrated on average a 2% normalized root mean square deviation. The results of in vivo recordings demonstrated signal stability, 50% noise reduction and up to 6 dB SNR improvement to the commercial electrodes. Following the long-term icEEG recording, brain histological results showed no abnormal tissue reaction in underlying cortex.

6.2   INTRODUCTION

Patients with refractory focal epilepsy may benefit from epilepsy surgery. Successful surgical treatment is highly dependent on adequate localization of the epileptogenic zone (EZ). Non-invasive localization techniques such as scalp EEG, Positron emission tomography (PET), Magnetic resonance imaging (MRI), ictal single-photon emission computed tomography (SPECT), magnetoencephalography (MEG) and EEG-functional MRI (EEG-fMRI) can help in the identification of this EZ, sometimes allowing some patients to directly go onto resective surgery (SPENCER, 2009). When non-invasive techniques fail to adequately localize the EZ, an invasive EEG study is generally required. These invasive EEG studies consist in the implantation of intracerebral electrodes to allow direct recording from the brain. A wide verity of intracranial electrodes is available for such invasive studies: subdural strip or grid, depth, epidural, and foramen ovale electrodes (SPENCER, 2009; GOLDRING, 1984, WYLLIE 1987; WIESER, 1985, DUBEAU 2007). They differ in method of insertion, accuracy, risks and limitations (TALAIRACH, 1958; BANCAUD, 1973, TALAIRACH, 1974, CRANDALL 1966). The choice
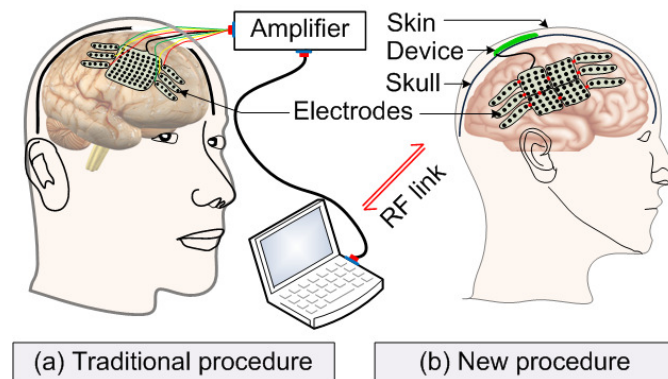
Figure 6-1: Schematic representation of intracerebral EEG recording systems: the traditional procedure using currently available commercial electrodes and the new procedure using the proposed novel subdural electrodes.

of electrodes depends on the suspected areas which need to be sampled. Figure 6-1(a) shows the traditional way of performing an invasive EEG study.

The intracranial electrodes are more sensitive to the brain activities than extracranial electrodes because they are closer to the EZ. Whereas the extracranial electrodes record signal generated from a large cortical surface, intracranial electrodes record synchronous firing of many neurons throughout a few millimeters of cortex across the diameter of an electrode contact. However, uses of intracranial electrodes have disadvantages, such as a small risk of infection, edema and hemorrhage. Thus it is best to limit the number of electrodes implantation to delineate the EZ for safety purposes (Fountas, 2007; Benbadis, 2006). Restriction on the number of electrodes however may cause insufficient coverage to allow identification of the EZ. Erroneous identification of the EZ obviously translates into a poor epilepsy surgery outcome.

Intracerebral electrodes have been in use since the 1950s but no significant development has been made since except for the development of microelectrodes to record high-frequency oscillations mainly for research purposes (DODGE, 1963; PENFIELD, 1954). Due to their smaller electrode-tissue interface, these microelectrodes have different electrical characteristics compared to the subdural electrodes. Commercial companies (i.e. Ad-Tech Medical Instrument Corporation, WI or PMT Corporation, MN) use common manufacturing methods for developing intracerebral subdural electrodes (diameter 4/5 mm). These commercial electrodes are based on silicone rubber (Polydimethylsiloxane-PDMS) as insulation and substrate material, platinum or

stainless steel as electrode material, and stainless steel for wiring (HENLE, 2011). Gold (Au) has been used in subdural electrodes (REN, 2010) but no significant improvement on icEEG recording has been reported.

Work presented here was motivated by the fact that currently used electrodes have several limitations. For one, mechanical resistance of electrode-wire generates noise that degrades the icEEG recording (REN, 2010). Higher chemical reactions at electrode-tissue interface produces toxic ions to the tissue (Merrill, 2005). Moreover, many materials (i.e. stainless steel, tungsten, and titanium) need corrosion protection (i.e. passive film) (MERRILL, 2005), but this protection often dissolves due to faradic reaction in the passive film (Norlin, 2002). Other unresolved issues include wiring material, poor connection at electrode-wire interface, and visualization of implanted electrodes on post-implantation scans or MRIs. Finally, current intracerebral EEG recordings use many wired connections which limit the patient's liberty to move and increase the risk of brain infections.

The icEEG recording is generally characterized by low-amplitude signals (microvolt range) and low-frequency bandwidth. The available instruments have relatively poor noise performance for the low-spectral neural signal amplification (SALAM, 2009(a)). Moreover, other low-spectral noises generated from electrodes and electrode-tissue interface combine with instrument noise to modulate the neural signal and degrade the signal-to-noise ratio (SNR). We have previously demonstrated several front-end preamplifiers for noise reduction (SALAM, 2009(a); SALAM, 2011(a)). However, optimum SNR value can also be obtained by improving intracranial electrode contacts (SALAM, 2011(b)).

In this paper, we propose a novel subdural electrode based recording system (Figure 6-1(b)) featuring attributes which could potentially facilitate larger sampling with lower morbidity: mini-grids connected as needed, single exit cable, wireless transmission, grid notches and holes, edge markers and numbering system, low-impedance electrodes and wiring, and wireless recording system.

6.3   PROPOSED NOVEL INTRACRANIAL RECORDING SYSTEM

The proposed subdural mini grid and/or strip electrodes are meant to be implanted independently over suspected areas of epileptogenicity through a craniotomy (Figure 6-2). One or two main grid electrode(s) hold(s) all the electrodes and connect(s) to the implantable wireless icEEG recorder (Figure 6-1(b)). Following the implantation of intracranial electrodes, the patient can undergo an MRI study to verify the positioning of implanted electrodes and finally long-term video-EEG recording for localization of the EZ. The shapes and attributes of the new subdural electrodes, and recording system are described below.
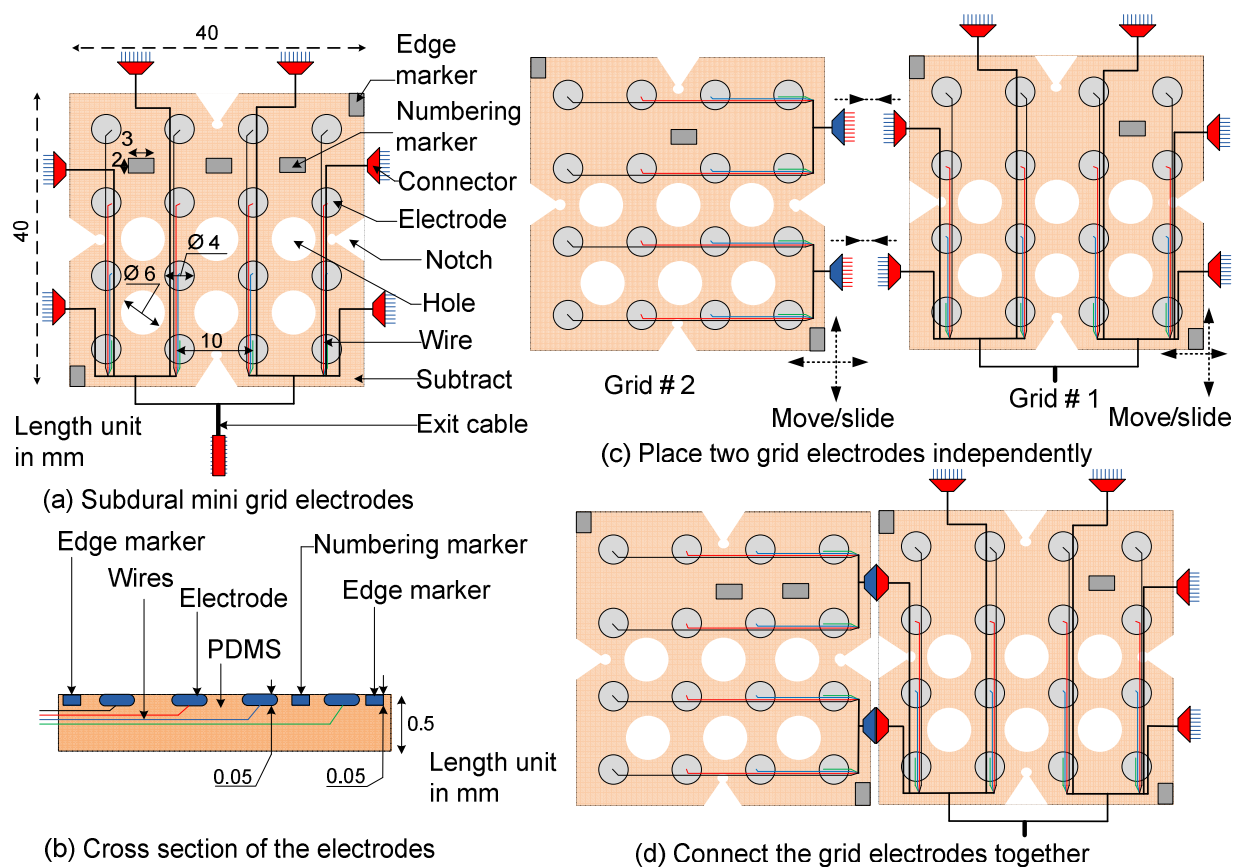
Figure 6-2: Illustration of the proposed novel subdural mini-grid electrodes: (a) new attributes and dimensions, (b) cross section of the mini grid, (c) placement, and (d) connection of the grid electrodes.

(i) Smaller grids

The mini subdural grid electrode is a 4 × 4 matrix (height 40 mm; width 40 mm; thickness 0.6 mm thick). The dimensions of grid electrodes are smaller to fit curved regions of brain.

(ii) Holes

Commercial subdural grid electrodes may cause brain swelling (LEE, 2000). In an attempt to minimize risk of brain swelling, each mini-grid has six holes to allow CSF circulation.

(iii) Notches

The mini grid electrode is designed to fit on human brain cortical surface. Each mini grid has 4 notches for better flexibility to allow a better fit with the curved cortical surface.

(iv) Markers

Edge and numbering markers are included in the grid electrodes to facilitate their identification on the post-implantation MRI. All materials used in the electrodes are MRI compatible and take into account the MR-susceptibility artifacts generated by metal contacts.

(v) Connectors

The mini grids are connected to each other using custom made contactors that enhance electrical and mechanical connection. The connectors provide internal routing of electrical wiring. Shorter wire length also reduces resistance in the electrical paths. Moreover, the connector provides stronger mechanical strength so that the mini-grids do not move and overlap. This mini grid electrode system can hopefully better adapt to the anatomy and different curvatures of various brain regions.

(vi) One exit cable

All the electrical paths are internally routed, thus all the cables are merged in one exit cable coated with Teflon that connects to the implantable device for wireless icEEG recording or to come out through the skin for wired recording. A single exit cable or wireless transmission should reduce risk of infections.

(vii) Electrode and wiring materials

Quality of icEEG recordings is dependent on the choice of electrode material. We have previously shown that pure platinum (Pt) or pure gold (Au) electrodes provided higher conductivity than the commercial electrodes (SALAM, 2011(b)). In accordance, contacts of the mini grid electrodes are made of pure Pt or Au material, and wire connections between the electrodes (thickness 0.05 mm) and amplifiers are made the using same materials used for the electrodes with 0.1 mm diameter wires.

(viii) Electrode-wire junction manipulation

Electrode impedance can potentially be further improved by manipulating the electrode-wire junction. Two types of junction are used for the *in vitro* impedance analysis experiments: electrode-wire touch junction and manipulation of electrode-wire junction by high conductive Silver epoxy (SE).

(ix) Wireless recording system

The wireless recording system contains preamplifiers and a wireless data transceiver. The preamplifier has tuneable gain with an input referred RMS noise of ~1 µV and an accurate ADC converter with 24-bits resolution. The wireless chip has a SPI interface and a MAC layer module. The low-power wireless system uses a custom FSK transceiver (402-405 MHz) for icEEG recordings transmission. The MICS transceiver offers high throughput up to 800 kbps and automatic error handling and flow control with BER below 10^{-10}.

6.4 METHODS AND MATERIALS

6.4.1 Fabrication of the mini grid electrodes

Figure 6-3 illustrates the subdural mini grid electrodes fabrication process. This process has three steps: mould construction, electrode-wire junction manipulation, and assembly and packaging.
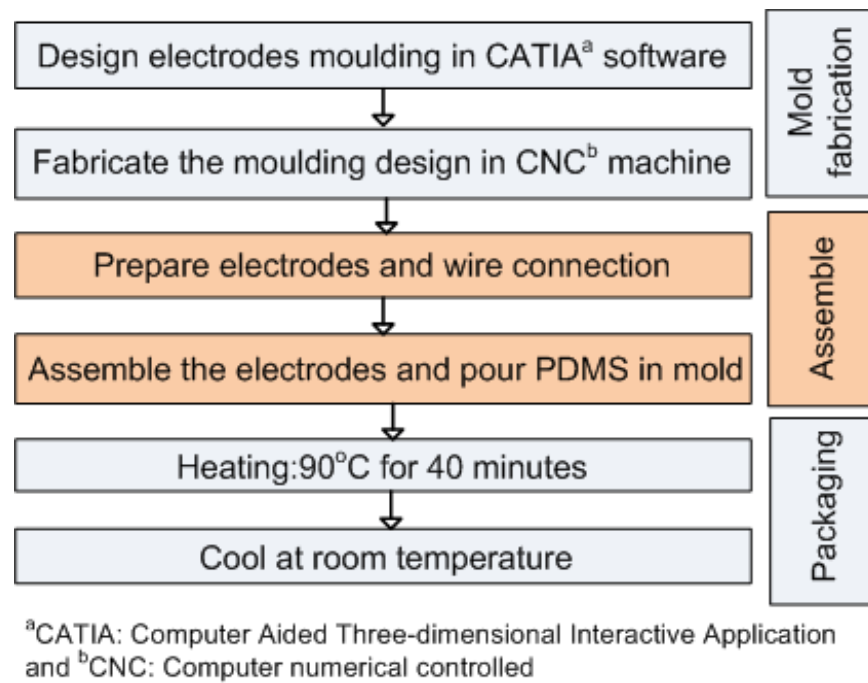
Figure 6-3: Flow chart of the subdural mini-grid electrode fabrication process.

(i) Mould design

The moulds were designed using CATIA software and fabricated using high speed precision 3-axis computer numerical controlled (CNC) vertical machining (Huron speed machine). The design and dimensions of the moulds are shown in Figures 6-4(a)-(b).

(ii) Electrodes-wires connection

Two types of electrode-wire connection were used to reduce impedance and improve icEEG recording performance. These connection types were electrode-wire touch connections and electrode-silver epoxy-wire connections.

(iii) Assembly and packaging

Electrodes and wires were assembled on the mould (Figure 6-4(c)) and PDMS was poured (Figure 6-4(d)). After 20 minutes of 110°C heating (Figure 6-4(e)), subdural electrode arrays were encapsulated with a thin PDMS substrate and were released from the mould (Figures 6-4 (f)-(g)).
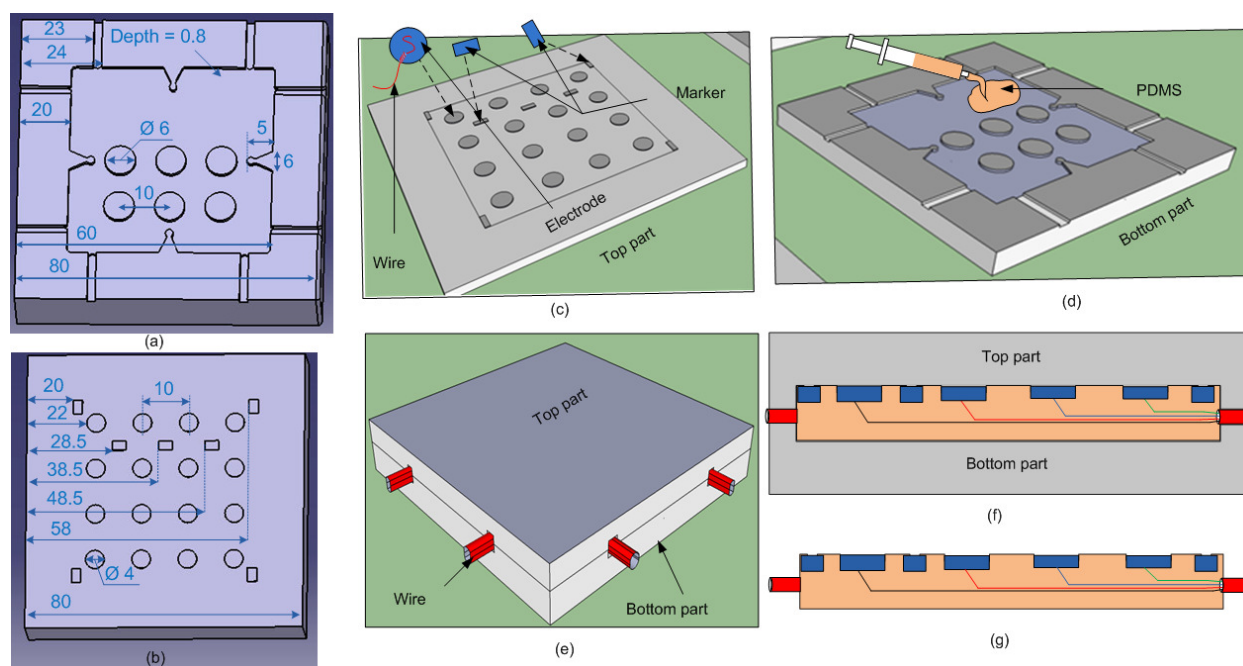
Figure 6-4: Fabrication process: (a)-(b) Design of mini-grid electrodes mould structures of top (a) and bottom (b) parts using CATIA software and (c)-(g) Assembling and packaging process: assembling of electrodes and markers (c), pouring of silicone on the mould (d), attachment of both parts (e) and cross section of assembly (f), and cross section of fabricated mini-grid electrodes (g).

6.4.1.1 Electron-probe microanalysis

Compositional analyses of the electrode contacts were performed using Scanning electron microscope (SEM) images and electron-probe microanalysis with energy dispersive spectrometry quantitative technique (Oxford Instrumentation Company).

6.4.1.2 Electrical impedance spectroscopy

Impedances of the proposed electrodes were electrically characterized *in vitro* using electrochemical impedance spectroscopy (Impedance analyzer HIOKI 3522 LCR) in standard physiological saline solution (0.9% NaCl). Conductivity of the solution (R_s) was measured using a conductivity meter (Cole-Parmer, model 1481-40). The impedances of the new electrodes and commercial electrodes were measured as bipolar configuration. Figure 6-7(a) shows the

experimental set up. The corresponding equivalent circuit is shown in Figure 6-7(b). The total equivalent impedance is

$$Z_T = R_{w1} + (C_{p1} \parallel R_{p1}) + R_s + R_{w2} + (C_{p2} \parallel R_{p2}) \qquad (6.1)$$

where, $R_{w1,2}$ is the wire resistance, $C_{p1,2}$ is the double layer capacitance, $R_{p1,2}$ the charge transfer resistance, and R_s the resistance of the solution. Thus the impedance of an electrode (Z_i) is the combination of $R_{w1/2}$, $C_{p1/2}$ and $R_{p1/2}$.

6.4.2 IcEEG recording performance of proposed subdural contacts and comparison with commercially available subdural contacts

These studies were conducted at the CHUM –Notre-Dame hospital and CHU-Ste-Justine hospital. All procedures for the use and care of animals for these experiments were conformed to the policy and guidelines of the Canadian Council for Animal Care (CCAC). Experimental protocols were approved by the Comité Institutionnel des Bonnes Pratiques Animales en Recherche (CIBPAR) at the CHU Ste-Justine Research Center, Université de Montréal. The recordings obtained with the proposed subdural contacts were compared with recordings made in human epileptics with commercial electrodes as part of their usual clinical care at the CHUM - Notre-Dame Hospital. Use of these recordings was approved by the CHUM's ethics committee.

6.4.2.1 Animals and surgical electrode implantation procedure

Two groups of male Sprague Dawley rats (P80, ~450-580g) underwent craniotomies (see below) with general anesthesia (i.e. induction: 4% isoflurane in 1 l/min of O_2 and 0.05 mg/kg Buprenorphin, maintenance: 2% isoflurane in 0.5 l/min of O_2 as shown in Figure 6-5(a). Twenty minutes before surgery the animals were pre-treated with atropine 0.1% (s.c. to minimize airways secretions), lactate ringer USP (2ml s.c. for hydration and electrolytes) and lidocaine 2.5% (s.c. for local anaesthesia). After that, a small slit (1cm) was done in the skin overlying the head to expose the skull.

First, three holes were drilled on skull to place two anchor screws and one reference screw (1.25 mm in diameter) on top of the cerebellum as shown in Figure 6-5(b). Second, craniotomy windows were drilled out starting at the level of the Bregma coronal suture on the skull and the dura was carefully opened using a 30 ½ G seringe needle tip. After that, the electrode implants
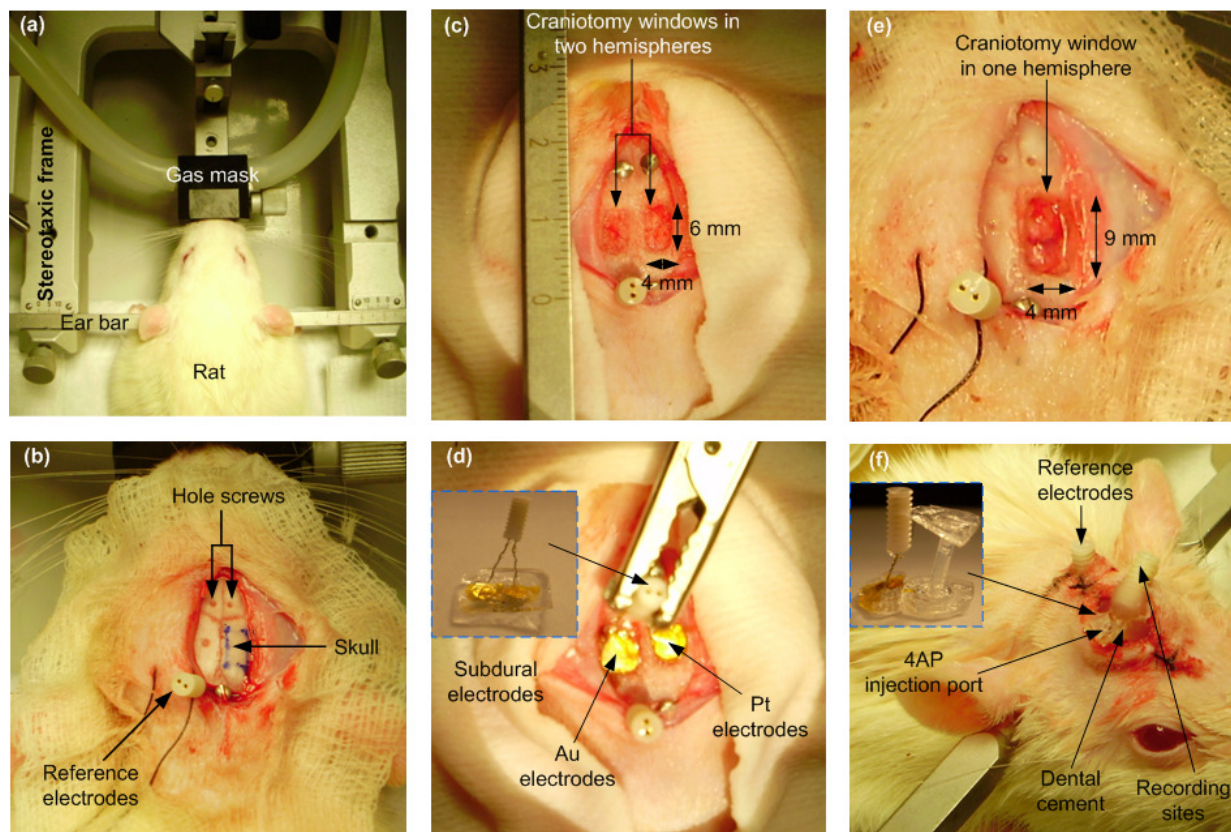
Figure 6-5: Surgical electrode implantation procedure in rats: (a) animal attached to stereotaxic instrument, (b) craniotomy windows, (c)-(d) electrode implantation in group 1 rats, and (e)-(f) implantation and coverage with dental cement on group 2 rats.

were placed directly on top of cortex using a stereotaxic micro manipulator apparatus with steady forceps arms (Stoelting Co. Germany) and left there for 2 minutes while the brain was hydrated. Meanwhile, a piece of gelfoam (<1mm in thickness), covering the craniotomy windows space, was placed on top of the implant to keep the site moist, to stabilize the electrode, to minimize vibrations and, to protect the brain from the extrinsic milieu. Finally, the entire surgical site surface, remaining skull, anchors, canula sides and reference screws were covered/sealed with dental cement leaving to be seeing only the tip of the injection site (canula silicon entry), recording sites and reference outputs (Plastics-1 Inc., Roanoke, VA, USA).

Following these implantations, the animals received post-operative care for three consecutive days (i.e. Enrofloxacine 10mg/kg, s.c. and Buprenorphin 0,05mg/kg, s.c.). After a 10-day post-operative recovery period, the freely-moving animals were placed in a Plexiglas cylinder cage surrounded by a Faraday tent to undergo video-EEG recording. EEGs and animal behaviour were

recorded simultaneously with a Stellate Harmonie system linked to a 32-channel Lamont amplifying unit and an infrared video camera positioned 1.5 meter in front of the cages (Stellate Systems v 6.2e, Victoria, Montreal, Qc, CAN). Three separate observers blinded to the treatment groups, reviewed the video-EEGs to detect spontaneous recurrent seizures and clinically associated behaviours.

6.4.2.2 IcEEG recordings and performance evaluation method

Recording performance of the proposed subdural contacts was first tested in two different rat experimental groups and compared with icEEG recordings of human patients group using commercial electrodes. Quality of the recording is evaluated in terms of SNR of icEEG recording and the SNR is measured using Eq. (6.2).

$$SNR \quad (dB) = 20 \log_{10} \frac{\sqrt{\sum_{i=1}^{N} V_{in}(i)^2 / N}}{\sqrt{\sum_{i=1}^{N} (V_{n,1}(i)^2 + \sum_{i=1}^{N} V_{n,2}(i)^2) / N}} \tag{6.2}$$

where, i = 1,2,3, ... N, V_{in} is icEEG recording, $V_{n,1}$ is noise$_1$ and $V_{n,2}$ is noise$_2$. SNR of icEEG recording improves with the signal strength in the icEEG frequency band while reducing noise$_1$ and noise$_2$.

6.4.2.2.1 Group-1: Basal activity recordings for three weeks with one subdural electrode contact on each side of the rat brain

The rat in group-1 underwent two rectangular craniotomies (4 x 6 mm) on top of both hemispheres (Figure 6-5(c)). The proposed subdural pure Au contact was positioned over left hemisphere and the pure Pt electrode contact over the other through craniotomy windows (Figure 6-5(d)). Basal icEEG activities and animal behaviours were monitored 12 hours per day (6 hours during the daytime, from 12 PM to 6 PM, and 6 hours at night, from 12 AM to 6 AM). Here, only basal activity was recorded to evaluate better SNR in recordings and electrode tissue reaction.

6.4.2.2.2 Group-2: Induction of cortical seizures in vivo in rats using 4-aminopyridine (4-AP)

For seizure induction and detection experiments, rats from group-2 were implanted with a subdural contact with a PDMS coated micro-cannula (1.5 mm diameter and 10 mm length) using

drilling of a wider rectangular craniotomy (4 x 9 mm) only on the right side of the skull (Figures 6-5(e)-(f) and zoom inset of Figure 6-6). To induce focal seizures of different duration in these rats, animals were injected with 4-aminopyridine (4-AP: a selective blocker of the Kv1 family of voltage-activated K,+ channels) at doses of 30, 100 and 200 nmol respectively (all diluted in 2ul of sterile 0.9% saline plus sonicated for two minutes to have uniform suspension and adequate dilution of the drug). This injection was done using a 10 µL reservoir of 4-AP solution in a Hamilton syringe (26G) that was positioned using a stereotaxic apparatus and injected through the PDMS micro-canula orifice into the adjunct region of the anterior part of the subdural electrode. The syringe needle orifice was stereotaxically positioned at 11 mm downward from the top of canula for intracortically ($\approx$ 0.5-1mm deep below the pial surface of the sensorimotor cortex) 4-AP solution injection (2µL, over a 10 minutes period, at 0.2µL/min). In this second group of rats, similarly to group 1, 12 hours of basal activities were recorded but only over 24 hours; the following day, the rats were anesthetized with isoflurane and injected with 4-AP before being put back into a recording chamber to recover while being monitored for seizures for 40 minutes. These experiments were done to prove better SNR in seizure activity recordings and in order to evaluate seizure signal recording performance using the proposed electrodes with commercially available subdural electrodes.

6.4.2.2.3   *Group-3: comparative studies with human patients*

For comparative studies, we also obtained recordings from two human patients (24 and 36 year-old male) with intractable partial epilepsy candidate for epilepsy surgery who had previously undergone an icEEG invasive study prior to epilepsy surgery. The signal analyzed in patient 1 came from commercially-available subdural electrode (AdTech Medical Instruments, WI, USA) positioned over the right fronto-temporal region and in patient 2 from the electrode contact positioned over the left orbitofrontal region. The icEEG signal was recorded for 2 to 3 weeks. The SNR in the recordings were compared with icEEG recordings performed in rats using the proposed electrodes.

6.4.2.3 Magnetic resonance visualization of subdural mini-grids

MRI appearance of the new electrodes was tested by placing them into a gel solution (0.9% NaCl with 14gm gelatin) and scanning them using a 1.5 T Phillips MR scanner.

6.4.2.4 Validation of wireless transmission of icEEG recordings

The icEEG was recorded in vivo from rats' cortex using Stellate Inc.'s video-EEG wired recording system and the wireless recording device was tested in vitro using the wired recordings by evaluating the distortion between the original wired and the wirelessly re-recorded EEG. Figure 6-6 shows the functional block diagram of the both recording system. Moreover, this wireless device is able to record 32 channels at 2 kHz sampling with 24-bit resolution.
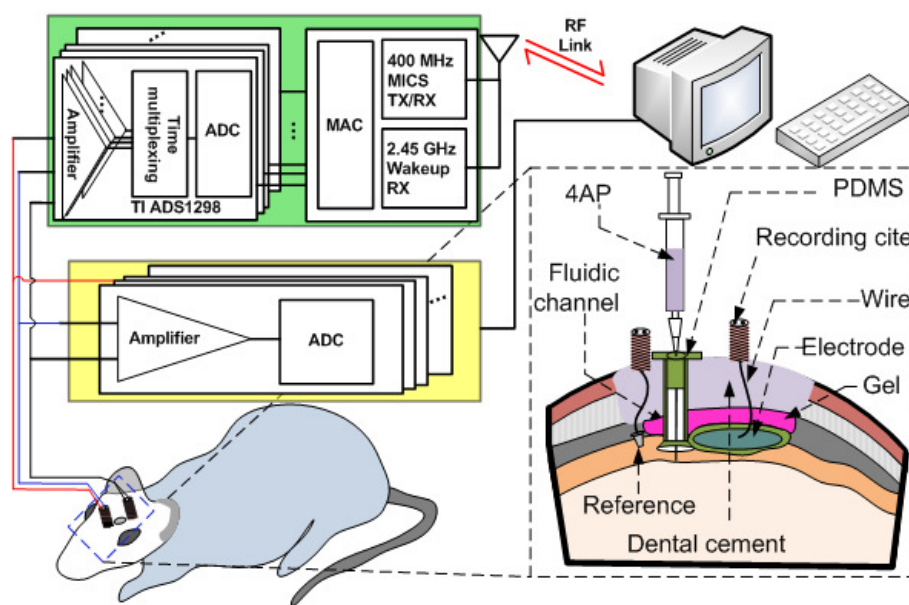
Figure 6-6: Method of icEEG recording using wired connections and the wireless system. Zoom inset illustrates implantation procedure and 4-AP drug injection into the brain for seizure induction.

6.4.2.5 Histological analysis

After long-term icEEG recordings using our proposed pure Pt and pure Au electrode contacts, histological examinations were carried out in the rats. The animals were first perfused through the heart using phosphate-buffered saline and 4% paraformaldehyde. The brains were blocked then

sterotaxically within the skull, removed, post-fixed for two hours at 4°C in a 4% paraformaldehyde phosphate-buffered solution (PB) and cryoprotected in graded sucrose in 0.1 M phosphate buffer (pH 7.4) for 48 hours and frozen until processed. The blocks were cut in series of 50 μm thick sections in the coronal plane, sections stained with cresyl violet for nissl substance and histological examinations were performed.

6.5   RESULTS

Figures 6-7 (a)-(b) show the fabricated moulds of the new subdural electrodes. Two types of subdural grid electrodes were fabricated, one with pure Au contacts (Figure 6-7(c)) and the other with pure Pt contacts (Figure 6-7(d)). These electrodes were scanned using SEM imaging and their material composition analyzed using energy dispersive spectrometry quantitative technique. The SEM images and compositional analyses of the electrode contacts showed 99.90% purity for both electrodes (Figures 6-7 (e) and (f)). Figure 6-7(g) shows a photograph of the 4 × 5.5 cm wireless icEEG recording device. Details of experimental results are described below.
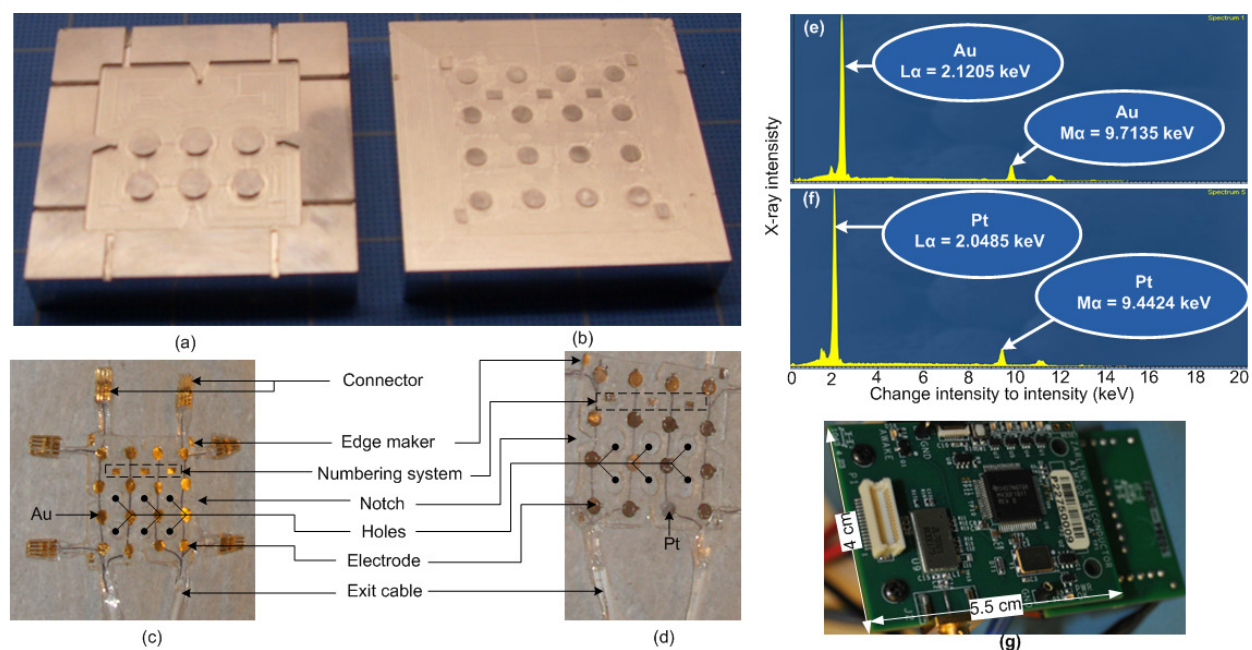
Figure 6-7: Fabrication of the mini grid-electrodes: (a)-(b) fabricated mould, (c)-(d) fabricated Au (c) and Pt (d) grid electrodes, (e) – (f) microanalysis of Au and Pt electrodes: X-ray fluorescence spectra recorded from Au (e) and Pt (f) electrode, and (g) wireless icEEG recording device.

6.5.1 Impedance measurement

The *in vivo* icEEG recording at 200 Hz sampling frequency is generally located in the low-frequency bandwidth (3 to 40 Hz). Flicker noise is predominant in lower frequency (<3Hz) and higher frequency noise is mainly located at >40Hz due to the sampling frequency limitation and thermal noise. Therefore, recorded signals are divided into three main frequency bands (i.e. $noise_1$, icEEG and $noise_2$ as shown in Figure 6-8(d)). Figures. 6-8 (d)-(f) show comparative studies on impedance magnitude of commercial subdural electrodes (AdTech Medical Instruments) and the proposed subdural electrodes. Figure 6-8(d) shows significantly lower impedance of the proposed pure Au and pure Pt electrodes compared to commercial electrodes. Moreover, Figure 6-8(e) shows that further impedance of Pt electrodes is reduced by attaching wire with Silver epoxy (SE). However, Au-electrode-Silver-Epoxy-Au-wire increases impedance compared to Au-electrode-Au-wire (Figure 6-8(f)).
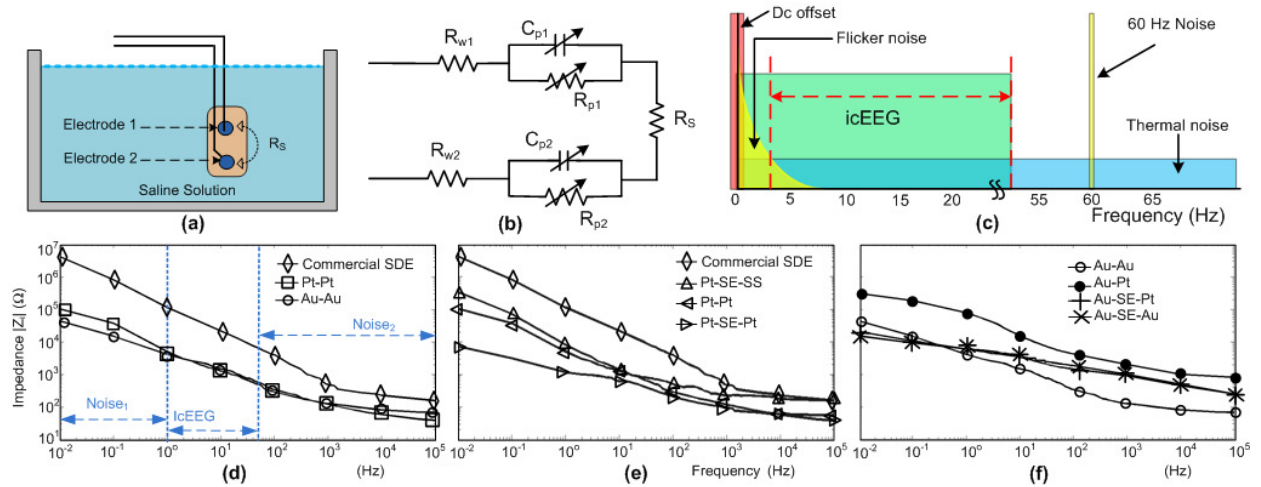
Figure 6-8: Impedance spectroscopy *in vitro*: (a) Bipolar impedance analysis configuration, (b) Equivalent electrical circuit of electrolyte-electrode interface, (c) Frequency analysis of icEEG recording with other noises, and (d) – (f) Measured impedance sweep of different electrodes, where Pt-Pt is Pt-electrode-Pt-wire, Au-Au is Au-electrode-Au-wire, Pt-SE-SS is Pt-electrode-Silver Epoxy (SE)-Stainless steel (SS)-wire, Pt-SE-Pt is Pt-electrode- Silver Epoxy (SE)-Pt-wire, Au-Pt is Au-electrode-Pt-wire, Au-SE-Pt is Au-electrode-Silver Epoxy-Pt-wire, and Au-SE-Au is Au-electrode-Silver Epoxy-Au-wire.

6.5.2 IcEEG recording performance

6.5.2.1 Basal activities recordings

Figure 6-9 shows five second samples of *in vivo* icEEG recordings using commercial subdural electrodes, proposed Pt and Au electrode contacts. The icEEG recording using commercial subdural electrodes (Figure 6-9(a)) has severe low- and high-spectral noise effect due to higher electrode impedance. The recordings using proposed pure Pt and pure Au electrode contacts (Figures 6-9(b)-(c)) had lower noises while recording neural activities efficiently. Moreover, higher conductivity of the proposed electrodes allows translating more neural activities into icEEG recordings. Power spectral densities (PSD) of Figures 6-9 (a)-(c) demonstrate recording
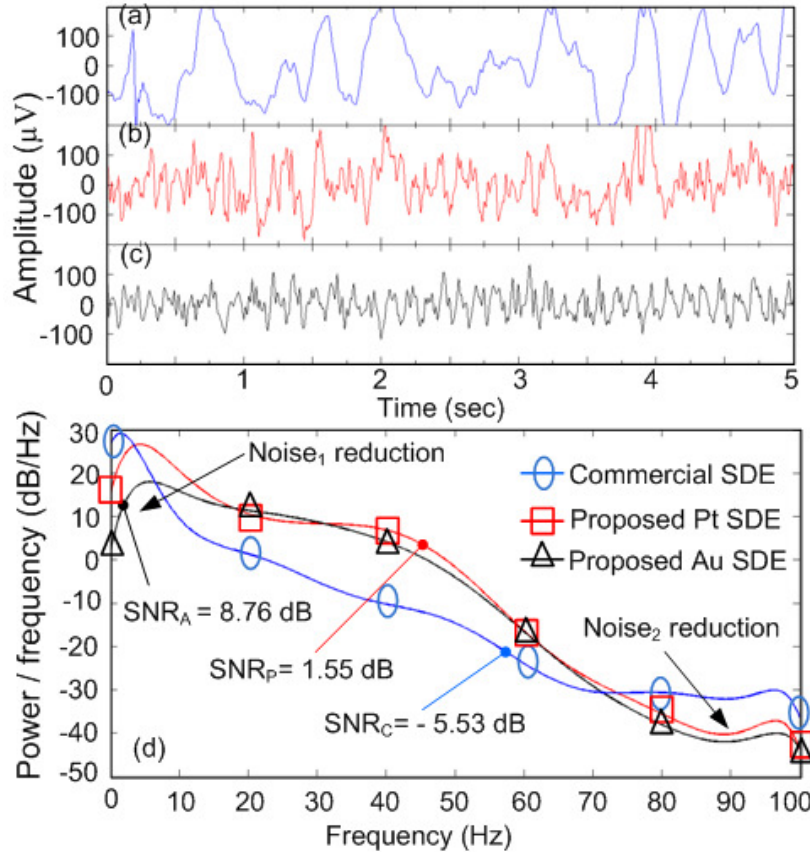
Figure 6-9: *In vivo* IcEEG recordings using: (a) Commercial subdural electrodes; (b) Proposed Pt subdural electrodes; (c) Proposed Au electrodes; and (d) Average power spectral density of the icEEG recordings (a)-(c).

efficacy in 3 to 40 Hz bandwidth while suppressing the noises in lower and higher frequencies. Figure 6-9(d) illustrates that PSD of the recording using commercial subdural electrodes had highest noise effect in lower and higher frequency bands; whereas, recordings using the proposed Pt and Au electrode contacts had lowest noise effect.

6.5.2.2 4-AP drug administration and seizure activities recording

Following the 4-AP injection, the rats were plugged to the video-EEG recording system and various seizure signals were recorded for ~40 minutes. The epileptiform activity induced was characterized by an initial hypersynchronous brain wave activity followed by trains of poly-spikes, with low-amplitude and low-frequency spike-wave complexes that increased after the first few minutes. The corresponding convulsive behaviors (e.g. myoclonus and tonico-clonic) were ranked at modified Racine's scale 0 to 5 (Table 6.1) in Figure 6-10 (RACINE, 1972).

Table 6.1: 4-AP induced seizure behavior in terms of modified racine's scale (RACINE, 1972)

Racine's scale	Convulsive behaviour
0	Behavioral arrest (motionless), hair raising, excitement and rapid breathing
1	Mouth movement of lips and tongue, vibrissae movements and salivation
2	Head clonus and eye clonus
3	Forelimb clonus, "wet dog shakes"
4	Clonic rearing
5	Clonic rearing with loss of postural control and uncontrollable jumping
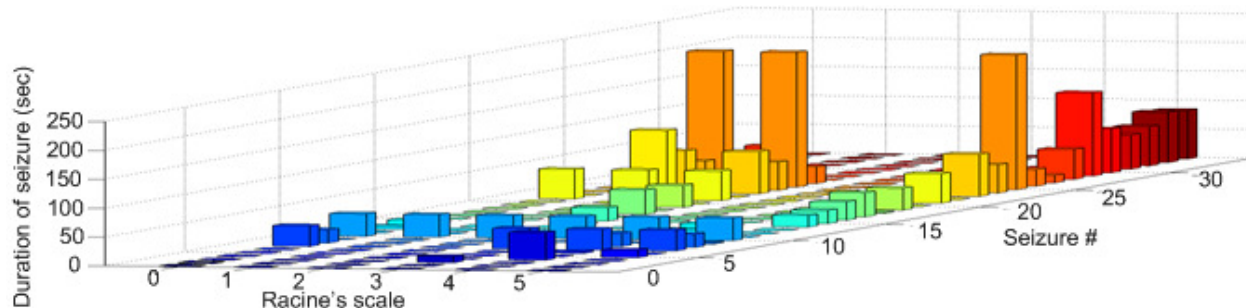
Figure 6-10: Histogram of seizure events induced by 200 nmol 4-AP injections: Durations of 34 seizure events with different intensity (Racine's scale) recorded in a rat.

In order to evaluate recording performance, electrographic seizure signals recorded from human group using commercial subdural electrodes (Figure 6-11(a)) were compared with 4-AP induced seizure signals recorded using the proposed pure Pt (Figure 6-11(c)) and pure Au (Figure 6-11(e)) electrode contacts. The corresponding frequency analysis of the recordings showed continuous degradation of lower-spectral noise in Figure 6-11(b) and reduced noise in Figures 6-11(d)-(f). Further noise reduction evidence is illustrated in Figure 6-12. The PSD of seizure activities in Figure 6-11(a) recorded using the commercial electrodes had highest noise effect in
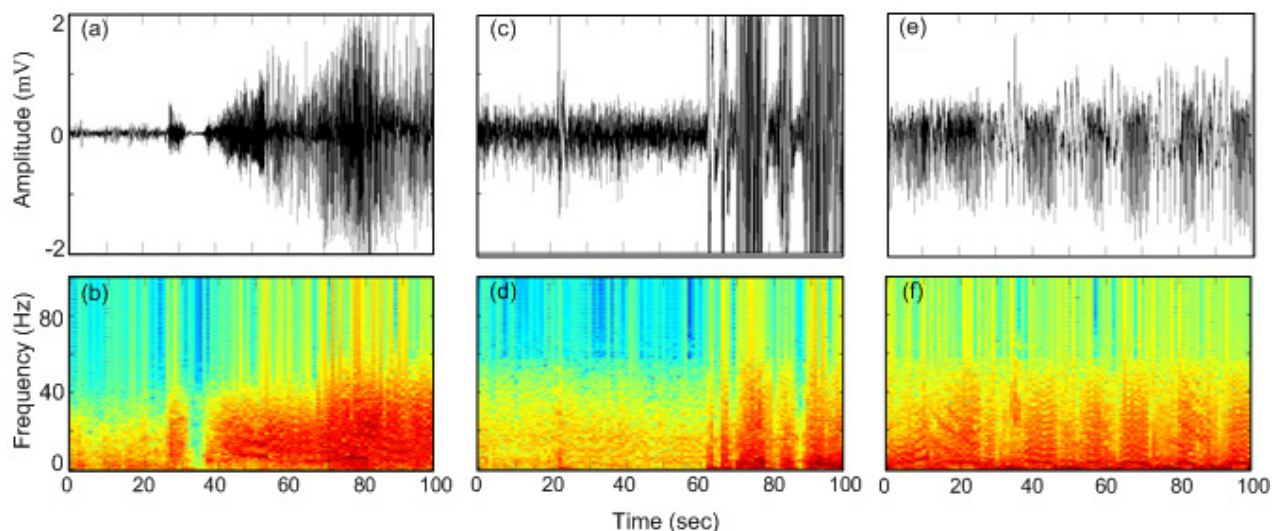
Figure 6-11: Electrographic seizure recording and corresponding frequency analysis using (a) – (b) commercially available subdural electrodes, (c) – (d) proposed Pt subdural electrodes, and (e) – (f) proposed Au subdural electrodes.

lower and higher frequency bands. However, the recordings using the proposed Pt and Au electrode contacts (Figure 6-11 (c) and (e)) had lowest noise effect. The impact of average noises and the SNR of the recordings are shown numerically in Table 6-2. The icEEG recording using commercial subdural electrodes has the worst SNR (-4.84 dB) at seizure onset due to higher RMS noise 47.49 µV in the low frequency band (LFB) and 1.61 µV in the high frequency band (HFB). The proposed Pt and Au electrode contacts reduced significant amount of noises and achieved higher SNRs. The highest SNR (6.67dB) was recorded at seizure onset using Au electrode contacts.
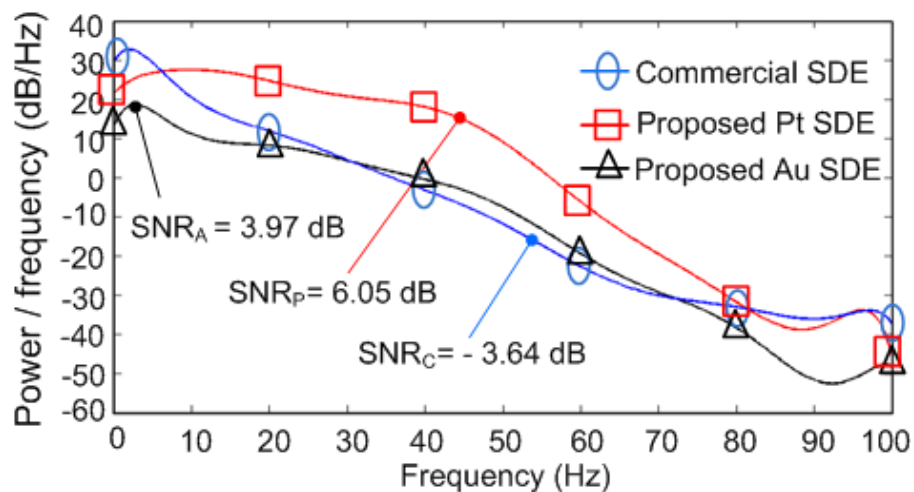
Figure 6-12: Power spectral density of the electrographic seizure recordings (same seizure as in Figure 6-11) using commercial subdural electrodes; proposed Pt subdural electrodes; and proposed Au electrodes.

Table 6.2: Comparative study on average icEEG recordings *in vivo*

	Basal					Electrographic seizure					
	Day			Night	Seizure onset			Seizure		
Electrode	[a]RMS Noise (µV)		[d]SNR (dB)	[a]RMS Noise (µV)	[d]SNR (dB)	[a]RMS Noise (µV)		[d]SNR (dB)	[a]RMS Noise (µV)		[d]SNR (dB)
	[b]LFB	[c]HFB		[b]LFB	[c]HFB		[b]LFB	[c]HFB		[b]LFB	[c]HFB	
Commercial SDE	47.49	1.618	-4.84	54.25	7.07	-3.06	60.23	3.38	-2.92	47.44	5.12	5.35
Proposed Pt electrodes	39.81	6.53	0.22	35.18	9.91	0.16	32.58	14.38	3.12	57.20	12.73	2.37
Proposed Au electrodes	22.12	4.23	1.85	21.46	4.44	3.69	55.91	15.81	6.67	75.75	15.78	3.74

[a]RMS: Root mean square, [b]LFB: Low frequency band, [c]HFB: High frequency band, and [d]SNR: Signal to noise ratio.

6.5.3 Magnetic resonance visualization of subdural mini-grids

All Au and Pt plates in the fabricated grid electrodes were clearly visualized in MRI images. Figure 6-13 shows MRI images of the proposed mini-grid electrodes, where electrodes, edge markers, and numbering markers were individually identified.
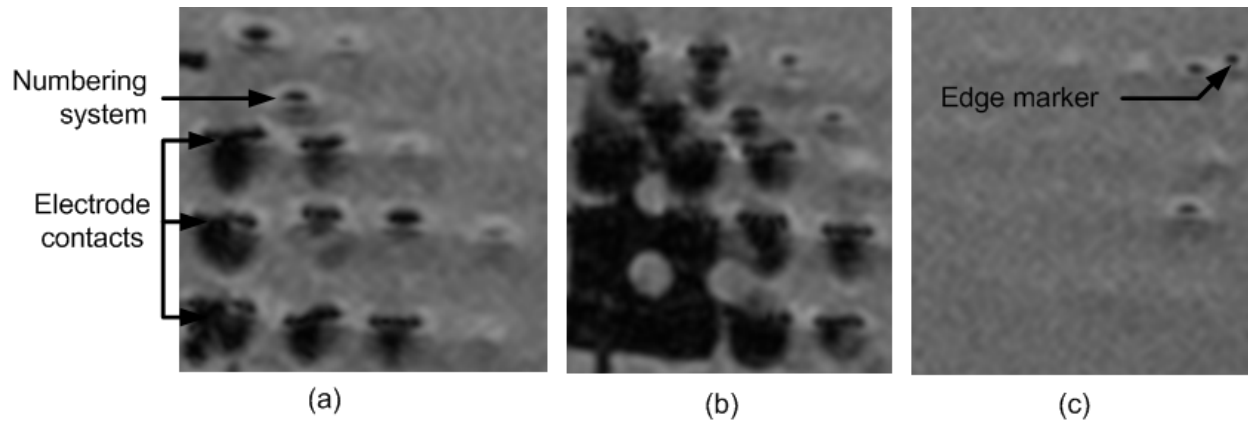
Figure 6-13: MRI image sequences of the new mini-grid Pt electrodes: Images (a) – (b) were taken by placing the electrodes into a gel solution (0.9% NaCl with 14gm gelatin) and scanning them using a 1.5 T Phillips MR scanner.

6.5.4 Validation of wireless transmission of icEEG recordings

The wireless icEEG recording system was implemented on printed circuit board and validated using the wired recorded icEEG from rats. Figures 6-14 (a)-(b) show icEEG recording from the wired Stellate Harmonie System and from the new wireless system. The icEEGs were recorded wirelessly at 250 Hz sampling frequency without degradation of signal quality. Normalized root-mean-square deviation in between the original and wirelessly recorded signal was average 2%. The total power consumption of wireless recording system was 15mW.
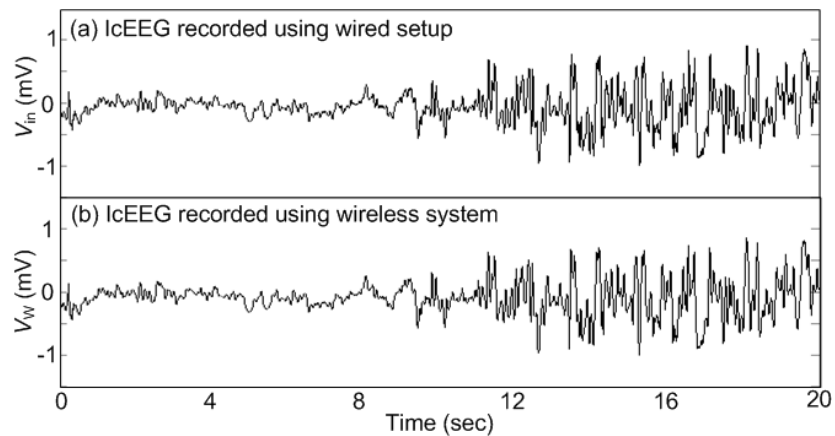
Figure 6-14: IcEEG recordings using: (a) Stellate Harmonie System (wired setup) and (b) Wireless system.

6.5.5 Post icEEG brain histology

Histology results showed nissl substance and labeled cells on the cerebral cortex. The cyto-architectures of the somatosensory cortices was similar between both brain hemispheres underneath the pure Pt (right) and pure Au (left) subdural electrode contacts in group 1 rats (Figure 6-15). The exposed regions were also compared to other sensory regions (not exposed to electrode contacts) such as the visual cortex. Clear cytoarchitectonic borders could still be defined between the primary and secondary sensory cortices. Neocortical laminar organization and cellular densities (e.g. neurons and glial cells) did not appear to be altered by the implants.
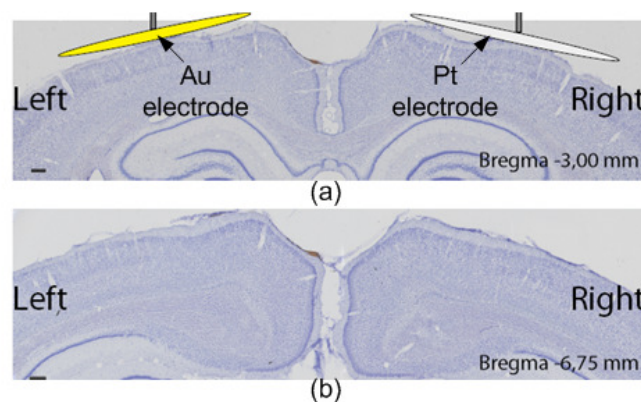
Figure 6-15: Representative micrographs illustrating the effect of the proposed subdural electrodes on the morphological appearance of cortex, 7 days after the 3 weeks *in vivo* recording experiment in group 1: (a) Somatosensory cortices (exposed to the electrodes) and (b) Visual cortices (unexposed).

The rest of exposed tissues by the electrodes were found normal compared to (PAXINOS, 2009).

6.6 CONCLUSION

In this paper, we present early work on a new intracerebral recording system to improve localization of the EZ with less morbidity. The proposed novel subdural mini grid electrodes have a new shape and several attributes to address problems with the currently available electrodes: notches, holes, connectors, single exit cable, and wireless transmission. The new subdural electrodes were fabricated using moulding process and the pure Pt/Au electrode contacts were encapsulated with PDMS. The electrical characteristics of the pure Pt/Au electrodes were analyzed in vitro and their impedances were significantly lower than commercial electrodes. The Au contact had better Electrical impedance spectroscopy properties in icEEG recording frequency band than the Pt contact. These electrodes were successfully implanted on rats and series of in vivo recording experiments were performed. The experimental results demonstrated 50% less flicker and thermal noises than commercial electrodes, excellent signal stability, improved SNR by up to 6 dB, and no evidence of tissue damage. The next step will be to test the entire system in larger animals.

6.7 ACKNOWLEDGMENTS

GENERAL DISCUSSION

In this thesis, we have presented neural signal acquisition systems, automatic signal processors and responsive stimulators for the construction of new prosthetic devices to treat epilepsy. Also, we have proposed new subdural porous and notched mini grid electrodes during epilepsy presurgical evaluation. The contributions were made at circuit-level, system-level and fabrication-level.

Implantable responsive device therapies offer a promising alternative treatment options outside of conventional medicine including the possibility of treating refractory epileptic patients who are not candidate for (or have failed) epilepsy surgery. The first step of constructing the therapeutic device is to design an electrographic seizure onset detector. However, electrophysiological seizure-onset patterns vary from patient to patient and a generic detector has higher level of complexity in circuit design and dissipates more power. The most frequently encountered ones are the low-voltage fast-activity, high-voltage fast-activity and rhythmic spiking patterns. The proposed seizure onset detection algorithm detects the most frequently seizure onset pattern (low-voltage fast-activity) in icEEG recordings. This algorithm includes a modified chopper stabilized preamplification and a real-time seizure onset detection method. Using this algorithm, we designed and implemented a integrated on chip detector that modulates icEEG recordings, amplifies the desired amplitude level of signal, extracts fast activity information using voltage window detectors, demodulates processed signal to the original frequency of acquisition using RC circuit, and detects seizure frequency by analyzing fast activities. Advantages of the proposed seizure detector are (i) reduction of the instrumentation and external noises, and enhancement of the sensitivity and specificity in seizure detection; (ii) increase of detection accuracy due to both high frequency and high amplitude detection criteria; (iii) decrease of false alarms due to seizure-unrelated physiological rhythmic activity and baseline activity variations; (iv) reduction of detection delay; and (v) the low-power consumption of the device. This detector was validated using icEEG recording from seven refractory epilepsy patients. The detection performance showed 100% sensitivity and specificity, and early detection of the abnormalities at electroclinical seizure onset demonstrates the capability of intervening quickly in the hope of disrupting before the seizure propagates to adjacent regions.

Responsive electrical stimulators composed of a seizure detector and a biphasic electrical stimulator. We proposed two prototypes of the responsive electrical stimulators. The first prototype combines the seizure detector and a FPGA based embedded stimulator. This device records icEEG continuously from the epileptogenic zone, monitors the recording, and triggers a burst of electrical stimulation on epileptic seizure onset detection. The second prototype of the responsive electrical stimulator which has lower power consumption, wider range of parameter variation, better precision, and larger memory. These responsive stimulators were validated offline using icEEG recording from ten refractory epilepsy patients and the early triggering of a burst of electrical stimulation is able to disrupt an upcoming seizure. Also, the second prototype stimulator was tested on cadaveric animal brain tissue in an *in vitro* morphologic electrical model. Spatial characteristics of the voltage distribution in cortex due to the stimulation were demonstrated and the experimental results suggested that lower frequency stimulation parameters caused significant amount of shunting of current through the cerebrospinal fluid; however higher frequency stimulation parameters produced effective spatial voltage distribution with lower stimulation charge.

Another interesting alternative focal treatment of epilepsy is responsive direct drug delivery. In this thesis, we proposed an implantable device which contains a new asynchronous seizure detector and a drug delivery system. The proposed device offers promises of low power dissipation, better data-dependent computation and higher detection performances compared to the previously proposed synchronous design. The synchronous devices continuously dissipate battery power for clock gating which ultimately shortens the interval for battery replacement or recharging. The asynchronous system is validated using icEEG recordings from seven patients, and detection performance is as accurate as that obtained with synchronous devices, but reduces power consumption by 49% in power saving mode. Sensitivity of the device is maximized to prevent unwarranted drug delivery; however, the average detection of the device is higher than the other the state-of-the-art detectors; but the proposed device has showed capability to detect seizure onset and deliver the antiepileptic drug well before the onset of clinical manifestations. All the detections have sufficient time to inject drugs and block seizure progression. The proposed device was mounted on two PCBs and proven to be reliable in an implantable device without risking false detections.

Efficacy of the responsive focal treatment depends on high quality icEEG recording. In chapter 5, we proposed high conductive intracranial electrodes for better icEEG recordings. Apart from their necessity for implantable responsive devices, intracranial electrodes are used in the epilepsy centers to delineate the EZ prior to epilepsy surgery in drug-refractory patients. Current clinical use of such electrodes is associated with some risk of complications, the most common being infection, hemorrhage and edema. Hence, it is important to limit the number of electrodes used without compromising the ability to localize the epileptogenic zone (EZ) adequately. As such, there is always a risk that an intracranial study may fail to identify the EZ from suboptimal coverage. We presented a new subdural electrode design which will hopefully allow large sampling of suspected areas of epileptogenicity at lower risk. The new subdural electrodes has several new attributes: (i) smaller in size but connectable grids which are intended to provide better conductivity with tissues in curvature regions and reduce electrode displacement or overlap; (ii) notches to provide better flexibility; (iii) holes to potentially reduce the risk of edema and hemorrhage; (iv) a numbering system and edge markers to facilitate their identification on post-implantation magnetic resonance imaging, (v) only two exit cables or wireless icEEG recordings in order to reduce the risk of infections. Moreover, the electrode contact and inter-connection wiring use pure Gold and Platinum material to obtain lower impedance (~116 kΩ) values compared to commercial contacts. The electrode contacts were tested for long-term *in vivo* neural recordings in rats. The recorded signal had excellent stability; moreover, noises were reduced and the signal-to-noise ratio was increased by ~6 dB. Following icEEG recordings using novel electrode contacts, histological examination of the rats' cortex showed no tissue damage.

CONCLUSION AND FUTURE WORKS

Herein, we conclude this thesis by a review of our contributions along with offering some suggestions for future works.

CONTRIBUTIONS

1. Design, implementation and validation of two seizure onset detectors with different level of complexity and power dissipation as broken into the following points:

    (i) Proposing new preamplification techniques: (a) a chopper stabilized preamplification methodology and (b) a three-stage preamplifier.

    (ii) Proposing seizure onset detection algorithms: (a) synchronous detection algorithm and (b) asynchronous detection algorithm.

    (iii) Implementing the preamplifiers and seizure detectors in PCBs with discrete components and 0.18µm CMOS process, and successfully testing using icEEG recordings from refractory epilepsy patients.

2. Modeling, implementation and validation of three new implantable closed-loops focal brain treatment devices as detailed below:

    (i) Proposing two architectures for the closed-loop electrical stimulators.

    (ii) Demonstration of spatial voltage distribution model in gray matter of brain due to the bipolar biphasic electrical stimulation.

    (iii) Proposing optimum electrical stimulation parameters for the suspected epileptic focus.

    (iv) Proposing an implantable asynchronous direct drug delivery device.

    (v) Construction of new hybrid electrodes.

    (vi) Implementing the closed-loop brain stimulators with microchip (0.18µm CMOS technology), FPGA (e.g. Actel EX256 and Igloo AGL125) and discrete components in miniature PCBs, and successfully testing using icEEG recording from ten refractory epilepsy patients.

3. Design and implementation of a new presurgical procedure to improve localization of the epileptogenic zone with less morbidity as detailed below:

(i) Design new attributes and shapes for novel subdural electrodes in order to provide better coverage of the suspected regions of epileptogenicity.

(ii) Improvement of signal-to-noise ratio of icEEG recording and better electrode-tissue reaction using higher conductive subdural electrode contact.

(iii) Construction of a new implantable wireless icEEG recording system to reduce bacterial infection and CSF leakage.

RECOMMENDATIONS FOR FUTURE WORKS

This thesis paves the way for several research topics. Moreover, the new microelectronic device therapies like focal electrical stimulation and direct drug delivery have obviously many important considerations from different aspect of this approach. Herein, we mention some of these issues based on our studies and experiments in this thesis.

(i) Preamplification: Design a modified chopper-stabilized amplifier using a conventional folded-cascode amplifier because of better noise performance. This conventional architecture requires additional four CMOS modulation switches to chopper stabilize the amplifier. Moreover, the demodulator and low-pass filter of the chopper amplifier can be replaced by a charge pump in order to reconstruct the signal in digital domain. This modified chopper-stabilized amplifier would be useful in low-power seizure detection applications.

(ii) Seizure detection: Investigate different types of electrographic seizure onset (e.g. high voltage fast activities and rhythmic patterns) for a generic seizure detection algorithm. Determine optimum seizure onset detection criteria, design a power efficient algorithm, and implement it using CMOS process.

(iii) High Frequency Oscillation (HFO): Increasing evidence indicate that pathological HFOs are good markers of the EZ. Thus, it is important to analyze the HFOs and determine optimum detection criteria and find out antiepileptic affect due to neuromodulation at HFO detection. Also, sampling frequency is important for the better HFO recoding. It is recommended to use 2 kHz or more sampling frequency to record HFOs and subsequent analysis and detections.

(iv) Closed-loop focal brain treatment device: Performance of a closed-loop neurostimulator can be improved several ways. We believe the following issues should be taken into count in future works:

- Design and implementation of a miniaturized low-power fully integrated closed-loop neurostimulator.

- Improvement of further electrical conductivity in intracranial electrodes and electrical path for better icEEG recoding.

- Implementation of a low-power electrical stimulator using freeze-mode FPGA.

- Design and implementation of low-power micropump rather than commercial micropump which has been used in this thesis.

- Model and implementation of responsive thermoelectric (Peltier) device for focal cooling therapy.

(v) Presurgical evaluation: Design and fabrication of hybrid subdural grid electrodes incorporating focal cooling. The grid electrodes can be fabricated using moulding process and microtubing would be integrated in the grid for cold water circulation.

BIBLIOGRAPHIE

Abdelhalim, K., Smolyakov, V. & Genov, R. (2011). Phase-Synchronization Early Epileptic Seizure Detector VLSI Architecture, *IEEE TBIOCAS*, vol. 5, No. 5.

Agarwal, V.S., Thakor, N.V., Lesser, R.P., Gordon, B., & Nathan, S. (1994). Modeling electrical stimulation of the human cerebral cortex; Engineering Advances: New Opportunities for Biomedical Engineers. *Proceedings of the 16th Annual International Conference of the IEEE*, 1, 185- 186.

Agnew, W.F., McCreery, D.B, (1990). Neural prostheses: fundamental studies. Englewood Cliff, NJ: Prentice Hall.

Aksenova, T. I., Volkovych, V. V., & Villa, A. E. P. (2007). Detection of spectral instability in EEG recordings during the preictal period, J. *Neural Eng.,* 4, 173.

Anschel, D. J., Ortega, E. L., Kraus, A. C., Fisher, R. S. (2004). Focally injected adenosine prevents seizures in the rat. *Experimental Neurology*, vol. 190(2), pp. 544-547.

Anschel, D. J., Ortega, E. L., Kraus, A. C., & Fisher, R. S. (2004). Focally injected adenosine prevents seizures in the rat. *Experimental Neurology,* 190, 544-547.

Arnhold, J., Grassberger, P., Lehnertz, K., & Elger, C. E. (1999). A robust method for detecting interdependences: application to intracranially recorded EEG. *Physica D: Nonlinear Phenomena,* 134, 419-430.

Aziz, J. N. Y., Karakiewicz, R., Genov, R., Bardakjian, B. L., Derchansky, M., & Carlen, P. L. (2006). Towards Real-Time In-Implant Epileptic Seizure Prediction. *IEEE Engineering in Medicine and Biology Conference.*

Aziz, J. N. Y., Karakiewicz, R., Genov, R., Bardakjian, B. L., Derchansky, M., & Carlen, P. L. (2006). Real-time seizure monitoring and spectral analysis microsystem. *IEEE ISCAS*, 2133–36.

Aziz, J. N. Y., Karakiewicz, R., Genov, R., Chiu, A. W. L., Bardakjian, B. L., Derchansky, M., & Carlen, P. L. (2007). In vitro epileptic seizure prediction microsystem. *IEEE ISCAS*, 3115-3118.

Babb, T. L., Lieb, J. P., Brown, W. J., Pretorius, J., Crandall, P. H. (1984). Distribution of pyramidal cell density and hyperexcitability in the epileptic human hippocampal formation. *Epilepsia*, vol. 25, pp. 721-728.

Bancaud, J. & Talairach, J. (1973). Methodology of stereo EEG exploration and surgical intervention in epilepsy," Rev Otoneuroophtalmol., vol. 45(4), pp.315-28.

Berdakh, A., & Don, S. H. (2009). Epileptic seizures detection using continuous time wavelet based artificial neural networks. *ITNG - Int. Conf. Inf. Technol.: New Gener*, 1456-1461.

Benbadis S., Wyllie, E. & Bingaman, W. (2006). Intracranial electroencephalography and localization studies", In: Wyllie E, ed., ch:77, The treatment of epilepsy: principles and practice.

Bhavaraju, N. C., Frei, M. G., & Osorio, I. (2006). Analog seizure detection and performance evaluation. *IEEE transactions on bio-medical engineering,* 53, 238-245.

Blad, N.B.L. (2007). An Electrical Impedance Model for Deep Brain Stimulation of Parkinson's Disease. *In 13th International Conference on Electrical Bioimpedance and the 8th Conference on Electrical Impedance Tomography.*

Boon, P., Raedt, R., de Herdt, V., Wyckhuys, T., & Vonck, K. (2009). Electrical stimulation for the treatment of epilepsy. *Neurotherapeutics*, 6(2):218-27.

Butson, C. R., & McIntyre, C. C. (2008). Current steering to control the volume of tissue activated during deep brain stimulation. 1, 1, 7-1.

Butsona, C. R., Maksa C. B., & McIntyre, C. C. (2006). Sources and effects of electrode impedance during deep brain stimulation. *Clinical Neurophysiology,* 117, 2, 447-454.

Celik, O., O'Malley, M. K., Boake C., *et al.* (2010). Normalized movement quality measures for therapeutic robots strongly correlate with clinical motor impairment measures. *IEEE Trans. Neural. Syst. Rehabil. Eng.*, vol. 18, no. 4, pp. 433-44.

Chabardes, S., Kahane, P., Minotti, L., Koudsie, A., Hirsch, E., Benabid, A.L. (2002). Deep brain stimulation in epilepsy with particular reference to the subthalamic nucleus. Epileptic Disord., 4 (Suppl. 3), S83–S93.

Chen, Y. C., Hsu, H. L., Lee, Y. T., et al. (2011). An active, flexible carbon nanotube microelectrode array for recording electrocorticograms. *J. Neural Eng.*, vol. 8(3).

Constandinou, T. G. Georgiou, J., & Toumazou, C. (2008). A Partial-Current-Steering Biphasic Stimulation Driver for Vestibular Prostheses. *IEEE Trans.Biomed. Eng.*, 2, 2, 106-113.

Coulombe, J., Sawan, M., & Gervais, J. F. (2007). A Highly Flexible System for Microstimulation of the Visual Cortex: Design and Implementation. *IEEE Trans. Biom. Circuits & Systems,* 1, 258–269.

Crandall, P.H., Brown, W.J. & Brinza, K. (1966). Stereotaxic accuracy in vivo of Talairach method in temporal lobes. *Confin Neurol.*, vol. 27, pp.149–53.

David, J. A., Ortega, E., & Robert S. F. (2004). Diazepam prophylaxis for bicuculline-induced seizures: a rat dose-response model. *Neuroscience Letters,* 356, 66-68.

DodGe, H.W., Bailey, A.A., Bickford, R.G., Petersen, M.C., Sem-Jacobsen, C.W. & Miller, R.H. (1953). Neurosurgical and neurologic application of depth electrography," *Proc Staff Meet Mayo Clin.*, Vol. 28(6), pp. 188-91.

Dubeau, F. & McLachlan, R. S. (2000). Invasive electrographic recording techniques in temporal lobe epilepsy. *Can J Neurol Sci.*, vol. 27 Suppl 1, pp. S29-34.

Engel, J. J. (2009). Overview of surgical treatment for epilepsy (3e éd.). *The Treatment of Epilepsy, Wiley-Blackwell,* 60, 743-756.

Fisher, R. S., & Ho J. (2002). Potential new methods for antiepileptic drug delivery. *CNS drugs,* 16(9), 579-593.

Fisher, R., Salanova, V., Witt, T., Worth, R., Henry, T., Gross, R., Oommen, K., Osorio, I., et al. (2010). Electrical stimulation of the anterior nucleus of thalamus for treatment of refractory epilepsy. *Epilepsia*, 51(5), 899–908.

Fountas, K. N. & Smith, J. R. (2007). Subdural Electrode-Associated Complications: A 20-Year Experience. *Stereotact Funct Neurosurg*, vol. 85, pp. 264–272.

Ghosh-Dastidar, S., Adeli, H., & Dadmehr, N. (2008). Principal component analysis-enhanced cosine radial basis function neural network for robust epilepsy and seizure detection. *IEEE Trans. Biomed. Eng.,* vol. 55, no. 2, pp. 512-8.

Goldring S. & Gregorie, E.M. (10984). Surgical management of epilepsy using epidural recordings to localize the seizure focus. Review of 100 cases. *J Neurosurg*., vol. 60(3), pp. 457-66.

Good, L. B., Sabesan, S., Iasemidis, L. D., Tsakalis, K., & Treiman, D. M. (2004). Brain dynamical disentrainment by anti-epileptic drugs in rat and human status epilepticus. *Conf. Proc. IEEE Eng. Med. Biol. Soc.,* vol.1, pp. 176-9.

Gordon, B., Lesser, R., Rance, N., et al. (1990). Parameters for direct cortical electrical stimulation in the human: histopathologic confirmation. *Electroenchepalog and Clin Neurophysiol*, 75, 371–377.

Gosselin, B., Simard, V., Roy, J. F., Marrouche, W., Dumortier, C., & Sawan, M. (2004). Multichannel wireless cortical recording: Circuits, system design and assembly challenges. *IEEE International Workshop on Biomedical Circuits and Systems*, Singapore.

Gosselin, B., Simard, V., & Sawan, M. (2004). Low-power implantable microsystem intended to multichannel cortical recording. *IEEE International Symposium on Circuits and Systems,* Vancouver, BC, Canada.

Gosselin, B., Simard, V., & Sawan, M. (2004). An ultra low-power chopper stabilized front-end for multichannel cortical signals recording. *IEEE CCECE*, 2259 – 2262.

Gosselin, B., Robert, P. Y., & Sawan, M. (2007). A Scalable Design for Signal Conditioning and Digitization in Implantable Multi-Channel Neural Sensors. *Computer Architecture for Machine Perception and Sensing, International Workshop,* 73-74.

Gosselin, B., & Sawan, M. (2007). A low-power integrated neural interface with digital spike detection and isolation. *14th IEEE International Conference on Electronics, Circuits and Systems*, Marrakech, Morocco.

Gosselin, B., & Sawan, M., & Chapman, C. A. (2007). A low-power integrated bioamplifier with active low-frequency suppression. *IEEE Trans. on BioCAS*, 1(3), 184-192.

Gosselin, B., & Sawan, M. (2008). An ultra low-power CMOS action potential detector. *IEEE International Symposium on Circuits and Systems,* Seattle, WA.

Gosselin, B., & Sawan, M. (2009). An ultra low-power CMOS automatic action potential detector. *IEEE Trans. on Neural Systems and Rehabilitation Engineering*, 17(4), 346-353.

Gosselin, B., Sawan, M., & Kerherv, E. (2010). Linear-phase delay filters for ultra-low-power signal processing in neural recording implants. *IEEE Trans. on BioCAS,* 4(3), 171-180.

Gosselin, B., & Sawan, M. (2010). A low-power integrated neural interface with digital spike detection and extraction. *AICSP*, vol. 64(1), 3-11.

Gotman, J., (1985). Seizure recognition and analysis**.** In Long-term Monitoring in Epilepsy**,** *Electroencephalography and Clinical Neurophysiology*, Suppl 37, Amsterdam: Elsevier, pp. 133-145.

Gordon B., Lesser R., Rance N., et al. (1990). Parameters for direct cortical electrical stimulation in the human: histopathologic confirmation. *Electroenchepalog and Clin Neurophysiol*, 75, 371–377.

Guerra, G. R., Davalos, R. V., Garcia P. A., *et al.* (2005). Heat transfer model to characterize the focal cooling necessary to suppress spontaneous epileptiform activity. *Proceedings of SPIE: Progress in Biomedical Optics and Imaging*, 240-246.

Handforth, A., DeSalles, A.A., Krahl, S.E. (2006) Deep brain stimulation of the subthalamic nucleus as adjunct treatment for refractory epilepsy. Epilepsia, 47 (7), 1239–1241.

Harrison, R. R. (2008). The design of integrated circuits to observe brain activity. *Proceedings of the IEEE*, 96, 1203-1216.

Henle, C., Raab, M., Cordeiro, J. G., Doostkam, S., Schulze-Bonhage, A., Stieglitz, T. & Ricker, J. (2011). First long term in vivo study on subdurally implanted Micro-ECoG electrodes, manufactured with a novel laser technology. *Biomed Microdevices*, vol. 13, pp.59–6.

Hodaie, M., Wennberg, R.A., Dostrovsky, J.O., and Lozano, A.M., (2002). Chronic anterior thalamus stimulation for intractable epilepsy. Epilepsia, 43 (6), 603–608.

Iasemidis, L. D., Deng-Shan, S., Chaovalitwongse, W., Sackellares, J. C., Pardalos, P. M., Principe, J. C., Carney, P. R., Prasad, A., Veeramani, B. & Tsakalis, K. (2003). Adaptive epileptic seizure prediction system. *IEEE Transactions on Biomedical Engineering,* 50, 616-627.

Iasemidis, L. D., Pardalos, P. M., Shiau, D.S., Chaowolitwongse, W., Narayanan, K., Kumar, S., Carney, P. R., & Sackellares, J.C. (2003). Prediction of human epileptic seizures based on optimization and phase changes of brain electrical activity. J. *Optimization Methods and Software*, 81-104.

Jacobs, J., Zijlmans, M., Zelmann, R., Olivier, A., Hall, J., Gotman, J., & Dubeau, F. (2010). Value of electrical stimulation and high frequency oscillations (80-500 Hz) in identifying epileptogenic areas during intracranial EEG recordings. *Epilepsia*, Vol. 51(4), pp. 573-82.

Jawed, S. A., Nielsen, J. H., Gottardi, M., Baschirotto, A., & Bruun, E. (2009). A multifunction low-power preamplifier for MEMS capacitive microphones. *Proceedings of the 35th European Solid-State Circuits Conference. ESSCIRC*, pp. 292-5.

Katz, B., & Miledi, R. (1965). The effect of temperature on the synaptic delay at the neuromuscular junction. *J. Physiol,* 181, 656–670.

Kossoff, E. H., Ritzl, E. K., Politsky, J. M., Murro, A. M., Smith, J. R., Duckrow, R. B., Spencer, D. D. & Bergey, G. K. (2004). Effect of an external responsive neurostimulator on seizures and electrographic discharges during subdural electrode monitoring. *Epilepsia,* 45, 1560-1567.

Kuncel, A.M., Cooper, S.E., Wolgamuth, B.R., Clyde, M.A., Snyder, S.A., Montgomery Jr, E.B., Rezai, A.R., & Grill, W.M. (2006). Clinical response to varying the stimulus parameters in deep brain stimulation foressential tremor. *Mov. Disord.,* 21, 11, 1920–1928.

Lee, W.S., Lee, J.K., Lee, S.A., Kang, J.K., & Ko, T.S. (2000) Complications and results of subdural grid electrode implantation in epilepsy surgery. *Surg Neurol.* Vol. 54(5), pp. 346-51.

Lega, B. C., Halpern, C. H., Jaggi, J. L. and Baltuch, G. H. (2009). Deep brain stimulation in the treatment of refractory epilepsy: update on current data and future directions. Neurobiol Dis., 38(3):354-60.

Lehnertz, A., & Elger, C. E. (1995). Spatio-temporal dynamics of the primary epileptogenic area in temporal lobe epilepsy characterized by neuronal complexity loss. *Electroencephalogr. Clin. Neurophysiol.*, vol. 95, no. 2, pp. 108-17.

Lester, D. B., Rogers, T. D., & Blaha, C. D. (2009). Neuronal pathways involved in deep brain stimulation of the subthalamic nucleus for treatment of Parkinson's disease, *IEEE EMBC*, 3302-5.

Manola L., Roelofsen B. H., Holsheimer J., Marani E., & Geelen J. (2005). Modelling motor cortex stimulation for chronic pain control: Electrical potential field, activating functions and responses of simple nerve fibre models. 43, 3, 335-343.

Masaya, Y., Akiyoshi, S., Keiichi, T., Nobuhiko, N. (2010). Multichannel biosensing and stimulation LSI chip using 0.18m complementary metal-oxide-semiconductor technology. *Japanese Journal of Applied Physics*, Vol. 49, No. 4 PART 2.

McIntyre C. C., Mori S., Sherman, D. L., Thakor N. V., & Vitek J. L. (2004). Electric field and stimulating influence generated by deep brain stimulation of the subthalamic nucleus. 115, 3, 589-595.

McSharry, P. E., He, T., Smith, L. A. & Tarassenko, L. (2002). Linear and non-linear methods for automatic seizure detection in scalp electro-encephalogram recordings. *Medical & biological engineering & computing,* 40(4), 447-461.

Meier, R., Dittrich, H., Schulze-Bonhage, A., *et al.* (2008). Detecting epileptic seizures in long-term human EEG: a new approach to automatic online and real-time detection and classification of polymorphic seizure patterns," *J. Clin. Neurophysiol.,* vol. 25, no. 3, pp. 119-131.

Merrill, D. R., Biksonb, M., & Jefferysc, J.G.R. (2005). Electrical stimulation of excitable tissue: design of efficacious and safe protocols. *Journal of Neuroscience Methods*, 141, 171–198.

Miocinovic, S., Lempka, S. F., Russo, G. S., Maks, C. B., Butson , C. R., Sakaie, K. E., Vitek, J. L., & McIntyre, C. C. (2009). Experimental and theoretical characterization of the voltage distribution generated by deep brain stimulation. *Exp Neurol*., 216, 1, 166-76.

Mormann, F., Lehnertz, K., David, P., & Elger, C. E. (2000). Mean phase coherence as a measure for phase synchronization and its application to the EEG of epilepsy patients. *Elsevier Science,* 144, 358-369.

Morrell, M. J. (2002). Brain stimulation for epilepsy: can scheduled or responsive neurostimulation stop seizures?. *Neurology*, 164–168.

Morrell, M. J. (2011). Responsive cortical stimulation for the treatment of medically intractable partial epilepsy, Neurology. 77, 13, 1295-304.

Mounaim, F., Sawan, M., & Bedard, S. (2006). Implantable Neuro-Monito-Stimulation System Dedicated to Enhance the Bladder Functions. *IEEE Biomedical Circuits and Systems Conference - Healthcare Technology*, 198–201.

Mounaim, F., & Sawan, M. (2007). Miniature Implantable System Dedicated to Bi-Channel Selective Neurostimulation. *IEEE ISCAS,* 2072-2075.

Mounaim, F., & Sawan, M. (2011). Integrated High-Voltage Inductive Power and Data Recovery Front-End Dedicated to Implantable. *IEEE TBIOCAS*, 5, 3, 283-291.

Moxon, K., Kuzmick, V., Lafferty, J., Serfass, A., Szperka, D., Zale, B., Johnson, J. & Nagvajara, P. (2001). Real-time seizure detection system using multiple single-neuron recordings. *Conference Proceedings of the 23rd Annual International Conference of the IEEE Engineering in Medicine and Biology Society*, 934-937.

Nadeau, P., & Sawan, M. (2006). A flexible high voltage biphasic current-controlled stimulator. *Conference on Biomedical Circuits and Systems*, 206–209.

Nagaraj, S., Shah, A., Shah, P., Szeto, V., & Bergen, M. T. (2006). Ambulatory preseizure detection device. *IEEE 32nd Annual Northeast Bioengineering Conference*, 41-42.

Nandan, M., Sachin, S. S., Myers, S., Ditto, W. L., Khargonekar, P. P., & Carney, P, R. (2010). Support vector machines for seizure detection in an animal model of chronic epilepsy. *J. Neural Eng.,* 7, 036001.

Nathan, S. S., Sinha, S. R., Gordon, B., Lesser, R. P., & Thakor, N. V. (1993). Determination of current density distributions generated by electrical stimulation of the human cerebral cortex. *Electroencephalography and Clinical Neurophysiology*, 86, 3, 183-92.

Nielsen, L. S. & Sparso, J. (1999). Designing asynchronous circuits for low power: an IFIR filter bank for a digital hearing aid. *Proceedings of the IEEE,* vol. 87, no. 2, pp. 268-81.

Nguyen, D. K., & Spencer, S. S. (2004). Invasive EEG in presurgical evaluation of epilepsy (2e éd.). *The Treatment of Epilepsy, Wiley-Blackwell*, 53, 633-658.

Niro, J., Manso, J., Ballina, F., Periolo, S., D'Atellis, C., Ponce, S., Barroso, M., Anessi, C., & Kochen, S. (2007). Development of a neurostimulator for studies of epileptic crisis. *J. Phys. Conf. Ser.,* 90, 012032.

Norlin, J. P. & Leygraf, C. (2002). Investigation of interfacial capacitance of Pt, Ti and TiN coated electrodes by electrochemical impedance spectroscopy, *Biomol. Eng.*, vol. 19, no. 67.

Oommena, J., Krausb, A. C., & Fisher, R. S. (2007). Intraventricular administration of gabapentin in the rat increases flurothyl seizure threshold. *Neuroscience Letters,* 417, 308-311.

Osorio, I., Frei, M.G., Manly, B.F., Sunderam, S., Bhavaraju, N.C., and Wilkinson, S.B. (2001).An introduction to contingent (closed-loop) brain electrical stimulation for seizure blockage, to ultra-short-term clinical trials, and to multidimensional statistical analysis of therapeutic efficacy. J Clin Neurophysiol, 18(6), 533-44.

Osorio, I., Frei, M. G., Sunderam, S., Giftakis, J., Bhavaraju, N. C., Schaffner, S. F. & Wilkinson, S. B. (2005). Automated seizure abatement in humans using electrical stimulation. *Annals of Neurology,* 57(2), 258-68.

Osorio, I., Frei, M. G., Sornette, D., & Milton, J. (2009). Pharmaco-resistant seizures: self-triggering capacity, scale-free properties and predictability? *European Journal of Neuroscience*, 30, 1554–1558.

Osorio, I., & Frei, M. G. (2009). Real-time detection, quantification, warning, and control of epileptic seizures: The foundations for a scientific epileptology. *Epilepsy & Behavior*, 16, 391–396.

Panescu, D. (2005). Vagus nerve stimulation for the treatment of depression. *IEEE Eng. Med. Biol. Mag.*, vol. 24, no. 6, pp. 68-72.

Patel, K., Chua, C. P., Faul, S., & Bleakley, C. J. (2009). Low power real-time seizure detection for ambulatory EEG. *Int. Conf. on PCTHealth - Pervasive Health*.

Pang, C. C. C., Upton, A. R. M., Shine, G. & Kamath, M. V. 2003. A Comparison of Algorithms for Detection of Spikes in the Electroencephalogram", *IEEE Trans. Biomed. Eng.*, vol. 50(4).

Paxinos G. & Watson, C. (2009). The rat brain in stereotaxis coordinates, *6th edition*: *Academic Press Elsevier*, London, Burlinton, San Diego.

Penfield, W. & Jasper, H. (1954). Epilepsy and the Functional Anatomy of the Human Brain. Boston, Little, Brown and Co.

Polychronaki, G. E., Ktonas, P. Y., Gatzonis, S., Siatouni, A., Asvestas, P. A., Tsekou, H., Sakas, D., & Nikita, K. S. (2010). Comparison of fractal dimension estimation algorithms for epileptic seizure onset detection. *J. Neural Eng.,* 7, 046007.

Racine, R. J. (1972). Modification of seizure activity by electrical stimulation. II. Motor seizure. *Electroencephalography and Clinical Neurophysiology*, vol. 32, pp. 281–94.

Raghunathan, S., Gupta, S. K., Ward, M. P., Worth, R. M., Roy, K., & Irazoqui, P. P. (2009). The design and hardware implementation of a low-power real-time seizure detection algorithm. *Journal of Neural Engineering*, 6(5), 1-13.

Raghunathan, S., Jaitli, A. & Irazoqui, P. P. (2011). Multistage seizure detection techniques optimized for low-power hardware platforms. *Epilepsy & Behavior*, vol. 22, pp. S61–S68.

Raghunathan, S., Gupta, S. K., Markandeya, H. S., Irazoqui, P. P., & K. Roy. (2011) Ultra Low-Power Algorithm Design for Implantable Devices: Application to Epilepsy Prostheses. *J. Low Power Electron. Appl.* vol. 1, pp. 175-203.

Rayport, M., & Sandler, B. (1969). Six-electrode method for the measurement of the passive electrical properties of brain envelopes. *Med Biol Eng*., 7, 3, 321-4.

Ren, T. L., Yan, B., Lin, J. H., Wu, X. M., Wang, L. G., Yang, Y. & Liu, L. T. (2010). A MEMS-Based Flexible Electrode Array Using Composite Substrate. *IEEE Electron Devices and Solid-State Circuits*.

Reese, T. J. (2009). Vagus nerve stimulation: A proven therapy for treatment of epilepsy strives to improve efficacy and expand applications. *IEEE EMBC.,* 4631-4634.

Ren, T. L., Yan, B., Lin, J. H., Wu, X. M., Wang, L. G., Yang, Y., & Liu, L. T. (2010). A MEMS-Based Flexible Electrode Array Using Composite Substrate. *IEEE EDSSC*.

Risinger, M. and Gumnit, R., (1995). Intracranial electrophysiologic studies. *Neuroimaging and Clin N Am*,.5, 559 –573.

Rothman, S. M., Smyth, M. D., Yang, X. F., & Peterson, G. P. (2005). Focal cooling for epilepsy: an alternative therapy that might actually work. *Epilepsy Behav,* 7, 214–221.

Rubinstein, J. T., Miller, C. A., Mino, H., & Abbas, P. J. (2001). Analysis of monophasic and biphasic electrical stimulation of nerve. IEEE Trans. Biomed. Eng., 48, 10, 1065–1070.

Rychlicki, F., Zamponi, N., Trignani, R., Ricciuti, R. A., Iacoangeli, M., & Scerrati M. (2006). Vagus nerve stimulation: clinical experience in drug-resistant pediatric epileptic patients, *Seizure,* 15(7), 483-490.

Saab, M. E., & Gotman, J. (2005). A system to detect the onset of epileptic seizures in scalp EEG. *Clin Neurophysiol.,* vol. 116, no. 2, pp. 427-4.

Safi-Harb, M., Salam, M. T., Nguyen, D. K., & Sawan, M. (2011). An Implantable Seizure-Onset Detector Based on a Dual-Path Single-Window Count-Based Technique for Closed-Loop Applications, *IEEE Journal on Emerging and Selected Topics in Circuits and Systems*, (Accepted for publication).

Safi-Harb, M., Salam, M. T., Sawan, M., Nguyen, D. K., & Mirabbasi, S. (2011) A High Sensitivity Low-Power CMOS Seizure-Onset Detector, *IEEE EMBC*, Boston, USA.

Salam, M. T., Sawan, M., Hamoui, A., & Nguyen D. K. (2009). Low-power CMOS-based epileptic seizure onset detector. *IEEE-NEWCAS*, pp. 1-4.

Salam, M. T., Sawan, M., & Nguyen, D. K., & Hamoui, A. A. (2009). Epileptic low-voltage fast-activity seizure-onset detector," *IEEE-BIOCAS*, pp. 169-172.

Salam, M. T., Sawan, M., & Nguyen, D. K. (2010). Low-power implantable device for onset detection and subsequent treatment of epileptic seizures: a review. *Journal of Healthcare Engineering*, 1(2), 169-184.

Salam, M. T., Sawan, M., & Nguyen, D. K. (2010). Epileptic seizure onset detection prior to clinical manifestation. *IEEE EMBC* 6210-3.

Salam, M. T., Sawan, M., & Nguyen, D. K. (2010). A Low-power Implantable Device For Epileptic Seizure Detection and Neurostimulation, *IEEE-BIOCAS*, pp. 154 – 157.

Salam, M. T., Sawan, M., & Nguyen, D. K. (2011). A Multichannel Intracerebral EEG Monitoring System For Epilepsy Presurgical Evaluation, *IEEE Canadian Conference on Electrical and Computer Engineering: Biomedical and Health Informatics Symposium,* Niagara, Canada.

Salam, M. T., Desgent, S., Duss, S., Carmant, L., Nguyen, D. K., & Sawan, M. (2011). New Subdural Electrode Contacts for Intracerebral Electroencephalographic Recordings: Comparative Studies on Neural Signal Recording *In Vivo*, *IEEE BioCAS,* San Diego, USA.

Salam, M. T., Sawan, M., & Nguyen, D. K. (2011). A Novel Low-Power Implantable Epileptic Seizure-Onset Detector, *IEEE Transactions on Biomedical Circuits and Systems* (online version available since 23 June 2011).

Salam, M. T., Nguyen, D. K., & Sawan, M. (2012). Implantable Closed-loop Epilepsy Prosthesis: Modeling, Implementation and Validation, *ACM Journal of Emerging Technologies in Computing*, 2011 (To be appeared).

Salam, M. T. , Mirzaei, M. Sawan, M., & Nguyen, D. K. (2012), A Implantable Asynchronous Responsive Drug Delivery System for Treatment of Epilepsy**,** *IEEE Transactions on Neural Systems & Rehabilitation Engineering* (To be appeared).

Salam, M. T., Mounaïm , F., Nguyen, D. K., & Sawan, M. (2012). Low-Power Circuit Techniques for Epileptic Seizures Detection and Subsequent Neurostimulation, *Journal of Low Power Electronics - American Scientific Publishers: Special Issue on Emerging Technologies*, Vol. 8, N°2 (To be appeared).

Salam, M. T., Gelinas, S., Desgent, S., Duss, S., Turmel, F. B., Carmant, L., Sawan, M., and Nguyen D. K. (2012). Subdural Porous and Notched Mini Grid Electrodes for Wireless Intracranial EEG Recordings. *IEEE Transactions on Biomedical Circuits and Systems*, (Submitted for publication).

Sarma, S. V., Eden, U. T., Cheng, M. L., *et al.* (2010). Using point process models to compare neural spiking activity in the subthalamic nucleus of Parkinson's patients and a healthy primate. *IEEE Trans. Biomed. Eng.*, vol. 57, no. 6, pp. 1297-305.

Sawan, M., Salam, M. T., Gelinas, S., Lesage, F., & Nguyen, D. K. (2012). Combined NIRS-EEG Remote Recordings for Epilepsy and Stroke Real-Time Monitoring. *IEEE ISCAS* special session, Korea (Accepted).

Sawan, M., Hu, Y., & Coulombe, J. (2005). Wireless Smart Implants Dedicated to Multichannel Monitoring and Microstimulation. *Invited paper in IEEE Circuits and Systems Magazine,* 5, 21-39.

Sawan, M., Ba, A., Mounaim, F., Corcos, J., & Elhilali, M. M. (2008). Biomedical Circuits and Systems Dedicated for Sensing and Neurostimulation: Case study on Urinary Bladder dysfunctions. *Turkish Journal of Electrical Engineering and Computer Science,* 16, 3, 171-187.

Schachter, S. C., Guttag, J., Schiff, S. J., Schomer, D. L., & Summit Contributors. (2009). Advances in the application of technology to epilepsy: the CIMIT/NIO epilepsy innovation summit. *Epilepsy & Behavior*, 16, 3–46.

Sethi, N., Labar, D., Ponticello, L., Torgovnick, J., Sethi, P., & Arsura, E. (2008). Treatment of Medically Refractory Epilepsy: A Review Of Vagus Nerve Stimulator. *The Internet Journal of Neurology,* 9(1).

Shoeb, A., Edwards, H., Connolly, J., Bourgeois, B., Treves, T. & Guttag, J. (2004). Patient-Specific Seizure Onset Detection, *Engineering in Medicine and Biology Society*, 5(4), 483-498.

Skarpaas, T. L., & Morrell, M. J. (2009). Intracranial stimulation therapy for epilepsy. *Neurotherapeutics,* 6(2), 238-43.

Smith, D. C., Krahl, S. E., Browning, R. A. & Barea, E. J. (1993). Rapid cessation of focally induced generalized seizures in rats through microinfusion of lidocaine hydrochloride into the focus. *Epilepsia*, vol. 34, pp. 43-53.

Sramka M, Chkhenkeli S. A., (1990). Clinical experience in intraoperational determination of brain inhibitory structures and application of implanted neurostimulators in epilepsy. *Stereotact Funct Neurosurg*, 54 –55:56 –59.

Stein, A. G., Eder, H. G., Blum, D. E., Drachev, A., & Fisher, R. S. (2000). An automated drug delivery system for focal epilepsy. *Epilepsy research*, 39, 103-114.

Spencer, S. S., Nguyen, D. K., & Duckrow, R. B. (2009). *Invasive EEG in presurgical evaluation of epilepsy* (3e éd.). *The Treatment of Epilepsy*, 53, 767-798.

Suffczynski, P., Da Silva, F. H. L., Parra, J., Velis, D. N., Bouwman, B. M., van Rijn, C. M., van Hese, P., Boon, P., Khosravani, H., Derchansky, M., Carlen, P. & Kalitzin, S. (2006). Dynamics of epileptic phenomena determined from statistics of ictal transitions. *IEEE Transactions on Biomedical Engineering,* 53(3), 524-532.

Sukhi, G. & Jean, G. (2005). An automatic warning system for epileptic seizures recorded on intracerebral EEGs. *Clinical neurophysiology*, 116, 2460–2472.

Sun, F. T., Morrell, M. J., & Wharen, R. E. Jr. (2008). Responsive cortical stimulation for the treatment of epilepsy. *Neurotherapeutics,* vol. 5, no. 1, pp. 68-74.

Talairach, J. & Tournoux, P. (1958). Stereotaxic localization of central gray nuclei. *Neurochirurgia (Stuttg)*, vol. 1, pp. 88–93.

Talairach, J., Bancaud, J., Szikla, G., Bonis, A., Geier, S. & Vedrenne, C. (1974). [New approach to the neurosurgery of epilepsy. Stereotaxic methodology and therapeutic results. 1. Introduction and history]. *Neurochirurgie*, vol. 20 Suppl 1, pp.1-240.

Tanaka, N., Fujii, M., Imoto, H., Uchiyama, J., Nakano, K., Nomura, S., Fujisawa, H., Kunitsugu, I., Saito, T., & Suzuki, M. (2008). Effective suppression of hippocampal seizures in rats by direct hippocampal cooling with a Peltier chip. *J Neurosurg,* 108(4), 791-797.

Tangel, A., & Choi, K. (2004). "The CMOS inverter" as a comparator in ADC designs. *AICSP,* 39, 147-55.

Terry, R. (2009). Vagus nerve stimulation: a proven therapy for treatment of epilepsy strives to improve efficacy and expand applications. *Conf. Proc. IEEE Eng. Med. Biol. Soc.*, pp. 4631-4.

Tetzlaff, R., Niederhofer, C., & Fischer P. (2006). Automated detection of a preseizure state: nonlinear EEG analysis in epilepsy by cellular nonlinear networks and Volterra systems. *International Journal of Circuit Theory and Applications,* 34, 89-108.

Tito, M., Cabrerizo, M., Ayala, M. *et al.* (2009). Seizure detection: an assessment of time- and frequency-based features in a unified two-dimensional decisional space using nonlinear decision functions. *J. Clin. Neurophysiol.,* vol. 26, pp. 381-91.

Theodore, W. H., & Fisher, R. S. (2004). Brain stimulation for epilepsy. *Neurology,* 3(8), 111-118.

Thompson, S. M., Masukawa, L. M., & Prince, D. A. (1985). Temperature dependence of intrinsic membrane properties and synaptic potentials in hippocampal CA1 neurons in vitro. *J Neurosci*, 817–824.

Verma, N., Shoeb, A., Bohorquez, J., Dawson, J., Guttag, J., & Chandrakasan, A. P. (2010). A micro-Power EEG acquisition SoC with integrated feature extraction processor for a chronic seizure detection system. *IEEE Journal of Solid-State Circuits*, 45(4), 804-16.

Volgushev, M., Vidyasagar, T. R., Chistiakova, M., Yousef, T., & Eysel, U. T. (2000). Membrane properties and spike generation in rat visual cortical cells during reversible cooling. *J Physiol*, 522, 59–76.

Wieser, H.G., Elger, C.E. & Stodieck, S.R. (1985). The 'foramen ovale electrode': a new recording method for the preoperative evaluation of patients suffering from mesio-basal temporal lobe epilepsy. *Electroencephalogr Clin Neurophysiol.*, vol. 61(4), pp. 314-22.

Wyllie, E., Lüders, H., Morris, H.H., Lesser, R.P., Dinner, D.S., Hahn, J., Estes M.L., Rothner, A.D., Erenberg, G. & Cruse, R. (1987). Clinical outcome after complete or partial cortical resection for intractable epilepsy. *Neurologym*, vol. 37(10), pp.1634-41.

Xiao-Feng, Y., Duffy, D. W., Morley, R. E., & Rothman, S. M. (2002). Neocortical seizure termination by focal cooling: Temperature dependence and automated seizure detection. *Epilepsia,* 43, 240-245.

Yadav, R., Agarwal, R. & Swamy, M. N. S. (2009). A new improved model-based seizure detection using statistically optimal null filter, *IEEE-EMBC*, 1318-22.

Yadav, R., Agarwal, R., & Swamy, M. N. S. (2008). A novel dual-stage classifier for automatic detection of epileptic seizures. *Engineering in Medicine and Biology Society, 30th Annual International Conference of the IEEE*, 911-914.

Zandi, A. S., Dumont, A. G., Javidan, M., & Tafreshi, R. (2009). An entropy-based approach to predict seizures in temporal lobe epilepsy using scalp EEG. *Proc. Annu. Int. Conf. IEEE Eng. Med. Biol. Soc.: Eng. Future Biomed., EMBC*, 228-231.

Zandi, A. S., Javidan, M., Dumont, G. A. *et al.* (2010) Automated real-time epileptic seizure detection in scalp EEG recordings using an algorithm based on wavelet packet transform. *IEEE Trans. Biomed. Eng.,* vol. 57, no. 7, pp. 1639-51.

Zarifi, M. H., Frounchi, J., Farshchi, S. & Judy, J. W. (2008). A Low-Power, Low-Noise Neural-Signal Amplifier Circuit in 90-nm CMOS," *IEEE EMBS Conference*, Canada.

Zhong, X. L., Yu J. T., Zhang, Q., Wang, N. D., Tan, L. (2011). Deep brain stimulation for epilepsy in clinical practice and in animal models. Brain Research Bulletin, 85(3-4), 81-8.

APPENDICE A: Ethics approvals for *in vitro* and *in vivo* experiments

All experiments in the thesis were conducted at the Polytechnique Montreal, Centre Hospitalier de l'Université de Montréal (CHUM) - Notre-Dame Hospital, and University Hospital Center (UHC) - Ste-Justine Hospital. Ethical issues in the experiments have been considered and approval for the research has been given by the research ethics committee of Polytechnique Montreal, CHUM ethical committee, and UHC Ste-Justine Research Center.

Ethic approval # 10.173 (page # 149) and Ethic approval # CER-10/11-05 (page #151) have been given for the clinical experiments in chapters 2, 3, 4, and 5. The low-power devices were validated using the icEEG recordings from human epileptics during epilepsy presurgical evaluation at the CHUM – Notre-Dame Hospital. Use of these recordings and validation procedure were approved by the CHUM's ethics committee and research ethics committee of Polytechnique Montreal.

Ethic approval # 10.176 (page #152) and Ethic approval reference # 444 (page #154) have been given for the clinical experiments of chapter 6. Moreover, all procedures for the use and care of animals for these experiments were conformed to the policy and guidelines of the Canadian Council for Animal Care (CCAC). Experimental protocols were approved by the Comité Institutionnel des Bonnes Pratiques Animales en Recherche (CIBPAR).

CHUM

COMITÉ D'ÉTHIQUE DE LA RECHERCHE DU CHUM

Édifice Cooper
3981, boulevard St-Laurent, Mezz 2
Montréal (Québec) H2W 1Y5

Le 11 octobre 2010

Dr Dang Khoa Nguyen
Hôpital Notre-Dame du CHUM
Service de neuro-épilepsie
Pavillon Deschamps – 3ème étage
Montréal, (Québec) H2L 4M1

a/s Micheline Gravel
Courriel : micheline.gravel.chum@ssss.gouv.qc.ca

Objet : | **10.173 – Approbation accélérée initiale et finale CÉR**

Validation d'un nouveau détecteur de crises à faible consommation d'énergie

Docteur

J'ai pris connaissance des documents suivants reçus au CÉR du CHUM en date du 5 octobre 2010 en vue de l'approbation du projet en rubrique :

- Lettre accompagnant la soumission du projet pour évaluation
- Formulaire de demande d'évaluation d'un projet de recherche non-multicentrique
- Formulaire A – information budgétaire
- Autorisation pour consultation de dossiers médicaux à des fins de recherche
- Protocole de recherche

En vertu des pouvoirs qui me sont délégués par le Comité d'éthique de la recherche du CHUM pour procéder à une évaluation accélérée, il me fait plaisir de vous informer que j'approuve votre projet puisqu'il s'agit d'un projet se situant sous le seuil de risque minimal.

La présente constitue l'approbation finale du comité suite à une procédure d'évaluation accélérée. Elle est **valide pour un an à compter du 11 octobre 2010,** date de l'approbation de

CENTRE HOSPITALIER DE L'UNIVERSITÉ DE MONTRÉAL

HÔTEL-DIEU (Siège social)
3840, rue Saint-Urbain
Montréal (Québec)
H2W 1T8

HÔPITAL NOTRE-DAME
1560, rue Sherbrooke Est
Montréal (Québec)
H2L 4M1

HÔPITAL SAINT-LUC
1058, rue Saint-Denis
Montréal (Québec)
H2X 3J4

CHUM

votre projet. Je vous rappelle que toute modification au protocole et/ou au formulaire de consentement en cours d'étude, doit être soumise pour approbation du comité d'éthique.

Cette approbation suppose que vous vous engagiez :

1. à respecter la présente décision;
2. à respecter les moyens de suivi continu (cf Statuts et Règlements)
3. à conserver les dossiers de recherche pour une période d'au moins deux ans suivant la fin du projet afin permettre leur éventuelle vérification par une instance déléguée par le comité;
4. à respecter les modalités arrêtées au regard du mécanisme d'identification des sujets de recherche dans l'établissement.

Le comité suit les règles de constitution et de fonctionnement de l'Énoncé de Politique des trois Conseils et des Bonnes pratiques cliniques de la CIH.

Vous souhaitant la meilleure des chances dans la poursuite de vos travaux, je vous prie d'accepter, Docteur, mes salutations distinguées.

Brigitte St-Pierre, conseillère en éthique
Présidente
Comité d'éthique de la recherche du CHUM

BSTP/go

C.C. – Bureau des contrats

Voici les coordonnées de la personne ressources pour ce projet :
Mme Ghislaine Otis
Téléphone : 514 890-8000, poste 14485
Télécopieur : 514 412-7394
Courriel : ghislaine.otis.chum@ssss.gouv.qc.ca

ÉCOLE POLYTECHNIQUE MONTRÉAL

CERTIFICAT D'ACCEPTATION D'UN PROJET DE RECHERCHE PAR LE COMITÉ D'ÉTHIQUE DE LA RECHERCHE AVEC DES SUJETS HUMAINS DE L'ÉCOLE POLYTECHNIQUE

Comité d'éthique de la recherche avec des sujets humains

Adresse civique :
Campus de l'Université de Montréal
2900, boul. Édouard-Montpetit
École Polytechnique
2500, chemin de Polytechnique
H3T 1J4

Adresse postale :
C.P. 6079, succursale Centre-ville
Montréal (Québec) Canada
H3C 3A7

Téléphone : (514) 340-4990
Télécopieur : (514) 340-4992

École affiliée à l'Université de Montréal

Membres réguliers du comité :

Marie-Josée Bernardi, juriste et éthicienne
Ginette Denicourt, IRSST
Daniel Imbeau, génie industriel
Bernard Lapierre, éthicien*
Delphine Périé-Curnier, génie mécanique
Élodie Petit, juriste et éthicienne
André Phaneuf, UdeMontréal
Farida Cheriet, génie informatique et génie logiciel

Céline Roehrig, secrétaire

* président du Comité

Montréal, le 27 octobre 2010

M. Muhammad Tariqus Salam
M. Mohamad Sawan
Département de Génie électrique
Ecole Polytechnique de Montréal

N/Réf : Dossier CÉR-10/11-05

Messieurs,

J'ai le plaisir de vous informer que les membres du Comité d'éthique de la recherche ont procédé à l'évaluation en comité restreint de votre projet de recherche intitulé « *Validation d'un nouveau détecteur de crises à faible consommation d'énergie* ».

Les membres du Comité ont recommandé l'approbation de ce projet sur la base des documents transmis par courriel à Mme Roehrig.

Veuillez noter que le présent certificat est valable pour le projet tel que soumis au Comité d'éthique de la recherche avec des sujets humains. La secrétaire du Comité d'éthique de la recherche avec des sujets humains devra immédiatement être informée de toute modification qui pourrait être apportée ultérieurement au protocole expérimental, de même que de tout problème imprévu pouvant avoir une incidence sur la santé et la sécurité des personnes impliquées dans le projet de recherche (sujets, professionnels de recherche ou chercheurs).

Nous vous prions également de nous faire parvenir un bref **rapport annuel** ainsi qu'un avis à la fin de vos travaux.

Je vous souhaite bonne chance dans vos travaux de recherche,

Bernard Lapierre, président
Comité d'éthique de la recherche avec des sujets humains

c.c.: Céline Roehrig, DRI

CHUM

COMITÉ D'ÉTHIQUE DE LA RECHERCHE DU CHUM

Édifice Cooper
3981, boulevard St-Laurent, Mezz 2
Montréal (Québec) H2W 1Y5

Le 11 octobre 2010

Dr Dang Khoa Nguyen
Hôpital Notre-Dame du CHUM
Service de neuro-épilepsie
Pavillon Deschamps – 3ème étage
Montréal, (Québec) H2L 4M1

a/s Micheline Gravel
Courriel : micheline.gravel.chum@ssss.gouv.qc.ca

Objet :	**10.176 – *Approbation accélérée initiale et finale CÉR***
	Monitorage intracrânien lors d'une chirurgie pour l'épilepsie : Qui en a besoin et qui en bénéficiera?

Docteur

J'ai pris connaissance des documents suivants reçus au CÉR du CHUM en date du 8 octobre 2010 en vue de l'approbation du projet en rubrique :

- Lettre accompagnant la soumission du projet pour évaluation
- Formulaire de demande d'évaluation d'un projet de recherche non-multicentrique
- Protocole de recherche
- Lettre d'approbation du CÉR de l'Université de Calgary
- Formulaire A – information budgétaire
- Autorisation pour consultation de dossiers médicaux à des fins de recherche

En vertu des pouvoirs qui me sont délégués par le Comité d'éthique de la recherche du CHUM pour procéder à une évaluation accélérée, il me fait plaisir de vous informer que j'approuve votre projet puisqu'il s'agit d'un projet se situant sous le seuil de risque minimal.

CENTRE HOSPITALIER DE L'UNIVERSITÉ DE MONTRÉAL

HÔTEL-DIEU (Siège social)	**HÔPITAL NOTRE-DAME**	**HÔPITAL SAINT-LUC**
3840, rue Saint-Urbain	1560, rue Sherbrooke Est	1058, rue Saint-Denis
Montréal (Québec)	Montréal (Québec)	Montréal (Québec)
H2W 1T8	H2L 4M1	H2X 3J4

CHUM

La présente constitue l'approbation finale du comité suite à une procédure d'évaluation accélérée. Elle est **valide pour un an à compter du 11 octobre 2010,** date de l'approbation de votre projet. Je vous rappelle que toute modification au protocole et/ou au formulaire de consentement en cours d'étude, doit être soumise pour approbation du comité d'éthique.

Cette approbation suppose que vous vous engagiez :

1. à respecter la présente décision;
2. à respecter les moyens de suivi continu (cf Statuts et Règlements)
3. à conserver les dossiers de recherche pour une période d'au moins deux ans suivant la fin du projet afin permettre leur éventuelle vérification par une instance déléguée par le comité;
4. à respecter les modalités arrêtées au regard du mécanisme d'identification des sujets de recherche dans l'établissement.

Le comité suit les règles de constitution et de fonctionnement de l'Énoncé de Politique des trois Conseils et des Bonnes pratiques cliniques de la CIH.

Vous souhaitant la meilleure des chances dans la poursuite de vos travaux, je vous prie d'accepter, Docteur, mes salutations distinguées.

Brigitte St-Pierre, conseillère en éthique
Présidente
Comité d'éthique de la recherche du CHUM

BSTP/go

C.C. – Bureau des contrats

Voici les coordonnées de la personne ressources pour ce projet :
Mme Ghislaine Otis
Téléphone : 514 890-8000, poste 14485
Télécopieur : 514 412-7394
Courriel : ghislaine.otis.chum@ssss.gouv.qc.ca

Dr Dang Khoa Nguyen
10.176   Approbation accélérée initiale et finale CÉR
Le 11 octobre 2010   Page 2 de 2

Le 31 mars 2011

**Centre de
Recherche du
CHU Sainte-Justine**
*Le centre hospitalier
universitaire mère-enfant*

Pour l'amour des enfants

Université
de Montréal

Docteur Lionel Carmant
Centre de recherche
Étage A, Bloc 7

OBJET: ***Projet intitulé*** : Optimisation d'un détecteur sous-durale automatisé pour le début de crises épileptiques corticales chez le rat : Une collaboration avec le Dr Dang Nguyan du CHUM et Dr Mohamad Sawan du laboratoire polystim neurotechnologies de l'école polytechnique de Montréal.
Catégorie : C
Référence : 444

Docteur,

Suite à la réunion du Comité institutionnel de bonnes pratiques animales en recherche tenue le 18 janvier 2011, votre nouvelle demande a été évaluée et approuvée suite aux modifications apportées. Veuillez prendre note que votre protocole porte le **# 444**.

Par conséquent, et *conditionnellement à l'espace disponible à l'animalerie*, vous êtes autorisé par la Direction du Centre de recherche à débuter votre projet pour l'année en cours.

Nous désirons également vous souligner l'importance de toujours indiquer le bon numéro se référant au protocole en titre, dans toute correspondance. Nous demeurons à votre disposition pour toute information complémentaire. Agréez, l'expression de nos sentiments les meilleurs.

Nadia Hilal, Agent de gestion à l'éthique
CIBPAR
/nh

p.j.: Certificat de bons soins aux animaux
c.c. : Sandra Duss

3175, Côte-Sainte-Catherine
Montréal (Québec)
H3T 1C5
www.chu-sainte-justine.org